J. Quant. Spectrosc. Radiat. Transfer Vol. 50, No. 4, pp. 363–429, 1993
Printed in Great Britain.

0022-4073/93 $6.00 + 0.00

SPECTRAL PARAMETERS OF SELF- AND HYDROGEN-BROADENED METHANE FROM 2000 TO 9500 cm^{-1} FOR REMOTE SOUNDING OF THE ATMOSPHERE OF JUPITER

K. STRONG,†‡ F. W. TAYLOR,† S. B. CALCUTT,† J. J. REMEDIOS,† and J. BALLARD§
†Clarendon Laboratory, University of Oxford, Parks Road, Oxford and §S.E.R.C. Rutherford Appleton Laboratory, Chilton, Didcot, Oxfordshire, U.K.

(Received 5 January 1993)

Abstract—Long-pathlength self- and H_2-broadened absorption spectra of CH_4 have been recorded from 2000 to 9500 cm^{-1} at a resolution of 0.25 cm^{-1}. These spectra were obtained for a wide range of conditions relevant to the atmosphere of Jupiter, including nominal temperatures of 190, 240, and 296 K, pathlengths from 64 to 512 m, and pressures from 0.2 to 700 torr, giving CH_4 column abundances from 0.016 to 530 m-amagat. A series of molecular band models were fitted to these spectra at 10 cm^{-1} resolution, showing that the Goody and Malkmus random band models with the Voigt lineshape provided the best fits to the data. The Goody–Voigt model was subsequently used to calculate the level in the Jovian atmosphere that will be sounded by observations of CH_4 absorption, and estimates were made of the accuracy to be expected if this model were used to retrieve atmospheric parameters.

1. INTRODUCTION

Absorption bands of CH_4 dominate visible and near-infrared spectra of Jupiter.[1,2] The interpretation of Jovian spectra is therefore critically dependent upon knowledge of the spectroscopic parameters of CH_4. The need for such parameters has long been recognized and is particularly relevant at the present time, with the *Galileo* spacecraft due to arrive at Jupiter in December 1995.

One of the instruments on the *Galileo* orbiter is the Near Infrared Mapping Spectrometer (NIMS), the first instrument designed for planetary exploration which is capable of both imaging and spectroscopic observations. NIMS is a grating spectrometer which will measure radiances over 0.7–5.2 μm, a region which is dominated by thermal emission at 5 μm and by reflected solar radiation at shorter wavelengths. Observations in both of these spectral regions and at a wide range of viewing angles will allow measurements of the chemical composition of the atmosphere and its spatial and temporal variability, the vertical temperature profile from 1 bar down to the first opaque cloud layer, and cloud height, thickness, and microstructure.[3,4] The spectral resolution of NIMS (0.025 μm) will allow the resolution of gaseous molecular bands and the determination of molecular abundances without resolving rotational lines.

In order to retrieve information about the Jovian atmosphere from NIMS observations, knowledge of the spectral parameters of those Jovian gases having absorption bands in the region from 0.7 to 5.2 μm is essential. As CH_4 is the dominant absorber at these wavelengths, the planning and interpretation of NIMS measurements will rely on the availability of CH_4 parameters. The preferred form of such spectral data is generally a compilation of individual line parameters, but the complexity of the visible and near-infrared spectrum of CH_4 makes such a compilation an enormous, if not impractical, task. In addition to the four fundamental vibrational bands, the infrared spectrum of CH_4 includes numerous overtone, combination, and difference bands, with the similarity between the ν_1, $2\nu_2$, ν_3 and $2\nu_4$ frequencies resulting in significant overlap of those bands which include these transitions. The overlapping of and interactions between bands also increases the difficulty of determining the quantum number assignments of lines, so that many lines have yet to be identified. Furthermore, at the long pathlengths found in the Jovian atmosphere,

‡To whom all correspondence should be addressed at: Department of Chemistry, University of Cambridge, Lensfield Road, Cambridge, U.K.

the centres of strong CH_4 bands are saturated, making the weak wings of these bands and the centres of weak bands more important for atmospheric studies.[4] Unfortunately, line-by-line analysis of these weak lines is particularly difficult. The calculation of theoretical line parameters is also difficult due to the complexity involved in modelling the spectrum of a spherical top molecule such as CH_4.

A review of the HITRAN[5,6] and GEISA[7,8] databases shows that in the NIMS spectral region (1923–14286 cm^{-1}) line data for CH_4 are only available for lines between 1923 and 6110 cm^{-1}. Not only are many of the CH_4 bands missing from these compilations, many weak lines are either omitted or of poor accuracy, thus presenting a serious limitation in using these line data for the

Table 1. Principal infrared $^{12}CH_4$ bands: H = HITRAN 1986 (Rothman et al[5]), G = GEISA 1984 (Chedin et al[7]), and other bands are from Herzberg[9] (p. 308), Taylor and Calcutt,[4] and Brown.[10] The number of lines in each band is given as HITRAN and (GEISA). The range is the maximum of the two.

BAND	CENTRE (cm^{-1})	SOURCE	RANGE (cm^{-1})	No. of LINES
ν_4	1310.7606	H, G	944–1628	1420 (4671)
ν_2	1533.3367	H, G	1163–1866	810 (3117)
$\nu_3 - \nu_4$	1720.	H, G	1474–1932	462 (2176)
$2\nu_4$	2596.	H, G	2458–2682	41
$2\nu_4$	2612.	H, G	2254–2848	1266 (1289)
$\nu_2 + \nu_4$	2830.	H, G	2572–3185	2300 (2347)
ν_1	2917.	H, G	2741–3092	52 (85)
$\nu_2 + \nu_3 - \nu_2$	3010.	H, G	2898–3106	264 (275)
$\nu_3 + \nu_4 - \nu_4$	3010.	H, G	2880–3136	712 (742)
ν_3	3018.9205	H, G	2809–3210	1903 (1908)
$2\nu_2$	3062.	H, G	2905–3254	755 (744)
unassigned lines		H	2511–3176	847
$3\nu_4$	3868.	Brown		
$\nu_2 + 2\nu_4$	4123.	Herzberg		
$\nu_1 + \nu_4$	4223.497	H, G	4136–4279	151 (172)
$\nu_3 + \nu_4$	4340.	H, G	4147–4490	958 (958)
$2\nu_2 + \nu_4$	4370.	Brown		
$\nu_1 + \nu_2$	4450.	Brown		
$\nu_2 + \nu_3$	4540.	H, G	4409–4667	388 (386)
unassigned lines		H, G	3900–4667	2116 (537)
$3\nu_2$	4600.	Brown		
$\nu_3 + 2\nu_4$	5585.	Herzberg		
$\nu_1 + \nu_2 + \nu_4$	5775.	Herzberg		
$\nu_2 + \nu_3 + \nu_4$	5861.	Herzberg		
$2\nu_3$	6004.991	H, G	5891–6107	142 (142)
$2\nu_2 + \nu_3$	~6086	Taylor&Calcutt		
$2\nu_1 + \nu_4$	~7145	Taylor&Calcutt		
$\nu_1 + \nu_3 + \nu_4$	~7247	Taylor&Calcutt		
$2\nu_3 + \nu_4$	~7349	Taylor&Calcutt		
$\nu_1 + \nu_2 + \nu_3$	~7469	Taylor&Calcutt		
$\nu_2 + 2\nu_3$	7514.	Herzberg		
$\nu_2 + 2\nu_3$	~7571	Taylor&Calcutt		
$2\nu_1 + 2\nu_4$	8421.	Herzberg		
$2\nu_3 + 2\nu_4$	8604.	Herzberg		
$2\nu_1 + \nu_3$	8807.	Herzberg		
$\nu_1 + 2\nu_3$	8900.	Herzberg		
$3\nu_3$	9047.	Herzberg		
$2\nu_1 + \nu_2 + \nu_3$	10114.	Herzberg		
$\nu_1 + \nu_2 + 2\nu_3$	10300.	Herzberg		
$\nu_2 + 3\nu_3$	~10590	Herzberg		
$3\nu_1 + \nu_3$	11270.	Herzberg		
$2\nu_1 + 2\nu_3$	11620.	Herzberg		
$\nu_1 + 3\nu_3$	11885.	Herzberg		
$4\nu_3$	~12076	Herzberg		
$3\nu_1 + \nu_3 + \nu_4$	12755.	Herzberg		
$2\nu_1 + \nu_2 + 2\nu_3$	~13405	Herzberg		
$4\nu_1 + \nu_3$	13790	Herzberg		
$3\nu_1 + 2\nu_3$	~14789	Herzberg		

interpretation of Jovian spectra. In Table 1, the major infrared bands of $^{12}CH_4$ are listed, including the 14 on HITRAN 1986 and GEISA 1984 (the databases available at the time of this work) and an additional 31 obtained from other sources; this illustrates the large number of bands in the NIMS spectral range as well as the lack of line data for many of these bands.

Evidence for the importance of weak lines under Jovian conditions is seen in Fig. 1, where the GENLN2 line-by-line model[11,12] has been used to calculate the transmittance of CH_4 in the Jovian atmosphere, using both HITRAN 1986 and GEISA 1984 line data. A description of this model and more details of the calculation can be found in Ref. 13. In this calculation, the Curtis–Godson approximation[14–16] was applied to the nominal Jovian model atmosphere of Orton[17] to obtain weighted mean pressures, temperatures, and CH_4 abundances for 130 layers from 100 to 10^{-11} bar, each of equal thickness in terms of Δ ln(pressure). GENLN2 assumes terrestrial isotopic abundances in weighting the line strengths and, given the uncertainty in the Jovian abundances of $^{13}CH_4$ and CH_3D relative to $^{12}CH_4$, the terrestrial values were used in this calculation. Nadir viewing was assumed and the CH_4 transmittance was calculated using three paths extending from 0.32, 2.0, and 5.0 bar, up to the top of the atmosphere, these pressures corresponding to the approximate levels of the three Jovian cloud layers.

The transmittance spectra in Fig. 1 are at 10 cm^{-1} resolution, approximately the same as the maximum resolution of NIMS. Both spectra show how the CH_4 transmittance to the top of the atmosphere decreases as the level of the reflecting or emitting cloud layer is located deeper in the atmosphere. This is as expected, since the radiation originating from deeper levels must traverse longer absorption paths. In addition, for the 2.0 and 5.0 bar clouds, the band centres are clearly saturated, with significant structure present only in the wings of the 3000 cm^{-1} band. More interesting are the differences between the HITRAN and GEISA spectra. The greater number of unassigned lines listed in HITRAN for the 3900–4667 cm^{-1} region (see Table 1) is reflected in the lower frequency edge of the 4200 cm^{-1} absorption band, which is located near 4100 cm^{-1} in the GEISA spectra but extends down to 3900 cm^{-1} in the HITRAN spectra. A potentially more significant difference between the spectra is the effect of the weak CH_4 lines which are present on GEISA, but not on HITRAN. These additional lines are located mostly below 3000 cm^{-1}, and it is over approx. 2000–2600 cm^{-1} that the GEISA spectra exhibit significantly more absorption than the HITRAN spectra. This is true for all three absorber amounts, and indicates that weak CH_4 lines give rise to measurable absorptions in the Jovian atmosphere. These results thus demonstrate that the use of line-by-line modelling as a means of calculating CH_4 transmittance in the Jovian atmosphere is severely limited by the availability of line data. The poor quality of the weak line data from 1800 to 6200 cm^{-1}, the known omission of certain strong line data from 1800 to 6200 cm^{-1}, and the complete lack of line data above 6200 cm^{-1} are all proof of the need for laboratory spectroscopic studies of CH_4, not only in support of NIMS, but for any applications requiring accurate knowledge of CH_4 spectral parameters.

Unfortunately the measurement and analysis of individual line parameters over the entire NIMS spectral range is a massive undertaking, impossible on the timescale of the *Galileo* mission, and unlikely to be completed for some time to come. However, the large number of lines in the near-infrared CH_4 spectrum and the low resolution of NIMS allow an alternative to the line-by-line calculation of atmospheric transmittance. For practical purposes, the spectral resolution of NIMS (9.25 cm^{-1} at 1923 cm^{-1}, and 510 cm^{-1} at 14386 cm^{-1}) is such that frequency-averaged transmittances are sufficient. Even if a comprehensive set of line parameters were available, the retrieval of atmospheric data from NIMS spectra would be likely to involve the fitting of low-resolution transmittance models to the line data. It is, therefore, more efficient to proceed directly from low-resolution spectra to low-resolution transmittance models. Such models, which involve the fitting of laboratory measurements of frequency-averaged transmittance directly as a function of laboratory temperatures, pressures, and abundances, are known as band models. These have long been used in radiative transfer calculations for the terrestrial atmosphere, the principle of the random band model having first been suggested by Mayer[18] and Goody.[19]

The applicability of band models to the analysis of CH_4 spectra has been recognized for some time. In the visible region, long-pathlength laboratory spectra were initially recorded simply for comparison with planetary spectra.[20–26] The first systematic laboratory measurements of the visible CH_4 spectrum were performed by Dick and Fink.[27] The complexity of these spectra and the lack

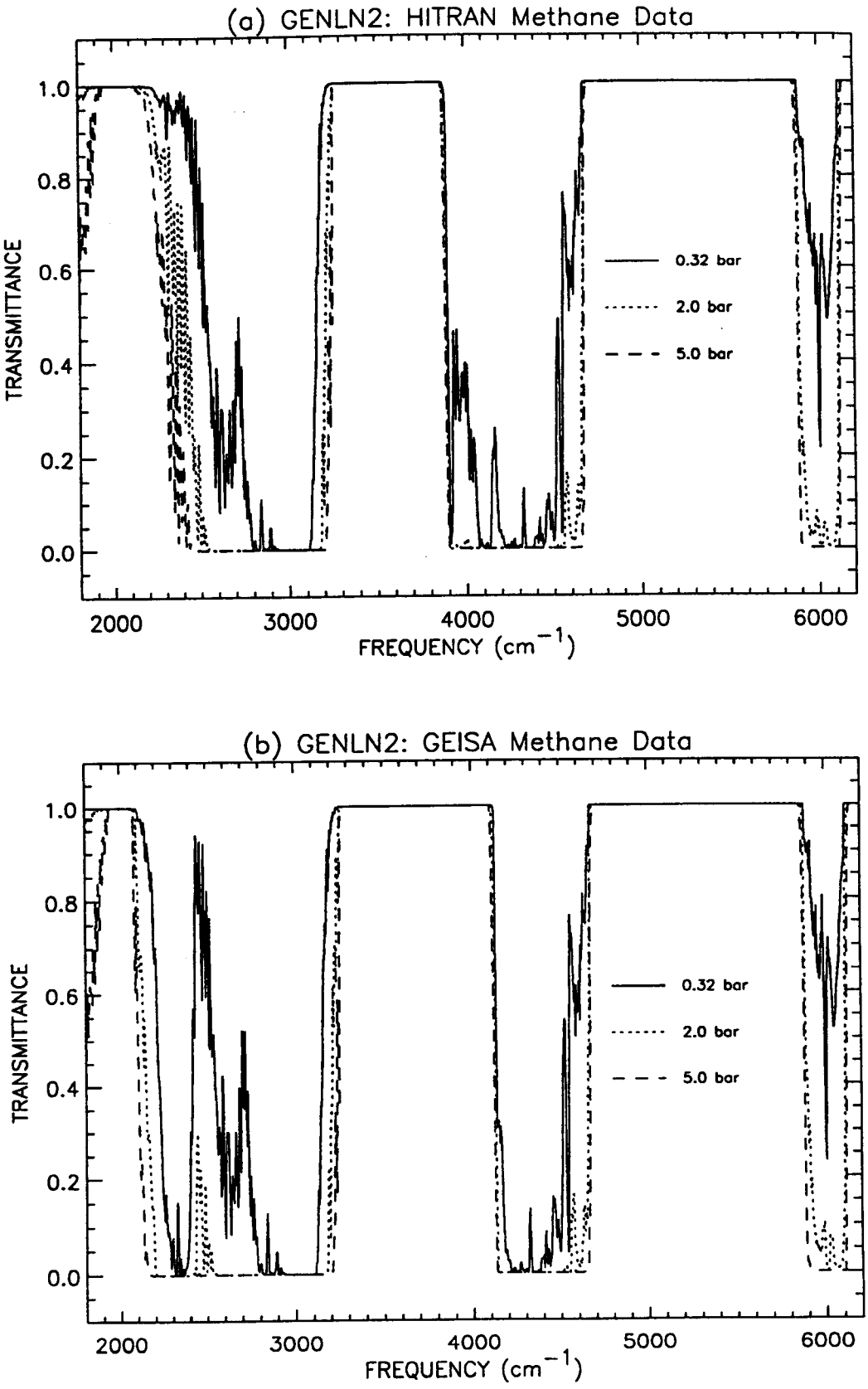

Fig. 1. The transmittance of CH_4 in the Jovian atmosphere from the 0.32, 2.0, and 5.0 bar levels up to the top of the atmosphere at 10^{-11} bar. The transmittance has been calculated with the GENLN2 line-by-line model, using (a) HITRAN 1986 line data, and (b) GEISA 1984 line data.

of quantum number assignments for any of the bands led Fink et al[28] to analyse them using the Goody random band model with the Lorentz lineshape, thus providing the first quantitative picture of the CH_4 spectrum up to 1 μm. This work was followed by that of Giver,[29] Podolak and Giver,[30] Lutz et al,[31] and more recently, Smith et al[32] and Mickelson et al.[33] Of these spectral studies, only that of Smith et al[32] included low-temperature measurements of spectral parameters, allowing the absorption coefficient for the 0.6190 μm band to be obtained from 100 to 290 K. Thus, while quantitative analysis of the CH_4 spectrum do exist for the 0.7–1.1 μm region of the NIMS spectral range, the lack of low-temperature data appropriate to the Jovian atmosphere remains a major limitation of these studies.

Similar conclusions can be drawn for the near-infrared region of the CH_4 spectrum. Although various sets of laboratory CH_4 spectra have been measured, only a few have been the subject of systematic analysis. Where long-pathlength spectra appropriate to Jovian conditions have been recorded,[34–36] this has been done at room temperature, while only Apt et al[37] have conducted any band model analysis, using the data of Benner and Fink,[35] and then only for the region from 4190 to 4590 cm^{-1}. Where low-temperature spectra have been measured and modelled, the pathlengths have been short and the abundances small. The three 77 K spectra of McKellar[38] were insufficient for modelling, while the 118 and 191 K spectra of Silvaggio[39] were omitted from the band-modelling analysis applied to his 273 K spectra, and even this was only performed from 4000 to 6500 cm^{-1}. Only Calcutt[40] and Giver et al[41,42] have performed band-model analyses of low-temperature CH_4 spectra over a significant range of the near-infrared. Even so, the spectra of Calcutt[40] were limited to 4000–10000 cm^{-1} and those of Giver et al[41] to 3760–9200 cm^{-1}, so that neither extends as far as the 5 μm Jovian window. Furthermore, Calcutt's 40 spectra were limited to a maximum abundance of 24 m-amagat and a minimum temperature of 213 K. Although the largest abundance and lowest temperature measured by Giver et al[41] were 192.8 m-amagat and 118 K, respectively, the CH_4 abundance is greater than 40 m-amagat for only eight of his 98 spectra. With Jovian Curtis–Godson weighted mean temperatures and CH_4 abundances being as low as 107 K and as high as 773 m-amagat, respectively, at heights relevant to atmospheric sounding, there is clearly a need for additional laboratory spectra of CH_4 recorded under conditions which simulate the Jovian atmosphere as closely as possible. The approach taken in the present study was therefore to measure laboratory spectra of CH_4 over the NIMS spectral range under conditions of low temperature, long pathlength, and H_2-broadening, and then to fit several different band models to these spectra, allowing an evaluation of which provided the best fit to the data.

2. EXPERIMENTAL APPARATUS

The experimental spectroscopy described below was performed at the Laboratory Spectroscopy Facility of the Rutherford Appleton Laboratory, as it was established that the maximum range of temperatures, pressures, and pathlengths available offered a useful advance over existing data. The CH_4 spectra were recorded with a BOMEM DA3.002 Fourier transform spectrometer, for which the maximum resolution achievable with the boxcar apodization imposed by the finite mirror travel of the spectrometer is 0.0028 cm^{-1} (see Ref. 43, p. 98). The spectrometer was initially purged with N_2 gas during the experiments, but as this was soon found to introduce H_2O and CO_2 contamination in the spectra, the spectrometer was evacuated for the remainder of the measurements.

The optical components used in this experiment were chosen to provide the greatest possible coverage of the 1923–14286 cm^{-1} NIMS spectral region. The combination of an LN_2-cooled InSb detector, a CaF_2 beamsplitter, and both a silicon-carbide globar and a quartz–halogen bulb, allowed spectra to be measured from 2000 to 9500 cm^{-1}, thus providing coverage of nearly all but the visible end of the NIMS region. A GaAs filter was also included in the system, mounted over the window of the InSb detector to eliminate contamination by any stray visible radiation of wavelength less than 0.9 μm.

The CH_4 gas samples were contained in a multiple-pass White cell,[44] referred to as the "long White cell" (LWC), which provided the longest pathlength (512 m) and lowest temperature (190 K) achievable at the facility, and therefore the closest simulation of Jovian conditions. This cell is described in detail by Strong[13] and by Ballard et al.[45] It consists of two stainless steel cylindrical shells with one mounted concentrically inside the other, the volume within the inner cylinder being

the gas absorption cell and the volume between the two cylinders thermally isolating the inner vessel. The mirrors in the LWC are made of Zerodur glass ceramic, coated with a gold finish which has a high reflectivity, typically 0.97–0.99, and is independent of wavelength over the spectral region of interest (see Ref. 46, p. 7-81). The radius of curvature of the mirrors is 8000 ± 10 mm and by using the double stacking optical design of Bernstein and Herzberg,[47] up to 64 traversals of the cell could be obtained, as determined by the maximum number of images that could be fitted onto the single mirror without overlapping or becoming too faint to distinguish. All three mirrors were adjustable from outside the LWC, allowing the pathlength to be varied from 64 to 512 m. Radiation from the BOMEM sources entered the cell through wedged CaF_2 windows which each provided >90% relatively flat transmittance over the entire NIMS spectral range (see Ref. 46, p. 7-40).

The LWC was cooled by pumping a circulating fluid, halon 2402, dibromotetrafluoroethane, through channels welded to the outer surface of the inner vessel. This fluid was itself cooled in an LN_2 heat exchanger, with the temperature of the cell ultimately determined by the LN_2 level in the heat exchanger pipes. This level was actively controlled by a microprocessor which used inputs from a LN_2 level gauge in the heat exchanger and from a platinum resistance thermometer (PRT) located on the cooling fluid circuit just beyond the output of the circulating pump to control the valve regulating the LN_2 flow.

The conduction of heat between the inner and outer vessels was reduced by the use of low-conductivity supports and connections, and conduction of heat by gas was minimized by operating with the vacuum vessel evacuated. The radiation of heat was reduced by multilayered interleaved aluminum foil and glass paper super-insulation wrapped around the outside of the inner vessel and over its endplates. The temperature of the LWC was monitored with a series of PRTs, 19 clipped to the outer surface of the inner vessel to monitor the temperature of the walls, and 26 suspended inside the inner vessel to monitor the temperature of the gas. The specified accuracy of these PRT temperatures was ± 0.1 K at 273 and 373 K, and ± 0.3 K at 78 K.

The vacuum and gas-handling systems for the LWC were constructed primarily of stainless steel, and included various provisions for the safe handling of CH_4 and H_2. Details can be found in Ref. 13. Gas pressures were measured with MKS Type 390 10-torr and 1000-torr Absolute Baratron Pressure Transducers. Both the 10-torr and 1000-torr baratron heads were calibrated to a claimed accuracy of 0.04% by MKS Instruments before installation in the gas-handling system.

In order to minimize contamination of gaseous impurities at the long pathlengths of the LWC, Ultra High Purity CH_4 (99.995%) and H_2 (99.999%) were used throughout the experiments, except in the case of some of the room-temperature self-broadened CH_4 measurements, when only High Purity CH_4 (99.95%) was available. Contamination by O_2 and H_2O was further reduced with the use of gas-purifying oxisorb cartridges. It should be noted that the CH_4 supplies contained terrestrial isotopic ratios of CH_3D and $^{13}CH_4$, both of which are higher than estimates of the Jovian ratios.[48,49] As these isotopic absorptions were included in the band-model fits, the band modelling over-estimates the absorptions of CH_3D and $^{13}CH_4$ relative to those of $^{12}CH_4$, compared to their relative absorptions in Jovian spectra.

3. EXPERIMENTAL METHOD

The laboratory conditions appropriate for simulations of the Jovian atmosphere were determined by calculating the Curtis–Godson weighted mean temperatures, pressures, and CH_4 abundances for 130 paths from levels between 100 and 10^{-11} bar up to the top of the atmosphere, using the five Jovian atmospheric profiles of Orton.[17] At infrared wavelengths, the Jovian atmosphere can be probed at atmospheric pressure levels between approx. 0.01 and 10 bar.[50] The Curtis–Godson parameters for the paths from levels between 0.01 and 10 bar, up to the top of the atmosphere, vary from 107 to 272 K, 0.00500 to 5.01 bar, and 0.710 to 773 m-amagat, for the temperature, the total pressure, and the CH_4 abundance, respectively. These parameters therefore defined the laboratory regime desirable for simulating the atmospheric regime of interest.

In practice, it proved possible to obtain temperatures from 189.7 to 293.1 K, CH_4 pressures from 0.0002680 to 0.9477 bar, and CH_4 abundances from 0.01723 to 527.7 m-amagat, thus getting reasonably good coverage of Jovian pressures and CH_4 abundances. Although the maximum values attained are lower than the Jovian values, the higher pressures and abundances are less important,

as the clouds present in the Jovian atmosphere block much of the radiation from the deeper levels. The inability to obtain temperatures less than 190 K is more unfortunate, because much of the absorption in the Jovian atmosphere does occur at these lower temperatures. However, it is possible that the weaker absorptions in the wings of the CH_4 bands will allow radiation to escape from slightly deeper and warmer regions of the atmosphere (see Ref. 40, p. 3-2). The long pathlengths available in the LWC therefore allow these weak absorptions to be measured.

In Fig. 2, the CH_4 abundance and the total atmospheric pressure have been plotted as functions of temperature for the Curtis–Godson paths to the top of the atmosphere. Three boxes have been superimposed on these profiles, the region within each representing the conditions achievable with a particular laboratory regime. The boxes identified as the "previous SWC conditions" show the range of temperatures, pressures, and CH_4 abundances that were obtained by Calcutt,[40] using the "short White cell" (SWC), a smaller cell with a maximum pathlength of 20 m. The boxes identified as the "current LWC conditions" show the range of conditions achieved for the spectra of the present study, clearly providing a greater coverage of temperature, pressure, and CH_4 abundance than the work of Calcutt.[40] The boxes labelled "future SWC conditions" refer to the design parameters of a new cooling jacket which has been built for the SWC, and which will operate at pressures up to 5 bar and at temperatures from 77 to 400 K.

During the period of spectroscopic measurements, a clearly defined procedure was followed each day, as can be found in Strong.[51] Chronologically, the spectra were recorded first at 296 K, then at the lowest possible temperature, 190 K, and finally at an intermediate temperature of 240 K. At each temperature, the usual procedure was to make measurements at a particular pathlength for several days, stepping through several pressures per day. Five spectra were recorded for every pressure–temperature–pathlength–source combination and were later averaged in order to reduce the effects of random variability. Each spectrum comprised 30 co-added scans, averaged to improve the signal-to-noise ratio, and taking about 10 min to record. Five empty-cell background spectra were also recorded at the start and end of each day.

The spectra were recorded at a nominal resolution of $0.25\,cm^{-1}$, the maximum resolution at which the entire wavelength region could be covered in one spectrum given the limitations of the available BOMEM computer memory. A minimum three-term Blackman–Harris apodization function[52] was applied to the interferograms in order to suppress the side lobes due to the instrument lineshape. This reduced the largest side lobes from 22 to 0.04% of the central peak amplitude, but also increased the FWHH of the measured lines to 116% of the nominal resolution. However, this remained significantly higher than the resolution required for the band-model analysis, allowing better assessment of the quality of the spectra and higher resolution analysis of the spectra if desired in the future.

Spectra of self-broadened CH_4 were recorded, using both the quartz–halogen and globar light sources to maximize the spectral coverage, at 108 temperature–pressure–pathlength combinations. These provided maximum coverage of the achievable conditions, thereby allowing the band models to be fitted to as wide a range of conditions as possible. A total of 1080 spectra were therefore recorded, 540 with the quartz–halogen lamp and 540 with the globar. At each of the three temperatures, spectra were recorded at four pathlengths and nine pressures. The pathlengths were 64.75, 128.75, 256.75, and 512.75 m with an uncertainty of 0.15%, except at 190 K, for which the maximum pathlength was reduced to 416.75 m due to difficulties in distinguishing the fainter images on the single mirror caused by the growth of a film of pump oil on the outside of the inner vessel windows. The nine nominal pressures were 0.2, 0.8, 3.2, 12.8, 51.2, 102.4, 204.8, 409.6, and 700 torr, chosen in logarithmic steps such that the ratio of successive pressures was 4 up to 51.2 torr and 2 beyond 51.2 torr, except for 700 torr, which was the highest LWC pressure safely obtainable.

In addition to the self-broadened CH_4 spectra, spectra of H_2-broadened CH_4 were recorded at 117 temperature–pressure–pathlength combinations. This provided a total of 1170 spectra, 585 recorded with the quartz–halogen lamp and 585 recorded with the globar. These conditions included the same range of temperatures and pathlengths, with the choice of CH_4 and H_2 pressures governed by the desire to simulate both Jovian CH_4 abundances and the Jovian CH_4 mixing ratio. Unfortunately, it is difficult to simulate both at the same time because of the small value of the Jovian CH_4 mixing ratio ($\sim 2 \times 10^{-3}$). Pressures of H_2 far greater than those attainable with the LWC would be required to obtain the larger Jovian CH_4 abundances with this mixing ratio.

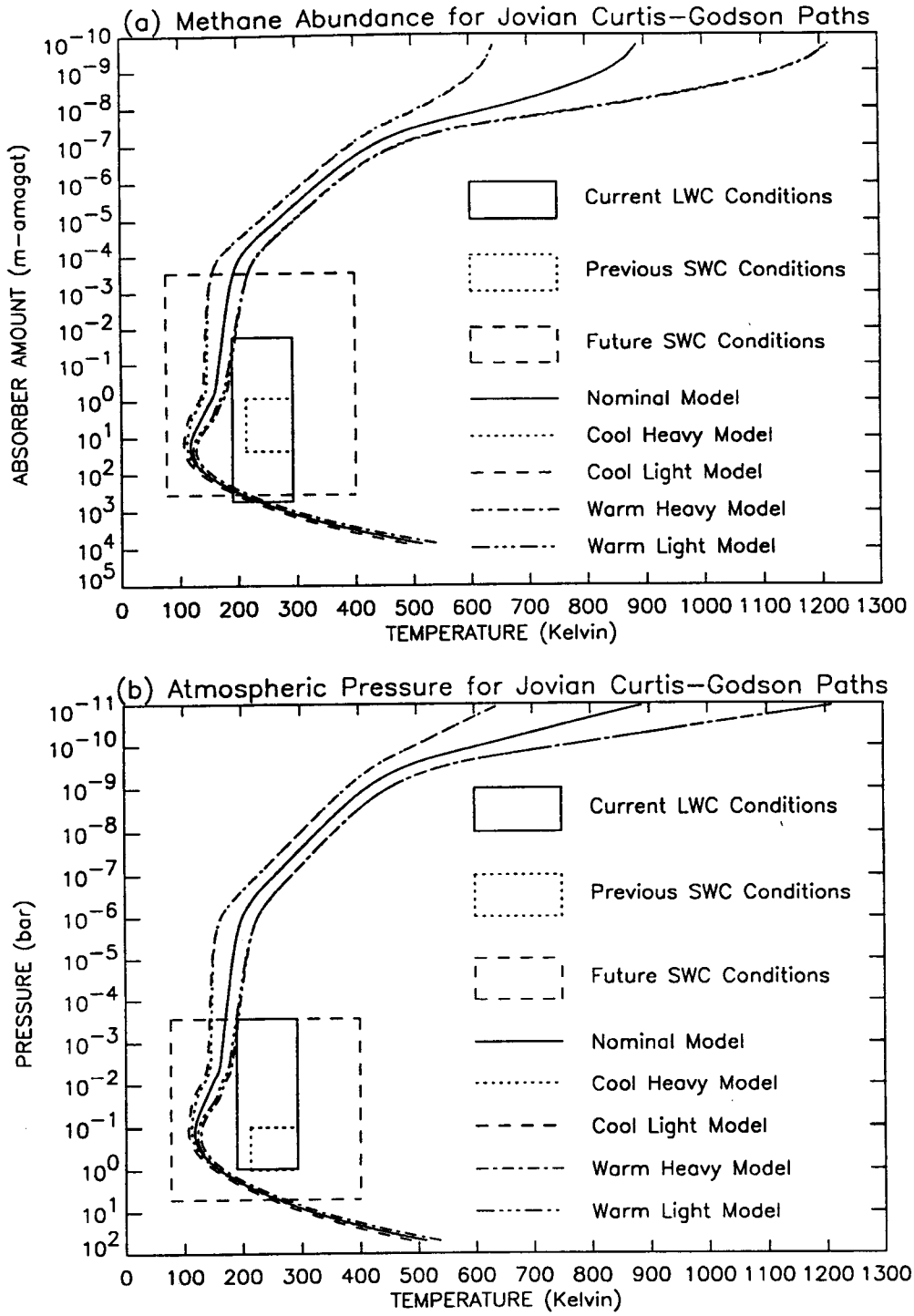

Fig. 2. The Curtis–Godson CH_4 absorber amount (a) and total pressure (b) for paths to the top of the atmosphere using the five Jovian atmospheric models of Orton.[17] Three laboratory regimes were superimposed on these profiles, representing the range of conditions achieved in this work ("current LWC"), by Calcutt[40] ("previous SWC"), and intended with the new SWC cooling jacket which has recently been designed and built ("future SWC").

However, the long pathlengths available with the LWC did allow the Jovian CH_4 mixing ratio to be simulated for the smaller Curtis–Godson abundances. For the CH_4 pressures, a subset of four of those used in the self-broadened measurements was chosen: 0.2, 3.2, 12.8, and 102.4 torr, and for the H_2 pressures, three values were chosen, 100, 245 and 600 torr, providing nominal CH_4-to-total mixing ratios ranging from 3.3×10^{-4} to 0.51.

Two distinct methods were employed for measuring the LWC temperature, depending upon whether the cell was at room temperature or cooled. For the room-temperature experiments, when the gas temperature was temporally stable with minimal spatial gradients, the temperatures of the 26 PRTs inside the LWC were recorded once for each pressure–pathlength run, about halfway through the recording of the spectra, using a 1 mA constant current source and a 15 V d.c. power supply. Tests of the current source give an average current value of 0.9935 mA, with a standard deviation (1σ) of ± 0.0018 mA. The standard deviation in the current corresponds to a temperature deviation of ± 0.5 K at room temperature, and so the instrumental uncertainty of the room-temperature measurements is the sum of this value and the quoted accuracy of the PRTs (± 0.1 K), i.e., ± 0.6 K. The maximum uncertainty in the temperature for each of the 296 K spectra is then the sum of this value and the standard deviation in the average of the 26 PRT readings. For the 296 K spectra, the largest standard deviation was ± 0.3, giving a maximum uncertainty of ± 0.9 K.

For the low-temperature experiments, a Phillips PM8237A/02 Multipoint Data Recorder with its own internal current source was used to monitor the LWC temperature. Tests of the 15 data logger channels showed that the temperatures were always within the specified accuracy of the data logger. The instrumental uncertainty of the low-temperature measurements was thus taken to be the sum of the quoted accuracy of the PRTs (± 0.3 K), and the accuracy of the data logger,[53] i.e.,

$$\Delta T = \pm 0.3 \pm [0.001 \times |T_{\text{in}}| + 0.25 \times 0.05|T_{\text{room}} - 23|] = \pm [0.7 + 0.001 \times |T_{\text{in}}|] \quad (1)$$

with T_{in} in °C and $T_{\text{room}} = 20$°C.

For the 190 and 240 K experiments, the PRTs were wired into the data logger, but with only 15 channels available, only 15 of the 26 gas sensors could be monitored in this way, requiring selection of a representative set. This included all eight along the left and right sides of the LWC, as these were at approximately the same height as the optical path, and seven of the PRTs distributed along the top and bottom of the LWC. The data logger was programmed to record the temperatures every 10 min. The accuracy of the PRT readings at low temperatures was evaluated using a temperature–pressure test, involving the application of the ideal gas law during a cool-down of the LWC from a known initial temperature and pressure. This revealed a slight cold bias of the average cold PRT temperatures (using all 26 PRTs and just the 15 data logger PRTs) relative to the theoretical temperature, suggesting that there may be warm pockets in the LWC which are not registered by any PRTs. However, the differences between the measured and theoretical temperatures were comparable to the standard deviations in the former, and so the accuracy of the low-temperature PRT readings was considered acceptable.

Because the temperatures for the 190 and 240 K spectra were recorded every 10 min, linear interpolation in time was used to derive the 15 PRT temperatures for every spectrum. For the averaged spectra generated from each set of five, the temperatures are thus the averages of 75 PRT temperatures. The maximum uncertainty in each cold temperature is again the sum of its standard deviation and the instrumental uncertainty. For the 240 K spectra, with the largest standard deviation being ± 1.6 K, the maximum uncertainty was ± 2.3 K. For the 190 K spectra, with the largest standard deviation being ± 3.2 K, the maximum uncertainty was ± 4.0 K.

The calibration of the baratrons was checked prior to both the room- and low-temperature measurements, and again after the latter. A barometric test of the 1000-torr head, conducted by exposing it to atmosphere and comparing the reading with that measured by a precision aneroid barometer, showed that the 1000-torr head measured 0.06, 0.05, and 0.09% higher than the aneroid barometer, slightly worse than its specified calibration error. The performance of the 10- and 1000-torr heads was also compared at five pressures over between 0 and 10 torr, giving maximum differences of 0.31, 0.60, and 1.1%. The individual pressure measurements were therefore considered to be accurate to at least 1.1%.

During the CH_4 experiments, the LWC was isolated as much as possible when full of flammable gas. The method of operation was to record the LWC pressure immediately after filling, then to isolate the LWC while spectra were being recorded, and finally to record the LWC pressure again once the spectra were finished. For both the room- and low-temperature spectra, the CH_4 pressures were calculated for each individual spectrum by linearly interpolating in time between the pressures measured just before and just after the spectra were recorded. For the averaged spectra generated from each set of five, the pressures are the averages of the five interpolated pressures. For the 296 K

spectra, there was negligible change in the pressure within a set, and so the uncertainty was the instrumental value of 1.1%. For the low-temperature spectra, there was a gradual temperature rise over the source of the day, as the LWC cryogenic system had to be turned off in order to eliminate vibration-induced noise in the spectra, and so the pressure of gas in the LWC increased slowly during the recording of a set of five spectra. The largest root-mean-square deviations in pressure were 0.28% for the 240 K spectra and 0.42% for the 190 K spectra, giving maximum uncertainties in the measured pressures of 1.4 and 1.5%, respectively.

4. DATA REDUCTION

Before beginning the band-modelling analysis of the self- and H_2-broadened CH_4 spectra, some initial processing was performed to generate transmittance spectra and to assess their quality. The procedure for generating the final set of CH_4 transmittance spectra from the raw intensity spectra was as follows. For each day of the experiment, a set of five start-of-day and another set of five end-of-day background spectra were recorded with the LWC evacuated, but otherwise using the same BOMEM configuration, sources, temperature and pathlength as were used for the CH_4 spectra recorded that day. The five spectra in each of these sets were averaged to obtain a daily start-of-day and a daily end-of-day averaged background for each source, thereby reducing the random variability within each set. Then the appropriate background for each CH_4 spectrum was computed by linearly interpolating the background intensity in time between the start- and end-of-day averaged backgrounds. Each individual CH_4 intensity spectrum was then ratioed to its interpolated background to generate the CH_4 transmittance spectra.

Due to the long duration of the spectral measurements and the delay between the recording of backgrounds and CH_4 spectra, significant drifts in the background levels were anticipated. Examination of the ratioed CH_4 spectra revealed that the 100% transmittance level often varied significantly from 1.0, in both the quartz–halogen and globar spectra. In some cases these drifts appeared to be random, and in other cases they were systematic, caused by small changes in the alignment of the LWC mirrors due to the presence of gas in the LWC, mirror movement, the relaxation of the LWC mirror adjustors, and temperature drifts, by changes in the alignment of the BOMEM source-switching mirror, and possibly by changes in the temperature of the detector or the light sources.

The same problem has been encountered in previous measurements of CH_4 spectra for the purposes of band modelling[27,29,40,54] and is particularly difficult to correct in those spectra with large CH_4 abundances for which the wings of the main bands eliminate the regions of zero absorption. In this work, it was decided that the spectra could best be corrected using two different methods, one for the "weakly absorbing" spectra, defined as those for which there was negligible absorption in the window regions, and one for the "strongly absorbing" spectra which exhibited weak line absorptions in the window regions. A convenient dividing point was 25 m-amagat of CH_4—for spectra with less than this abundance, the transmittance in the windows was assumed to be 1.0. This assumption ignored the possibility of any CH_4 continuum absorption in these regions, the measurement of which is clearly a difficult problem without a highly stable background level.

Each weakly absorbing spectrum was corrected by fitting a straight line to the transmittances at frequencies located in regions of zero absorption, and then ratioing the spectrum to this line to correct the 100% transmittance level for all points. For the globar spectra this line was fitted to the average transmittances at $2000 \pm 5\,cm^{-1}$ and $3510 \pm 5\,cm^{-1}$. For the quartz–halogen spectra, this line was fitted to the transmittances at 3510, 4870, 6450, 7780, and $9300\,cm^{-1}$ again averaged over $\pm 5\,cm^{-1}$, except for the H_2-broadened spectra, for which the transmittance at $4870\,cm^{-1}$ was excluded as it lay in a region of H_2 absorption.

For the strongly absorbing spectra, slightly different methods of correction were required for the globar and quartz–halogen spectra. For the globar spectra, the transmittance in the $3510\,cm^{-1}$ window was significantly lower than that in the $2000\,cm^{-1}$ window, decreasing to about 85% for the largest CH_4 abundance due to the presence of weak CH_4 lines near $3510\,cm^{-1}$. Each of these spectra was therefore normalized by scaling it by the maximum transmittance between 2000 and $4000\,cm^{-1}$, averaged over $\pm 5\,cm^{-1}$. The quartz–halogen spectra proved to be more difficult to correct because CH_4 absorptions appeared in all five windows, with no particular window showing

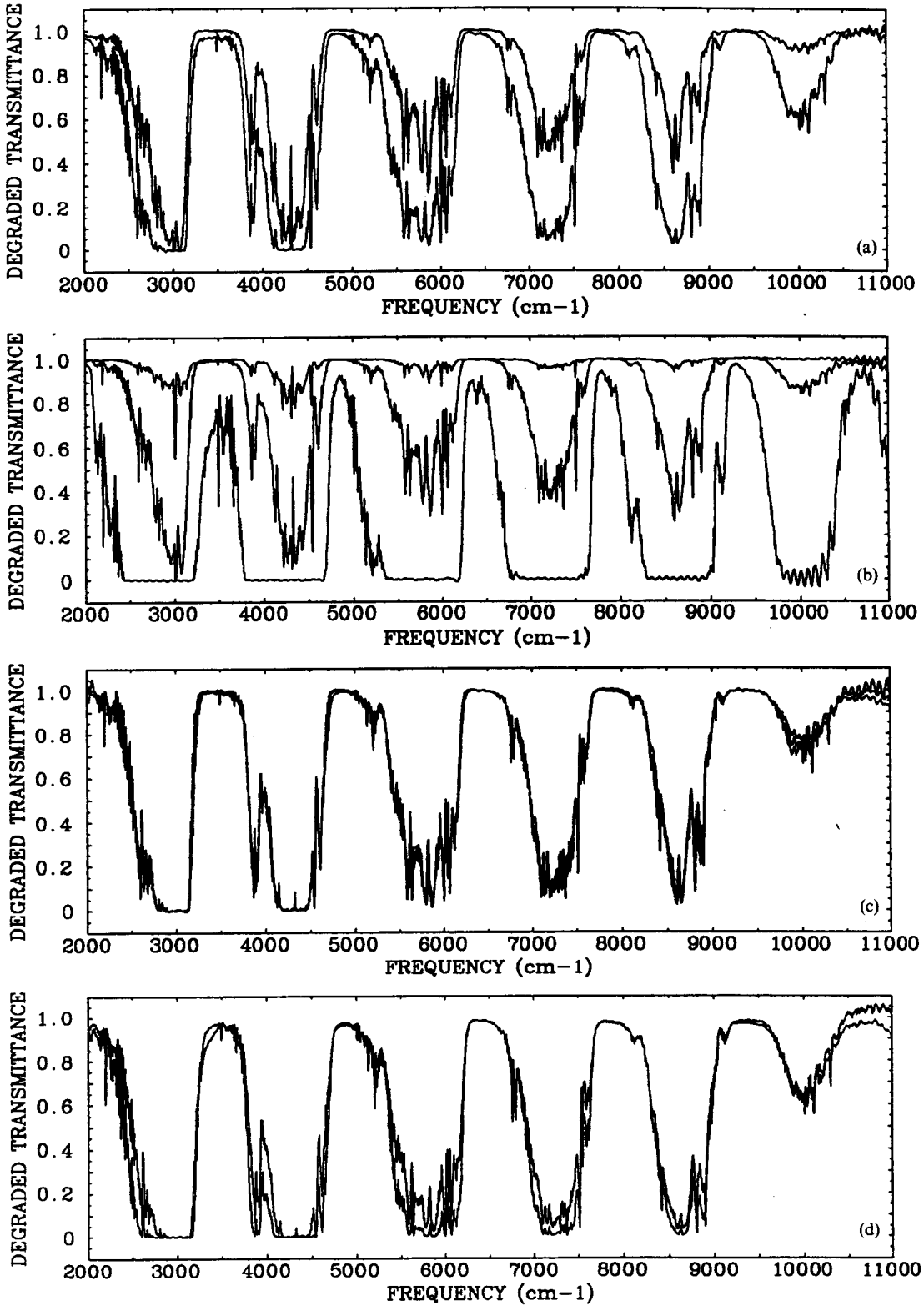

Fig. 3. Self-broadened CH_4 spectra recorded with the quartz–halogen source, corrected, averaged, and degraded to 10 cm^{-1}. (a) Constant T (~240 K) and P (~51.2 torr), with varying L (64.75 m for upper curve, and 512.75 m for lower curve). (b) Constant T (~240 K) and L (512.75 m), with varying P (~0.2 torr for upper curve, ~12.8 torr for middle curve, and ~700 torr for lower curve). (c) Constant P (~102.4 torr) and L (128.75 m), with varying T (290.8, 239.3, and 193.2 K: barely distinguishable). (d) Constant T (~296 K) and CH_4 abundance (~32.5 m-amagat), with varying P and L (~51.2 torr and 512.75 m for upper curve, ~409.6 torr and 64.75 m for lower curve).

consistently stronger or weaker absorption than the other windows. The method of normalization for these spectra used the fact that each set of globar and quartz–halogen spectra were recorded under the same conditions, and should therefore have the same transmittance in the region of overlapping frequency. This region of overlap included the 3510 cm^{-1} window, and so each quartz–halogen spectrum was scaled by the ratio of the corrected globar transmittance at $3510 \pm 5\,cm^{-1}$ to the uncorrected quartz–halogen transmittance at $3510 \pm 5\,cm^{-1}$. These various methods of correcting the 100% transmittance level resulted in shifts of 3–20% in transmittance.

Having corrected all of the self- and H_2-broadened CH_4 transmittance spectra, the next step in generating the final set of spectra was to average the five corrected spectra in every set, producing a total of 225 corrected and averaged spectra at the original resolution of $0.25\,cm^{-1}$. For the purposes of band modelling, these spectra were then degraded to a resolution of $10\,cm^{-1}$. This value was chosen primarily because it represents the highest resolution achievable with NIMS, but also because it facilitates comparison with other band-modelling studies, such as those of Silvaggio[39] and Giver et al.[41,55] The spectra were degraded using a square weighting function and averaging all of the transmittances within $\pm 5\,cm^{-1}$ of each output frequency. With a spectral increment of $0.1244\,cm^{-1}$ in the original-resolution spectra, the degraded transmittances were the average of 80 or 81 points. In order to avoid undersampling of the degraded spectra, an output frequency spacing of $5\,cm^{-1}$ was selected. Figure 3 displays some typical self-broadened CH_4 spectra at $10\,cm^{-1}$ resolution, illustrating how changes in pathlength, pressure, and temperature affect the CH_4 absorption. Similarly, in Fig. 4, two CH_4 spectra are shown, both having the same CH_4 pressure, with one spectra having no H_2 and the other broadened by 613.2 torr of H_2.

Unlike the 100% transmittance level, the accuracy of the zero-signal level assigned by the BOMEM was easily assessed because there were large regions of total absorption in the strongly absorbing CH_4 spectra. The zero-signal level was examined in the five bands of the quartz–halogen spectra and in the two bands of the globar spectra, for those spectra with the largest CH_4 abundances at all three temperatures. For both the original resolution and the degraded CH_4 spectra, the assigned zero in the transmittance spectra was within 0.01 (i.e. 1% at full scale) of the true zero transmittance level, consistent with previous BOMEM results (see Ref. 43, p. 174) and therefore considered acceptable.

In order to quantify the random noise on the averaged and corrected original-resolution CH_4 transmittance spectra in a reproducible manner, the average transmittance, τ_{avg}, and its standard deviation, 1σ, were calculated over $\pm 5\,cm^{-1}$ for selected frequencies in the window regions, the ratio τ_{avg}/σ providing a measure of the signal-to-noise. This calculation was performed at 2000 and $3510\,cm^{-1}$ for the globar CH_4 spectra, and at 3510, 4870, 6450, 7780, and $9300\,cm^{-1}$ for the quartz–halogen CH_4 spectra. Spectra with more than 25 m-amagat of CH_4 were not included in the calculation due to the presence of weak absorptions in the selected regions. The signal-to-noise ratio varied from 52 to 1985 for the global spectra, and from 52 to 6766 for the quartz–halogen spectra. The signal-to-noise ratio was generally higher for the quartz–halogen spectra, and for both

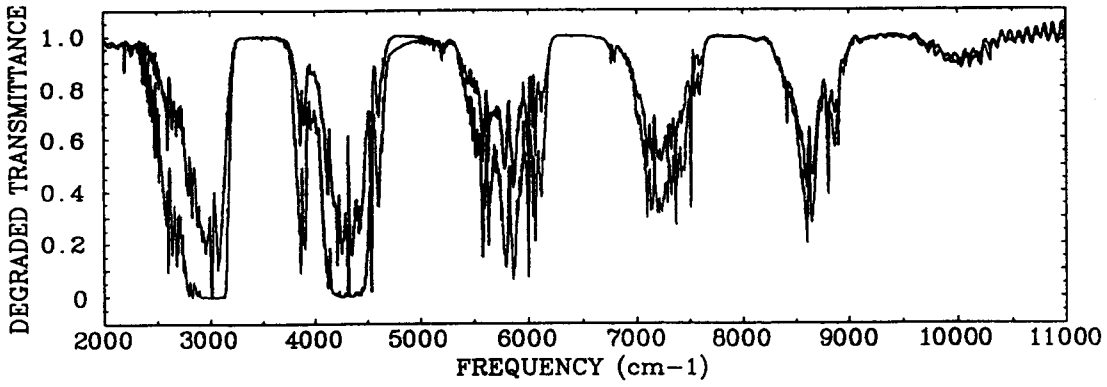

Fig. 4. Self- and H_2-broadened CH_4 spectra recorded with the quartz–halogen source, corrected, averaged, and degraded to $10\,cm^{-1}$: constant temperature (~240 K), CH_4 pressure (~12.8 torr), and pathlength (256.75 m), with no H_2 for the upper curve and 613.2 torr of H_2 for the lower curve.

sources it decreased as the background signal dropped off and also decreased with an increasing number of reflections off the LWC mirrors. The signal-to-noise was also noticeably better in the 190 and 240 K spectra compared to the 296 K spectra due to better securing of the mirrors in their mounts prior to the start of the low-temperature spectroscopy and the readjustment of the LWC mirrors to maximize the detector DC signal level after every gas fill, an action which was only taken at 296 K if there was a serious loss of signal. In all cases, when the transmittance spectra were degraded to 10 cm^{-1} resolution, the random noise became negligible.

Various factors, common to spectroscopic measurements, were found to affect the quality of the spectra. Some of the resulting spectroscopic features were reduced or eliminated during the experimental work, and many of the features were present in only a subset of the spectra or affected only a limited spectral region. By recording such a large data set, good characterization of these features was obtained, and where possible, the unwanted features were minimized computationally. A detailed assessment of the quality of the spectra can be found in Ref. 13; a brief summary follows here.

(1) Prior to its correction, the 100% transmittance level in some of the CH_4 transmittance spectra was found to slope from low to high frequencies, indicating changes in signal level with frequency, possibly due to an instrumental effect such as misalignment of the mirrors in the spectrometer.[56] Although the method of correcting the 100% level in the weakly absorbing spectra removed these slopes, this was not true of the methods of correction for the strongly absorbing spectra. However, it was possible to assess the error in the latter by first recorrecting the weakly absorbing spectra using the methods applied to the strongly absorbing spectra and then calculating the r.m.s. deviation from 1.0 of the recorrected transmittances at each of the frequencies of zero absorption. For all of the self- and H_2-broadened CH_4 spectra, the method of correcting the strongly absorbing spectra gave maximum r.m.s. deviations of 0.014 and 0.026 for the globar and quartz–halogen spectra, respectively, due to the inability to remove slopes in the 100% level.

(2) Some of the CH_4 transmittance spectra were subject to a broad ripple of varying amplitude, with a minimum between 3500 and 4500 cm^{-1} and another beyond 9000 cm^{-1}, and a maximum between 6000 and 7400 cm^{-1}. The growth of the ripple amplitude was well correlated with the growth of a broad absorption feature centered on 3220 cm^{-1} which was traced to an intense broad band of H_2O ice[57] that formed when residual water vapour in the dewar vacuum of the LN_2-cooled InSb detector froze onto the detector element. The broad ripple therefore appeared to be a channel spectrum, produced by internal reflections within the ice layer. Efforts to remove the contaminating water vapour from the detector–dewar vacuum were unsuccessful, but it did prove possible to keep the detector cold overnight for all of the 190 and 240 K experiments, thereby stabilizing the ice deposition and minimizing the rate of change of the ripple and of the ice absorption over the course of the day.

As a measure of the error introduced by the broad ripple, its amplitude was calculated as the maximum difference between any two of the window transmittances at 3510, 4870, 6450, 7780, and 9300 cm^{-1} ± 5 cm^{-1} (omitting the transmittance at 4870 cm^{-1} from the calculation for the H_2-broadened spectra). For all 164 of the weakly absorbing CH_4 spectra, the r.m.s. amplitude was 0.015 in transmittance, making this the estimate of the overall error introduced into the CH_4 transmittance spectra by the broad ice ripple. The error in transmittance due to the 3220 cm^{-1} ice absorption feature, which extends from 3000 to 3500 cm^{-1}, was difficult to determine from the CH_4 spectra because of the presence of a strong CH_4 band. However, estimates obtained from three background tests suggested that the maximum error in transmittance due to the absorption at 3220 cm^{-1} was 0.079. On days when the detector was cold at the start of the day, the error would be significantly less.

(3) Channelling with a period of approx. 3.2 cm^{-1} and a maximum amplitude of 0.030 in transmittance was present in the 296 K self-broadened CH_4 spectra. This was caused by internal reflections in the GaAs filter which was mounted over the window of the detector, and was eliminated from all subsequent spectra by remounting the filter at an angle of $17° \pm 0.5°$ to the face of the detector window. For those spectra that did exhibit this channelling, degrading them to a resolution of 10 cm^{-1} resulted in a negligible error in transmittance due to the channelling.

Another oscillatory feature, with a period of approx. 80 cm^{-1}, was present in many of the quartz–halogen spectra, apparently caused by a gain change problem in the spectrometer which

generated spikes in the quartz–halogen interferograms and hence oscillations in the spectra. It appeared as an irregular oscillation of varying period and amplitude, making it difficult to characterize, reduce, or remove. Analysis of all the corrected and averaged original-resolution quartz–halogen self- and H_2-broadened CH_4 spectra showed that the maximum error in the degraded transmittances due to this effect was 0.040. For most of the quartz–halogen spectra, particularly those with lower CH_4 abundances and weaker absorptions, the error in the transmittances at 10 cm^{-1} resolution due to the irregular oscillation was much less than this value.

(4) Contaminating line absorptions were present in the 296 K self-broadened CH_4 intensity spectra due to H_2O and CO_2 impurities in the N_2 purge of the spectrometer and the transfer-optics tanks. This contamination was eliminated from all other spectra by evacuating the system instead of purging. However, the absorptions that were present in the intensity spectra were largely eliminated on generating the transmittance spectra. At 10 cm^{-1} resolution, the CO_2 absorptions were estimated to be less than 0.01 for all but four days for which the maximum absorption was 0.04 at 2360 cm^{-1}, with CO_2 absorption affecting the region from 2290 to 2390 cm^{-1}. The H_2O contamination affected three regions, 3500–4000, 5150–5550 cm^{-1}, and 7000–7400 cm^{-1}, but in all of these regions, the absorptions disappeared on generating the transmittance spectra, the residual H_2O absorption being well below 0.01 for all spectra examined.

The possibility of significant absorption arising from H_2O and CO_2 impurities in the CH_4 and H_2 gas supplies was investigated using the GENLN2 line-by-line program to calculate the H_2O and CO_2 absorption for the largest CH_4 abundance at room temperature (442.6 m-amagat). For the specified purity of the gas after passing through the oxisorb cells (0.5 ppm), the H_2O absorptions were found to be negligible. For the CO_2, at both 10 ppm (the purity of the HP CH_4) and 2 ppm (the purity of the UHP CH_4), the absorptions, present from 2200 to 2400 and 3550 to 3750 cm^{-1}, were stronger, making some contamination of these two regions likely, although it was not possible to distinguish CO_2 absorption from CH_4 absorption.

(5) The H_2-broadened CH_4 spectra include absorption by the 1–0 band of H_2. In order to distinguish this band from overlapping CH_4 absorptions and to determine its extent, a set of pure H_2 spectra was recorded at 240 K and 256 m, using the three H_2-broadened pressures of 100, 245, and 600 torr. In these spectra, six individual absorption lines were seen to be superimposed on a broad continuum absorption. The positions of these lines are in excellent agreement with those listed by Margolis,[58] while the continuum feature extends from approx. 3700 to 5600 cm^{-1} and is less than 1% in absorption except for 600 torr of H_2, for which it is as high as 7% at the pathlength of 256 m. Those CH_4 spectra broadened by 600 torr of H_2 therefore have H_2 absorption in this region, somewhat less than 7% for pathlengths of 64 and 128 m, and somewhat more than 7% for pathlengths of 416 and 512 m.

(6) The final contaminating feature found in the spectra was a broad-band absorption extending from 2820 to 3020 cm^{-1}, and having three sharp absorption maxima at approx. 2850, 2920, and 2960 cm^{-1}. This was due to pump-oil contamination in the system, and was particularly noticeable at low temperatures, when pump oil in the LWC vacuum vessel condensed on the outside of the inner-vessel viewing and infrared windows. For the 296 K spectra, the pump-oil absorption remained stable over the course of a day and ratioed out completely in the transmittance spectra. For the 190 and 240 K spectra, the pump-oil absorption was much stronger and no longer stable, and as it overlapped the strongest CH_4 band, it was impossible to use the CH_4 transmittance spectra to assess how well the pump-oil absorption ratioed out. However, an estimate of the maximum error introduced by the pump oil was obtained by generating the ratio of the end- to start-of-day averaged backgrounds for all 33 days of cold spectra, calculating the maximum absorption (over ± 5 cm^{-1}) due to the pump oil, and then calculating the r.m.s. of these 33 values. This gave a value of 0.025 as the worst estimate of the error for the 190 and 240 K CH_4 transmittance spectra. The true error should be much less than this as the residual pump oil spectra features were much smaller when the CH_4 spectra were ratioed to interpolated background spectra.

5. BAND MODELLING

Discussions of the theory of band modelling and the various models that have been developed can be found in Goody[59] and Rodgers.[60] When fitting a band model to laboratory spectra, two types

of transmittance functions may be used: those that attempt to model physical absorption processes and those that are purely empirical. The latter are often more successful, but the former are preferable as they should give physically based and therefore more reliable transmittances for conditions interpolated and extrapolated from measurement conditions.

The method of analysis used in this work was to first fit the self-broadened CH_4 spectra with the Goody and Malkmus random band models, the generalized Zachor–King and Gibson–Pierluissi models, and the empirical Smith model. The Goody and Malkmus models, which are the models most commonly used in fitting CH_4 transmittance, were selected because their assumption of a random line distribution is appropriate to the irregular and complex near-infrared CH_4 spectrum. The three other models were fitted in order to allow a comparison of the results obtained by different models and an assessment of which models provided the best representation of the data. In the second stage of the fitting process, the band models that were most successful at fitting the self-broadened CH_4 spectra were adapted to include foreign-broadening. They were then used to fit both the self- and H_2-broadened CH_4 spectra together. Given a band-model equation for the frequency-averaged transmittance in terms of temperature, pressure, abundance, and several parameters, the aim of a band-model fit is to find the set of parameters for which the band model provides the best match to the measured transmittances. In this study, non-linear least squares fitting was used, specifically, routine E04FDE of the Numerical Algorithms (NAG) Library, which finds the unconstrained minimum of the sum of the squares of N non-linear terms with M parameters, given a set of initial estimates for these parameters, and does not require specification of first or second derivatives. Details of this method can be found in Refs. 61 and 62.

The self-broadened CH_4 spectra were fitted with four sequences of progressively more complex models, using the parameters fitted by one model as the input for the next model. Because the fitting routine showed some sensitivity to the initialization of the parameters, this method ensured that the value of a parameter was optimized as far as possible before being used as an initial value in a succeeding model. All four sequences began with the fit of the one-parameter Weak Limit model,

$$\bar{\tau} = \exp[-k_\nu(T_0)U] \tag{2}$$

where $k_\nu(T_0)$ is the absorption coefficient at reference temperature T_0, U is the amount of absorbing gas per unit area, and $k_\nu(T_0)$ for each frequency interval was initialized to the average value of $-\ln(\bar{\tau})/U$ for the 108 transmittances in the interval.

This fit was followed by the fit of a two-parameter Weak Limit model in which k_ν was given a temperature dependence. A common limitation of band models is that their only temperature dependence is that of the Lorentz and Doppler line widths, the usual method of band-model analysis being to fit the averaged transmittance as a function of pressure and abundance, but only at a specific temperature. Calculation of the band-model transmittance at temperatures other than those measured involves extrapolating from or interpolating between the models fitted at different temperatures. This is an unsatisfactory method, being computationally inefficient and liable to inconsistencies between users. Calcutt[40] (p. 5-8) and Calcutt et al[63] proposed that the temperature dependence of the absorption be explicitly included in the band model by giving the fitted absorption coefficient the same temperature dependence as that of the line strength, i.e.,

$$k_\nu(T) = k_\nu(T_0)\left(\frac{T_0}{T}\right)^{1.5} \exp\left[1.439E_1\left(\frac{1}{T_0} - \frac{1}{T}\right)\right], \tag{3}$$

where E_1 is analogous to the energy of the lower level in units of cm^{-1}, with the vibrational partition function assumed to be unity, and the simulated emission term ignored. This expression is easily incorporated into most band models, simply using $k_\nu(T)$ wherever k_ν appears, and fitting both $k_\nu(T_0)$ and E_1. Thus, for the temperature-dependent Weak Limit model, both of these parameters were fitted, $k_\nu(T_0)$ being initialized to the best-fit values of the preceding Weak Limit fit, and E_1 being given an initial value of $100\,cm^{-1}$, typical of values for CH_4 listed in the HITRAN 1986 database.

These two parameters, optimized for the Weak Limit approximation, were then supplied as the initial values for four subsequent independent fitting sequences, two involving random band models, and two involving empirical models. The former assume that the lines in a spectral interval are randomly distributed, and define the model transmittance of the interval to be the transmittance

averaged over all possible arrangments of line positions.[60] The transmittance in the general random model can be expressed in terms of a line-strength-distribution function $N(S)$, where $N(S)\,\mathrm{d}S$ is the number of lines in interval $\Delta\nu$ which have a line strength between S and $S+\mathrm{d}S$ (see Ref. 59, p. 154 and Ref. 60, pp. 18–19):

$$\bar{\tau} = \exp\left(\frac{-1}{\Delta\nu}\int_0^{\infty} N(S)\int_{-\infty}^{+\infty}[1-\mathrm{e}^{-SUf(\nu)}]\,\mathrm{d}\nu\,\mathrm{d}S\right). \tag{4}$$

Evaluation of this expression for the transmittance thus requires specification of the lineshape function, $f(\nu)$, and the line-strength-distribution function, with the two most widely used distributions being those of Goody[18,19] and Malkmus.[64]

Thus, in the first fitting sequence, the Goody random band model[18,19] was fitted to the spectra, first using the Lorentz lineshape and then using the Voigt lineshape. This model assumes an exponential line-strength distribution having a total of N_0 lines of mean strength S_0 randomly spaced over the interval $\Delta\nu$, with a mean line spacing of $\delta = \Delta\nu/N_0$. This distribution has the form

$$N(S) = \frac{N_0}{S_0}\exp\left(\frac{-S}{S_0}\right). \tag{5}$$

Substituting this expression into Eq. (4), integrating over S, and incorporating the Lorentz lineshape gives

$$\bar{\tau}_{\text{Goody–Lorentz}} = \exp\left(-1\Big/\sqrt{\frac{1}{(k_\nu U)^2}+\frac{1}{\pi k_\nu y_\nu UP\sqrt{T_0/T}}}\right), \tag{6}$$

where the absorption coefficient is defined as

$$k_\nu = \frac{S_0}{\delta} = \frac{\text{mean line strength}}{\text{mean line spacing}} \tag{7}$$

and the pressure coefficient is defined as

$$y_\nu = \frac{\alpha_{\mathrm{L}}^0}{P_0\,\delta} = \frac{\text{self-broadened Lorentz half-width at } T_0, P_0}{P_0 \times \text{mean line spacing}}. \tag{8}$$

In the Goody–Lorentz model, parameters k_ν, E_l, and y_ν were fitted to the spectra. Parameter y_ν was initialized to give the strong term in Eq. (6) the same effect as the weak term for the spectrum with the strongest absorption (largest U/P), after a series of trial fits it showed that the fits improved (i.e., the r.m.s. residual error decreased) as the effect of the strong term was increased through 10, 20, and 50–100% of the weak term, but showed negligible improvement beyond this.

Once the Goody–Lorentz model had been fitted, the resulting best-fit parameters were used to initialize the parameters in the Goody–Voigt model. If the Voigt lineshape is substituted into Eq. (4), the Goody model becomes

$$\bar{\tau}_{\text{Goody–Voigt}} = \exp\left(-2k_\nu U\int_0^{\infty}\frac{V(x,y)}{1+k_\nu U\,\delta V(x,y)/\alpha_{\mathrm{D}}^0\sqrt{T}}\,\mathrm{d}x\right), \tag{9}$$

where

$$V(x,y) = \frac{y}{\pi^{3/2}}\int_{-\infty}^{\infty}\frac{\exp(-t^2)}{y^2+(x-t)^2}\,\mathrm{d}t, \tag{10}$$

$$x = (\nu-\nu_0)/\alpha_{\mathrm{D}}, \quad y = \alpha_{\mathrm{L}}/\alpha_{\mathrm{D}} = \frac{\alpha_{\mathrm{L}}^0}{\alpha_{\mathrm{D}}^0}\frac{P}{P_0}\frac{\sqrt{T_0}}{T}, \tag{11}$$

and

$$\alpha_{\mathrm{D}}^0 \equiv \alpha_{\mathrm{D}}/\sqrt{T} = \frac{\nu_0}{c}\sqrt{\frac{2R}{M}}, \tag{12}$$

where c is the speed of light, R is the gas constant, and M is the molecular weight of the molecule. Four parameters were fitted in the Goody–Voigt model: $k_\nu(T_0)$ and E_l were directly translated from the Goody–Lorentz fit, $\delta/\alpha_{\mathrm{D}}^0$ was calculated from the Goody–Lorentz fit of y_ν, being equivalent

to $\alpha_L^0/P_0\alpha_D^0 y_v$, and α_L^0/α_D^0 was initialized from a given α_L^0, v, and the molecular mass of CH_4. The value of the self-broadened Lorentz half-width, α_L^0, chosen for the initialization was 0.085 cm^{-1}, as used by Silvaggio[39] and Giver et al[41] in their CH_4 band modelling. Evaluation of the Voigt lineshape $V(x, y)$ was accomplished using the computer code of Drayson.[65] Evaluation of the second integral (over x) was performed using Simpson's rule with 101 points[66] computed over both high- and low-resolution grids.

The second sequence to be fitted from the Weak Limit with $k_v(T)$ involved the Malkmus random band model,[64] again using both the Lorentz and Voigt lineshapes. The Malkmus model uses a line-strength distribution with an infinite number of lines and a $1/S$ weighting, having the form

$$N(S) = \frac{N_0}{S} \exp\left(\frac{-S}{S_0}\right). \tag{13}$$

Introducing $N(S)$ and the Lorentz lineshape into Eq. (4) yields

$$\bar{\tau}_{\text{Malkmus-Lorentz}} = \exp\left(-1 \Big/ \left[\frac{1}{2k_v U} + \sqrt{\frac{1}{(2k_v U)^2} + \frac{1}{4\pi k_v y_v UP\sqrt{T_0/T}}}\right]\right). \tag{14}$$

Similarly, using the Voigt lineshape,

$$\bar{\tau}_{\text{Malkmus-Voigt}} = \exp\left(\frac{-2\alpha_D^0\sqrt{T}}{\delta}\int_0^\infty \ln\left[1 + \frac{k_v U\delta}{\alpha_D^0\sqrt{T}} V(x, y)\right] dx\right). \tag{15}$$

The parameters fitted in the Malkmus–Lorentz and Malkmus–Voigt models are equivalent to those in the Goody–Lorentz and Goody–Voigt models, respectively. The pressure coefficient in the Malkmus–Lorentz model was given the same initial value as it was in the Goody–Lorentz model, after trial fits similar to those described above showed that initializing the strong term to 100% of the weak term again optimized the fit. Thus, all of the parameters in the Malkmus models were initialized in the same way as the equivalent parameters in the Goody models. The evaluation of the Voigt lineshape and of the second integral (over x) were both identical to the methods used for the Goody–Voigt model.

The third sequence of models to be fitted from the Weak Limit with $k_v(T)$ were empirical generalizations of the general random band model. Two such models were fitted, the first being a simplification of the model of Zachor,[67,68] which assumes the Lorentz lineshape, but includes a parameter v which describes the line-strength distribution. In this model,

$$\bar{\tau}_{\text{Zachor-King}} = \exp\left[-1 \Big/ \sqrt{\left(\frac{1}{k_v U}\right)^2 + \left(\frac{-1}{\ln \tau_{\text{strong}}}\right)^2}\right] \tag{16}$$

where τ_{strong} is the transmittance in the strong limit which was derived by King[69] to account for line distributions which differed from the ideal regular and random cases. In this formula, the transmittance is defined in terms of the incomplete gamma function, $P(n, x)$:

$$\tau_{\text{strong}} = 1 - P(n, [n\Gamma(n)\sqrt{4k_v y_v UP\sqrt{T_0/T}}]^{1/n}) \tag{17}$$

where

$$P(n, x) = \frac{1}{\Gamma(n)}\int_0^x t^{n-1} e^{-t}\, dt, \tag{18}$$

$\Gamma(n)$ is the gamma function, and n is an adjustable parameter.

A further generalization of this model was proposed by Gibson and Pierluissi,[70] who introduced a scaling parameter for the $(-1/\ln \tau_{\text{strong}})^2$ term. Retaining the term for intermediate absorption in Zachor's original model, the Gibson–Pierluissi model becomes

$$\bar{\tau}_{\text{Gibson-Pierluissi}} = \exp\left[-1 \Big/ \sqrt{\left(\frac{1}{k_v U}\right)^2 + B_s\left(\frac{-1}{\ln \tau_{\text{strong}}}\right)^2 - M\left(\frac{1}{k_v U}\right)\left(\frac{1}{\ln \tau_{\text{strong}}}\right)}\right] \tag{19}$$

with $|M| < \sqrt{B_s}$, and τ_{strong} again defined by Eq. (17).

In the fit with the Zachor–King model, parameters $k_v(T_0)$, E_l, y_v (initialized as for the Goody–Lorentz model), and n (initialized to 1) were fitted to the spectra. Evaluation of τ_{strong}

required evaluation of the gamma and incomplete gamma functions, which was performed using Numerical Recipes routines GAMMLN and GAMMP found in Ref. 71 (pp. 157, 161). The best-fit values obtained with the Zachor–King model were then used to initialize four of the six parameters in the Gibson–Pierluissi model. The additional two parameters, B_s and M, were initialized to 1 and 0, respectively, making the initial model identical to the simplified Zachor–King model.

The last model to be fitted to the self-broadened CH_4 spectra was the empirical Smith model[72] refitted from the Weak Limit. This has the form

$$\bar{\tau} = \exp(-k_v U^a P^b T^c) \tag{20}$$

where a, b, and c are fitted exponents. Two such fits were performed. In the first, the original four-parameter Smith model was refitted from the one-parameter Weak Limit, with the only temperature dependence being the T^c term. However, this power law temperature dependence is unlikely to fit all data sets because for some wavenumber intervals, the optical depth may be a minimum or maximum at an intermediate temperature, not at the highest or lowest temperature measured. Therefore, a second fit was performed in which the $k_v(T)$ temperature dependence was added to the Smith model. The resulting five-parameter model was fitted from the two-parameter Weak Limit with $k_v(T)$. The exponents a, b, and c in the Smith model were initialized to 1, 0, and 0, respectively, making the initial Smith model identical to the Weak Limit model.

The self-broadened CH_4 spectra were thus fitted using all four of these sequences. Two independent sets of fits were performed, one of the 108 globar spectra and one for the 108 quartz–halogen spectra. Once the fits were completed, the results obtained for these two sources were merged, the globar results being used for the 2000–3900 cm^{-1} region and the quartz–halogen results being used for the 3905–9500 cm^{-1} region. The results of this band modelling are discussed in the following sections.

6. RESULTS FOR THE SELF-BROADENED CH_4

The success of each of the fitted models in reproducing the measured transmittances at each frequency was quantified by the r.m.s. residual error, σ, defined by

$$\sigma^2 = \sum_{i=1}^{N} \frac{[y_i - y(x_i; a_1, \ldots, a_M)]^2}{N} \tag{21}$$

where N is the number of original data points (x_i, y_i), and the fitted values are given by model $y(x_i; a_1, \ldots, a_M)$ having M parameters. This r.m.s. error is plotted in Fig. 5 for all 10 of the models that were fitted to the self-broadened CH_4 spectra.

The first four plots, Figs. 5(a)–5(d), are for the four models fitted in the Goody sequence. As expected, the one-parameter Weak Limit model provides a poor fit to the data, particularly in the strongly absorbing band centres. The addition of the temperature dependence of k_v improves the Weak Limit fit, but is still unable to reduce σ significantly. Further improvement is obtained with the addition of the strong term in the Goody–Lorentz model, but the Voigt lineshape is required before σ is consistently reduced across the entire spectrum. This follows from the range of laboratory conditions obtained during the experiments, as they included the regimes of both Doppler and Lorentz broadening. A similar improvement in σ is seen for the Malkmus model. Figures 5(e) and 5(f) show σ for the Malkmus–Lorentz and Malkmus–Voigt models, again following from the fits in Figs. 5(a) and 5(b). Again, the Malkmus fit is significantly improved by the use of the Voigt lineshape. In the third sequence, the Zachor–King model, Fig. 5(g), again provides a significant reduction in σ, compared to the preceding Weak Limit fits. However, the addition of two more parameters in the subsequent fit with the Gibson–Pierluissi model, Fig. 5(h), has little effect on σ, the difference between σ for these two models being well below 0.005 over the entire 2000–9500 cm^{-1} range. In the final sequence, the Smith exponential model was fitted with and without $k_v(T)$. As seen in Figs. 5(i) and 5(j), the addition of the temperature dependence of k_v improves the fit at the high frequency edge of each of the five bands.

With the exception of the generalized empirical models, the increasingly complex models in each of the four fitting sequences thus provide progressively better fits to the self-broadened CH_4 spectra. All models except the last in each sequence served as a means of obtaining the optimum initial

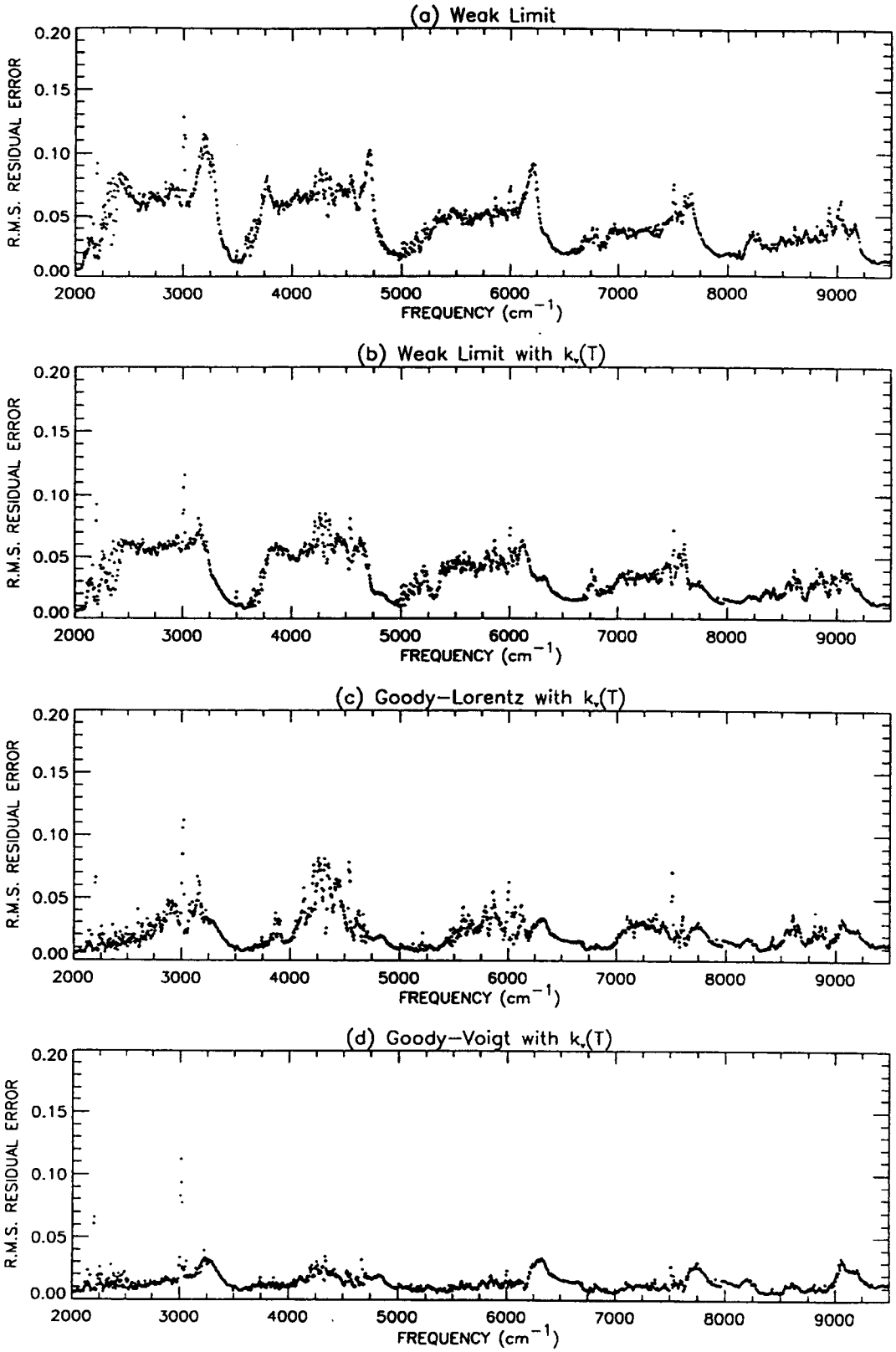

Fig. 5. *Caption on p. 383*

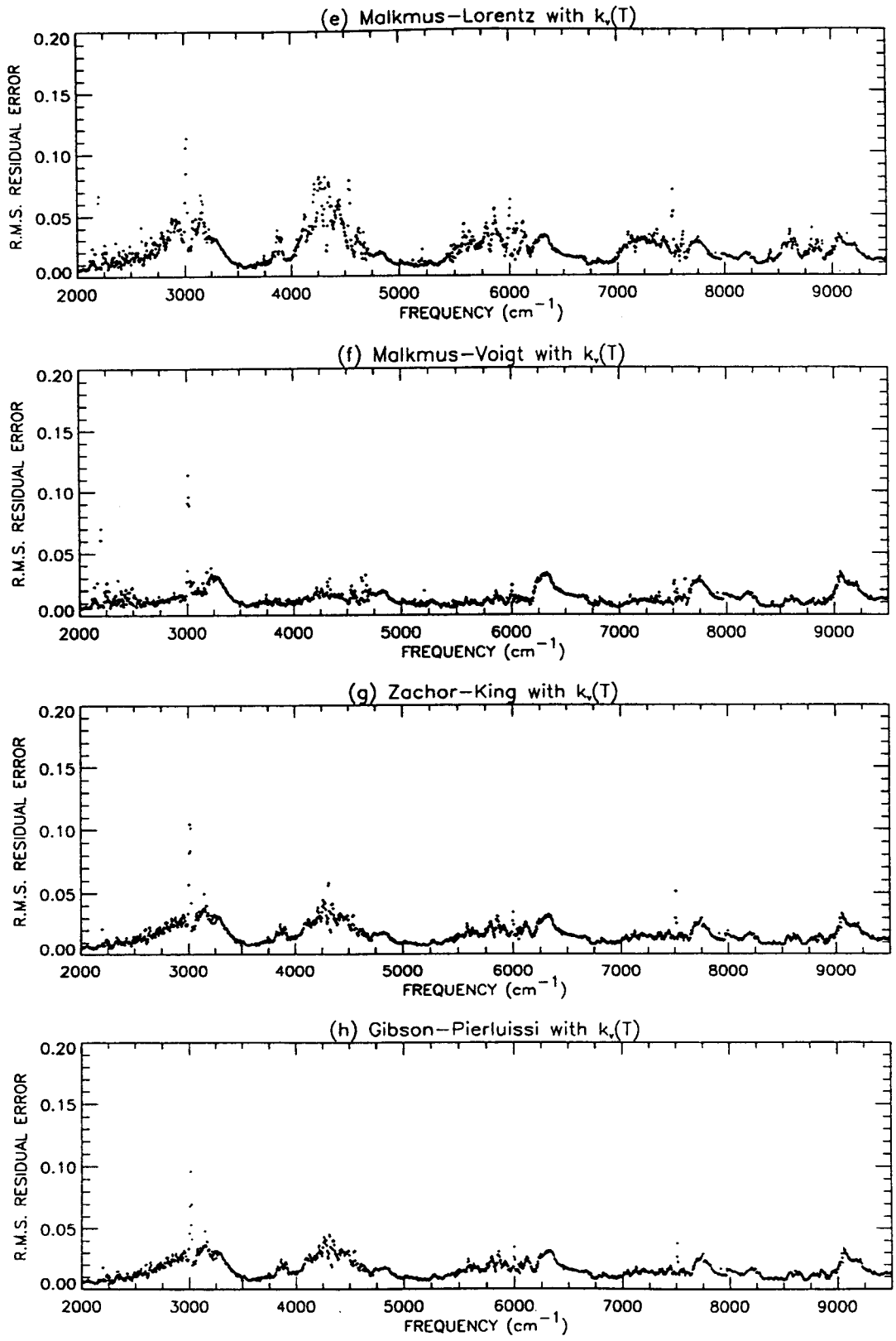

Fig. 5. *Caption on opposite page.*

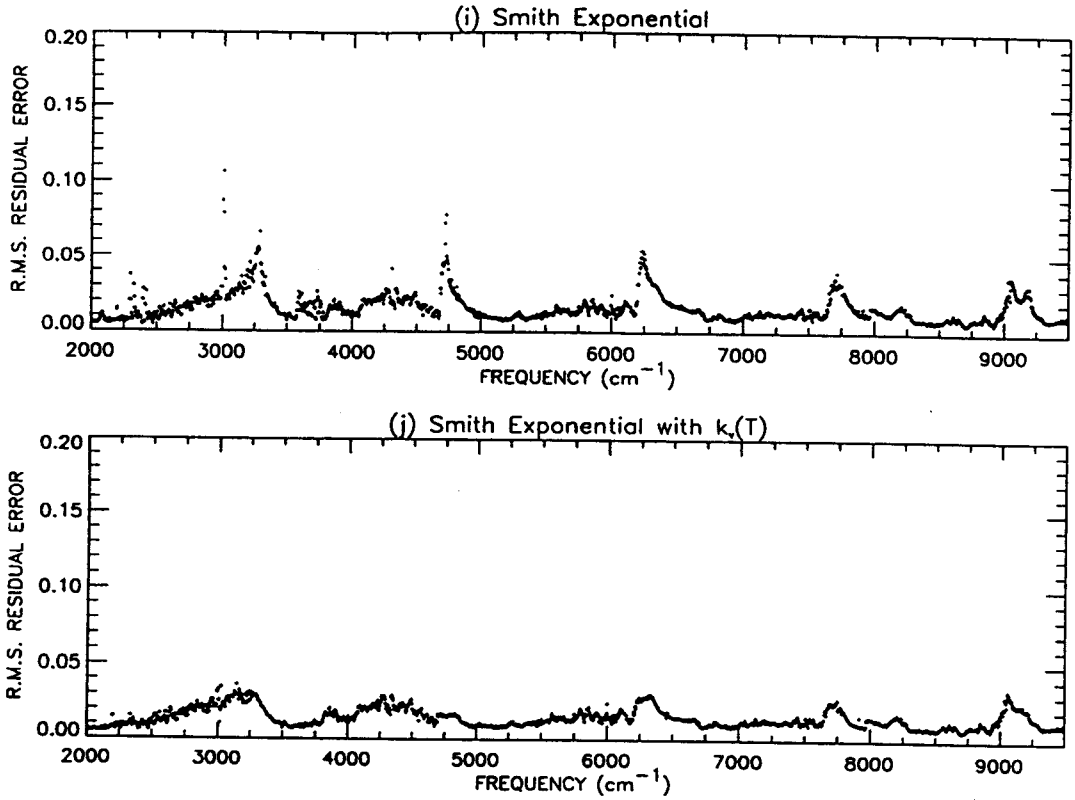

Fig. 5. The r.m.s. residual error in transmittance for the 10 models fitted to the self-broadened CH_4 spectra.

values for parameters to be fitted by the next model. Closer examination of the five best fits reveals that the Goody–Voigt and Malkmus–Voigt band models provide closer fits to the spectra than do the Zachor–King, Gibson–Pierluissi, or Smith models. The Goody–Voigt and Malkmus–Voigt fits agree to within 0.005 in transmittance except in the band centre at 4000–4300 cm^{-1}, where σ is slightly larger for the Goody–Voigt fit, but the agreement is still within 0.01. Thus, the $1/S$ weighting and the larger number of weakly absorbing lines included in the Malkmus model offer only a small improvement over the Goody model.

The fits with the Goody–Voigt and Malkmus–Voigt models are consistently better than those with the Zachor–King, Gibson–Pierluissi, and Smith models, particularly for the CH_4 bands. Only in the region from approx. 2000 to 2500 cm^{-1}, and for some isolated points at other frequencies, do these three models apparently provide a better fit. The region from 2000 to 2500 cm^{-1} includes the ν_2 band of CH_3D which has a regular PQR structure seen in the spectra at the original resolution, making the assumption of random line spacing made by the Goody and Malkmus models inappropriate in this region. Furthermore, contamination by CO_2 in this region may also contribute to the poorer fit.

Despite the differences in σ from fit to fit, the regions where σ is largest are the same for all five models, suggesting that errors in the measured transmittances are largely responsible for the larger values of σ. This r.m.s. residual error only provides a measure of the agreement between the fitted and measured transmittances. If the spectra were known to be free of errors, σ would represent the uncertainty in the fit, whereas, if the fit were assumed to be correct, σ would represent the standard deviation in the original data. In this case, σ combines both the measurement errors of the data and the goodness of fits. As was discussed in Sec. 4, the original spectra were subject to a variety of errors, of which the sloping ratios and the ice ripple had the largest overall effect. With the upper r.m.s. error estimate of 0.020 for the former and an r.m.s. error estimate of 0.013 for the latter, for the self-broadened CH_4 spectra, these measurement errors account for a significant fraction of the r.m.s. residual error in the fits. The values of σ for the Goody–Voigt and Malkmus–Voigt models lie between 0.005 and 0.02 for most of the 2000–9500 cm^{-1} range. The

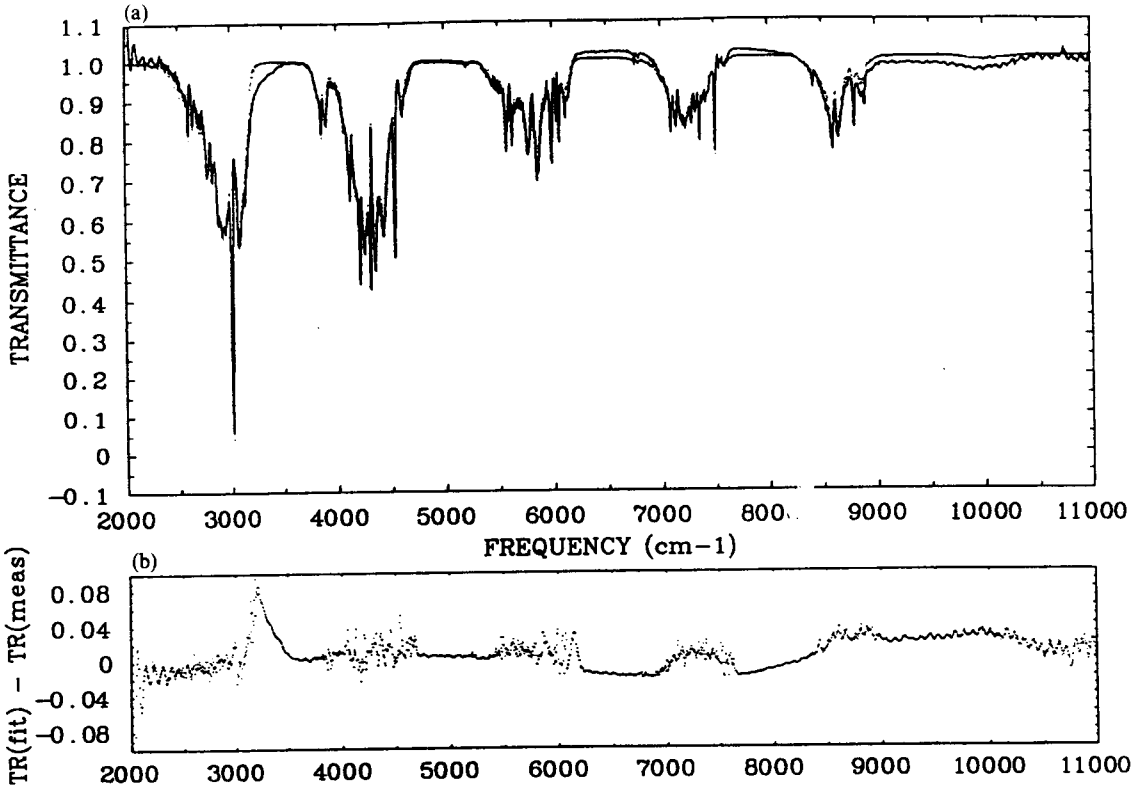

Fig. 6. (a) A weakly absorbing spectrum recorded at 289.8 K, 0.004304 bar, 256.75 m, and 1.028 m-amagat CH_4 (——) and the Goody–Voigt fit to this spectrum (· · · ·). (b) The difference between these two spectra.

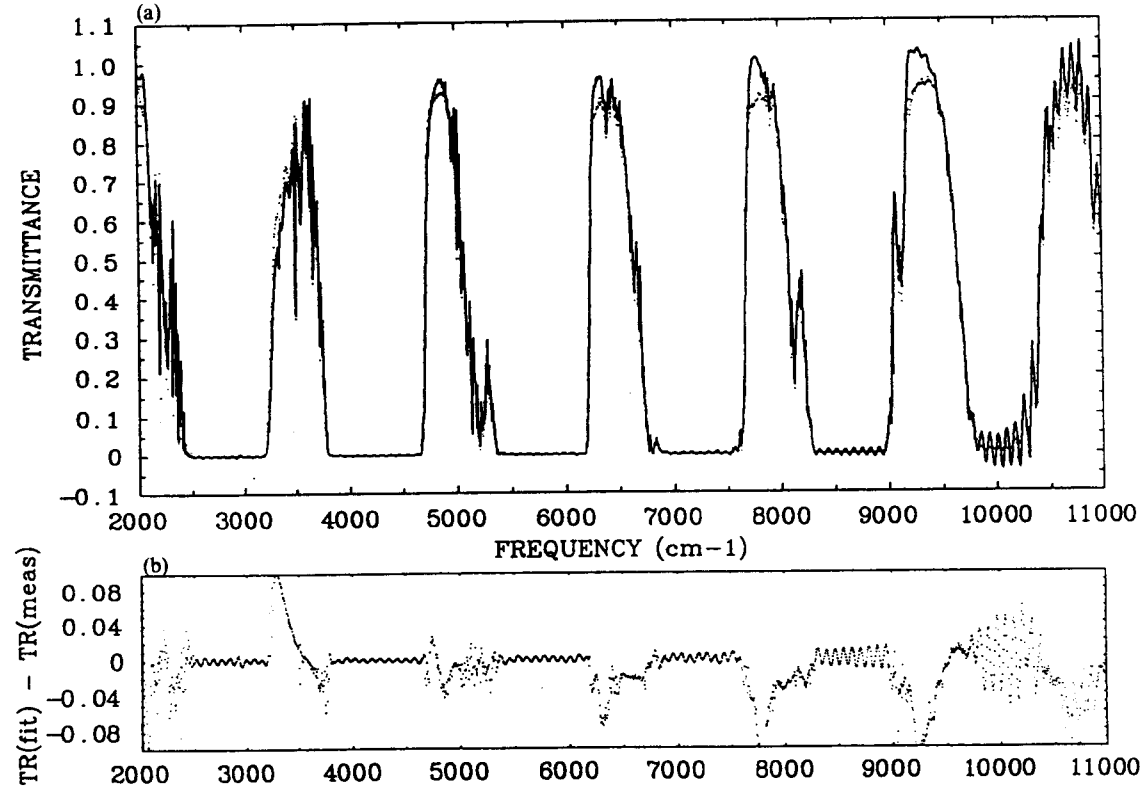

Fig. 7. (a) A strongly absorbing spectrum recorded at 206.0 K, 0.9361 bar, 416.75 m, and 510.5 m-amagat CH_4 (——) and the Goody–Voigt fit to this spectrum (· · · ·). (b) The difference between these two spectra.

exceptions are some points near 3000 cm^{-1} which are poorly fitted due to contamination by pump oil and the presence of the sharp, strongly absorbing Q branch of the ν_3 band of CH_4, and points at the edges of absorption bands ($\sim$3200, 6300, 7700, and 9100 cm^{-1}) where the transmittance drops sharply and the assumption of statistically similar intervals on either side of the fitted interval, implicit in the derivation of the random band models, is no longer valid. However, even in these regions, σ remains $\leqslant 0.035$ for the fits with the Goody–Voigt and Malkmus–Voigt models.

Further insight into the deviation between the fitted models and the original spectra is gained by using a fitted model to generate synthetic spectra for the experimental conditions and comparing these spectra with the original measured spectra. This was carried out for all 108 of the quartz–halogen self-broadened CH_4 spectra, using the fit with Goody–Voigt model. Three such plots are presented in Figs. 6–8. Because these plots are of quartz–halogen spectra, they include the Goody–Voigt fit over the entire 2000–11000 cm^{-1} quartz–halogen spectral range, showing the poor quality of the measured transmittance and therefore of the band-model fit below 2500 cm^{-1} (for which spectral region the globar spectra were used in the fitting) and above 9500 cm^{-1}.

The first plot, Fig. 6, illustrates the fit to a weakly absorbing spectrum which is badly affected by the broad ice ripple and by the ice absorption at 3000–5000 cm^{-1}. This shows how the ripple is eliminated by the band model, and how the model has difficulty in fitting the ice absorption, with the difference between the fitted and measured transmittance (hereafter, $\Delta\bar{\tau}$) obviously being due to errors in the latter. The second plot, Fig. 7, illustrates the fit to a strongly absorbing spectrum which was corrected by scaling to match the globar transmittance and is badly affected by a sloping ratio, and possibly also by the ice ripple. As a result, the windows at 4870, 6450, 7780, 9300, and 10700 cm^{-1} all have anomalously high measured transmittances. For three of these bands, the apparent "transmittance" is greater than 1, however, the fitting procedure ignores any "transmittances" which are less than 0 or greater than 1. The large values of $\Delta\bar{\tau}$ in these regions are thus again due to errors in the measured spectrum. Figure 7 also shows how the 80 cm^{-1} channelling is effectively ignored by the band model, being completely absent in the fitted spectrum, and how

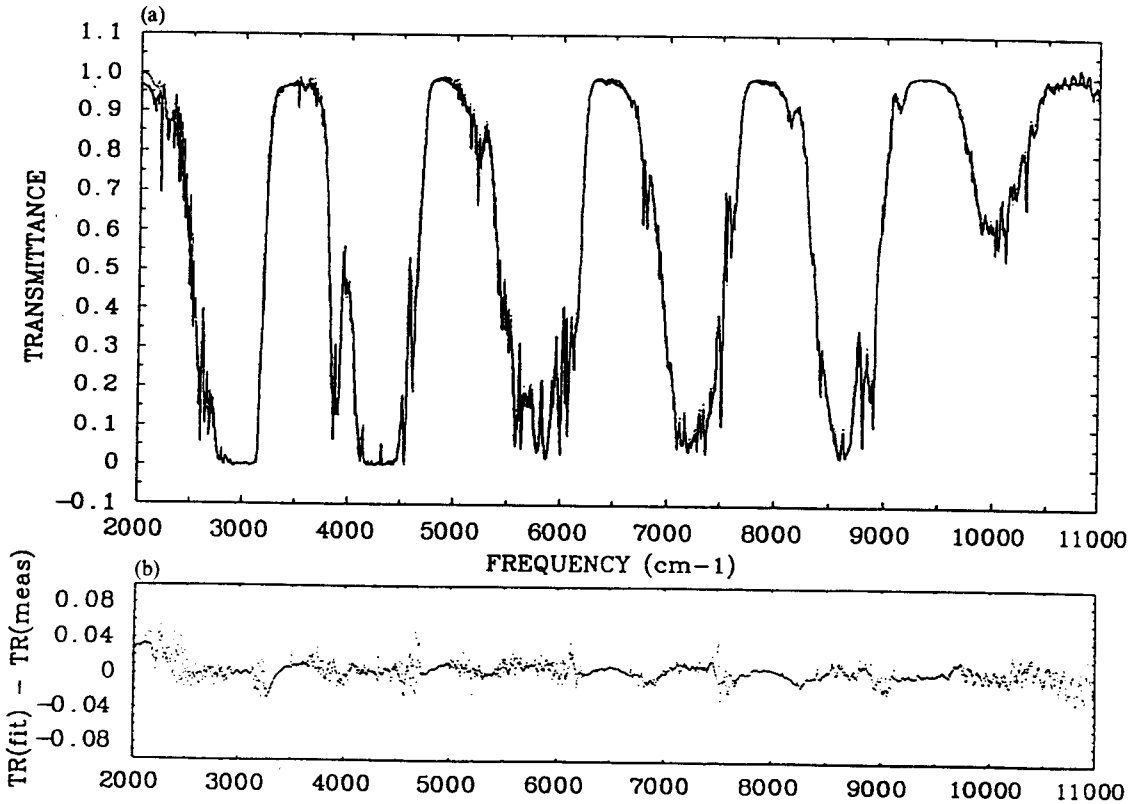

Fig. 8. (a) A spectrum of intermediate absorption recorded at 243.3 K, 0.06851 bar, 512.75 m, and 38.92 m-amagat CH_4 (——) and the Goody–Voigt fit to this spectrum (· · · ·). (b) The difference between these two spectra.

the model has difficulty fitting the high frequency edges of the bands. The third plot in this series, Fig. 8, shows the fit to a spectrum of intermediate absorption, which is essentially free of the ice ripple, the 3000–3500 cm^{-1} ice absorption, the sloping ratio, the 80 cm^{-1} channelling, and the sharp band edges seen in the previous two plots. As a result, the match between the original spectrum and the synthetic Goody–Voigt spectrum is much better than it was for either of the two previous cases.

Also of interest is how the fitted band models and the available CH_4 line data compare. For this purpose, the GENLN2 line-by-line program was used to generate synthetic spectra for the laboratory paths of the measured spectra shown in Figs. 6–8. The HITRAN 1991 database[6] became available just as the present study was being completed and so it was used in these calculations. In Fig. 9, the three line-by-line spectra are superimposed on spectra calculated for the same conditions using the fit with the Goody–Voigt model. In these plots, the GENLN2 absorptions are consistently weaker than those of the Goody–Voigt model, most probably due to missing line data, as the Goody–Voigt fit has already been shown to reproduce the three measured CH_4 spectra reasonably well. The line-by-line and band model spectra show the best agreement [within 0.05, 0.15, and 0.10 in transmittance for Figs. 9(a), 9(b), and 9(c), respectively] in the region below 3255 cm^{-1}, where the greatest number of CH_4 lines in the HITRAN database are found. As expected, poorer agreement is obtained in the 4300 and 5800 cm^{-1} bands, where the CH_4 line data is known to be inadequate. Finally, Fig. 9 clearly reveals the lack of line data for CH_4 in the weakly absorbing 3200–3700 and 4700–5500 cm^{-1} regions, where there are obviously CH_4 absorptions which will be important at Jovian abundances, but no available line parameters, even on the most recently compiled database.

For the work reviewed in Sec. 1, assessment of the quality of band-model fits to experimental CH_4 data, if provided at all, is often inconsistent from one work to another, making it difficult to compare with the results of this work. Only Calcutt[40] provides a similar interval-by-interval estimate of the deviation between the fitted and measured transmittances, but these are only indirectly relevant, as they are expressed as the mean deviation rather than the r.m.s. deviation, for fits in wavelength rather than frequency space, and for individual fits at three temperatures rather than a single fit to data at all three temperatures. However, as in the present study, the Goody–Voigt model was found to provide a better fit than the Goody–Lorentz model, although both the Zachor–King and Smith models provided better fits than the Goody–Voigt model.

Of the various other near-infrared CH_4 band-modelling studies discussed above, only a few include brief discussions of the fit quality. Cruikshank and Silvaggio,[73] who fitted the 273 K CH_4 spectra of Silvaggio[74] at 100 cm^{-1} intervals from 4000 to 4800 cm^{-1} using the Goody–Voigt band model, estimated the goodness of their fit with a reduced χ^2 test, replacing N in Eq. (21) with $N-3$. Their final error estimate was equivalent to $\sigma \leqslant 0.002$ in transmittance. This deviation is significantly better than the values obtained in the present study, and may be attributed to three factors. The first is the fact that the spectra of Silvaggio[74] were recorded over a smaller range of laboratory conditions, with a single temperature, pressures of only 0.0013–0.13 bar, and path-lengths of 3.31–36.75 m, therefore resulting in a smaller range of transmittances to be fitted at each frequency. The second factor, related to the first, is that the spectra were fitted at one temperature with no temperature dependence necessary in the model. The third factor is the larger fitting interval, which may smooth out fluctuations and by increasing the number of lines in an interval may give a better approximation of the statistical distribution assumed by the Goody band model. However, similar values of 0–0.003 for $\Delta\bar{\tau}$ in the 10 cm^{-1} interval centred on 4305 cm^{-1} were obtained by Silvaggio[39] (p. 592) using the same 273 K CH_4 spectra and again fitting the Goody–Voigt model. In contrast, a value of $\sigma = 0.022$ was obtained for 4305 cm^{-1} using the Goody–Voigt model in this present work. Unfortunately, Silvaggio[39] only presented values of $\bar{\tau}_{\text{measured}}$ and $\bar{\tau}_{\text{fitted}}$ for this single frequency interval, so no further comparison with his 10 cm^{-1} fits was possible.

A full quantitative assessment of the near-infrared band-model analysis of CH_4 performed by Giver et al[41,42] is also lacking. In this extensive study, the CH_4 spectra were fitted with the Malkmus–Voigt band model at three individual temperatures. The only published data providing any indication of the quality of the fits is a list of the measured and fitted transmittances for the 10 cm^{-1} interval centred on 4650 cm^{-1}, given by Giver et al.[55] Using these values, it was possible

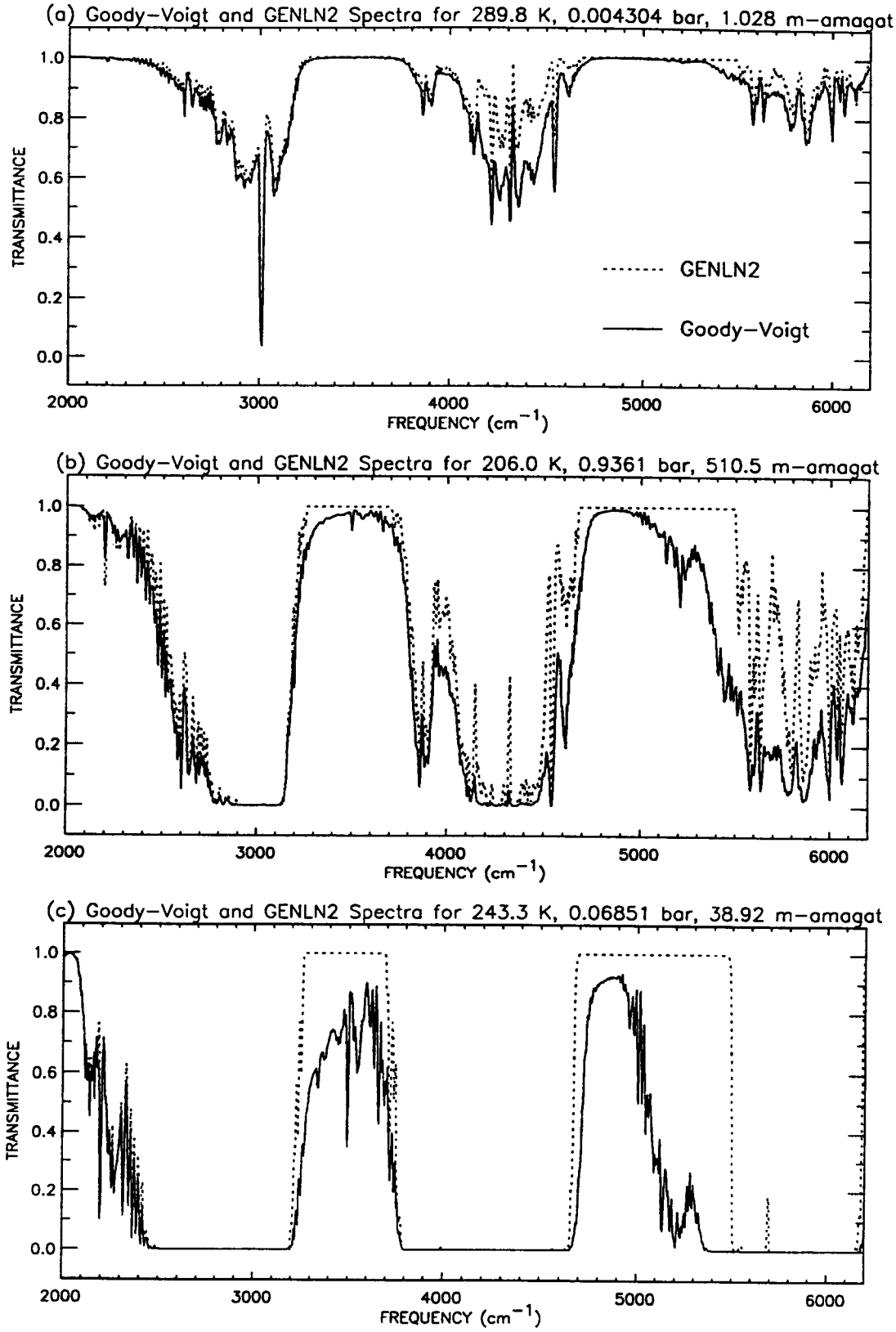

Fig. 9. Synthetic spectra generated for the laboratory paths of Figs. 6, 7, and 8, [(a), (b), and (c) respectively] using both the Goody–Voigt model (fitted to the self-broadened CH_4 spectra) and the GENLN2 line-by-line model with CH_4 line data from the HITRAN 1991 database.

to calculate the r.m.s. residual error for the fit at each temperature, yielding 0.016, 0.015, and 0.008, for the 295, 188, and 112 K fits, respectively. For comparison, the Malkmus–Voigt fit to all three temperatures performed in the present study yielded a value of 0.014 for σ at 4650 cm^{-1}. The similarity of the results thus provides some confidence in the fits of the present study. The larger values of σ obtained by Giver et al[55] compared to Cruikshank and Silvaggio[73] above may also be due to the greater range of pressures (0.0020–12.4 bar), pathlengths (3–61 m) and CH_4 abundances (0.0149–192.8 m-amagat) fitted by the former, particularly as the smallest σ, 0.008, was obtained for the 112 K spectra for which the pressure was limited to 0.538 bar.

In the visible band-modelling studies of CH_4 described in Sec. 1, the quality of the fits is usually characterized by an error estimate for the fitted parameters rather than a comparison of the fitted and measured transmittances. Thus, Fink et al[28] and Benner,[54] who used the Goody–Lorentz model, derived standard deviations for their absorption and pressure coefficients and combined these with the errors in the measured spectra, to estimate uncertainties of up to 10% for k_ν and 30% for y_ν. Similar uncertainties of 4–15% for k_ν and 18–31% for y_ν were obtained by Podolak and Giver,[30] for three intervals fitted with the Goody–Lorentz model. If these uncertainties in k_ν and y_ν are converted to uncertainties in transmittance, values of approx. 0.01 in transmittance are obtained, comparable to σ in the present work.

7. RESULTS FOR THE H_2-BROADENED CH_4

Having found that the Goody–Voigt and Malkmus–Voigt models provided the best fits to the self-broadened CH_4 spectra, these two models were subsequently used to fit the combined set of both the 108 self-broadened CH_4 spectra and the 117 H_2-broadened CH_4 spectra. Two independent fits were again performed, one for the globar spectra and one for the quartz–halogen spectra, with the globar fits again adopted from 2000–3900 cm^{-1} and the quartz–halogen fits adopted for 3905–9500 cm^{-1}.

As was the case for the self-broadened CH_4 spectra, the combined set of self- and H_2-broadened CH_4 spectra were fitted using sequences of progressively more complex models. These began with the one-parameter Weak Limit model followed by the two-parameter Weak Limit model with temperature dependence, initializing $k_\nu(T_0)$ and E_l as described in Sec. 6. The resulting optimized values of these parameters were then used to initialize the parameters for the temperature-dependent Goody–Lorentz and Malkmus–Lorentz models.

For the next fit in both sequences, a new parameter, the ratio of self-to-foreign broadening, was introduced into the Goody–Lorentz and Malkmus–Lorentz models in order to account for the modification of the CH_4 line width due to the presence of H_2. This ratio, SFB, is defined as the ratio of the self-broadened Lorentz half-width to the foreign-broadened Lorentz half-width. It appears in the equation for α_L, which can be expressed in terms of the CH_4-to-total mixing ratio, q, and the total pressure, P, as

$$\alpha_L(P, T) = \alpha_L^0 \frac{P}{P_0}\sqrt{\frac{T_0}{T}}\left[q + \frac{(1-q)}{\mathrm{SFB}}\right]. \tag{22}$$

In all following discussions, SFB will be taken to be the self-to-foreign broadening ratio for CH_4 broadened by H_2. When this expression is introduced into the Goody–Lorentz random band model, $\bar{\tau}$ becomes

$$\bar{\tau}_{\text{Goody–Lorentz}} = \exp\left(-1\Big/\sqrt{\frac{1}{(k_\nu U)^2} + \frac{1}{\pi k_\nu y_\nu UP[q + (1-q)/\mathrm{SFB}]\sqrt{T_0/T}}}\right). \tag{23}$$

Similarly, the Malkmus–Lorentz random band model becomes

$$\bar{\tau}_{\text{Malkmus–Lorentz}} = \exp\left(-1\Big/\left[\frac{1}{2k_\nu U} + \sqrt{\frac{1}{(2k_\nu U)^2} + \frac{1}{\pi k_\nu y_\nu UP[q + (1-q)/\mathrm{SFB}]\sqrt{T_0/T}}}\right]\right). \tag{24}$$

For both models, SFB was initialized to 1, making each model initially the same as the preceding self-broadened model.

Once the Goody–Lorentz and Malkmus–Lorentz models, both with temperature dependence and foreign broadening, had been fitted to all of the self- and H_2-broadened spectra, their final best-fit

parameters provided the initial values for the Goody–Voigt and Malkmus–Voigt models. In addition to the newly introduced parameter SFB, these models were used to fit the same four parameters $k_v(T_0)$, E_l, δ/α_D^0, and α_L^0/α_D^0 that were fitted to the self-broadened CH_4 spectra, with all four parameters being initialized as described above. The ratio of self-to-foreign broadening was again introduced into these models through the definition of α_L, in this case appearing in the definition of y in $V(x, y)$:

$$y = \frac{\alpha_L}{\alpha_D} = \left(\alpha_L^0 \frac{P}{P_0}\sqrt{\frac{T_0}{T}}\left[q + \frac{(1-q)}{\text{SFB}}\right]\right)\left(\frac{1}{\alpha_D^0\sqrt{T}}\right) = \frac{\alpha_L^0}{\alpha_D^0}\frac{P}{P_0}\frac{\sqrt{T_0}}{T}\left[q + \frac{(1-q)}{\text{SFB}}\right]. \tag{25}$$

For these models, SFB was initialized directly from the best-fit values obtained with the preceding fits with the Lorentz lineshape.

The combined set of 225 self- and H_2-broadened CH_4 spectra was thus fitted with a total of eight models, culminating in the Goody–Voigt and Malkmus–Voigt models, both of which included both temperature dependence and foreign broadening. Following the methods used with the self-broadened CH_4 spectra, the r.m.s. residual error, σ, was again used to quantify how well the fitted models matched the original measured transmittances. The first two fits, using the Weak Limit model and the Weak Limit model with temperature dependence, provided poor agreement with the data, particularly in the bands. This is not surprising as neither model includes pressure dependence or foreign broadening.

In the three models subsequently fitted in the Goody sequence, the addition of the term for strong absorption in the Goody–Lorentz model provided a more significant reduction in σ. The addition of the self-to-foreign broadening ratio to the Goody–Lorentz model further improved the fit, but both of the Goody–Lorentz models had trouble fitting points in the 3000 and 4300 cm^{-1} bands. With the introduction of the Voigt lineshape, the large values of σ found in these regions were reduced for all but a few points. With the exception of these points, which correspond to pump-oil contamination and peaks of absorption, σ for the Goody–Voigt fit is less than 0.04 throughout the 2000–9500 cm^{-1} spectral range, and less than 0.03 for all frequencies outside the 3000 and 4300 cm^{-1} bands. This is seen in Fig. 10(a). These values are considered acceptable as they are again comparable to the measurement errors in the spectra, the estimate for the error due to sloping ratios being 0.026 for the combined set of self- and H_2-broadened CH_4 spectra, and the estimate for the error due to the ice ripple being 0.015.

A similar improvement in σ is seen in the progression from the Malkmus–Lorentz fit to the Malkmus–Lorentz fit with SFB to the Malkmus–Voigt fit with SFB. The major exceptions to this are the 3000 and 4300 cm^{-1} bands, where the large values of σ obtained with the Malkmus–Lorentz models were not reduced by the Malkmus–Voigt model. For frequencies from 2785 to 3145 cm^{-1} and 4125 to 4545 cm^{-1}, σ is >0.10, and for all of these points, the Numerical Algorithms least squares minimization routine warned of a convergence problem. This problem was reduced by refitting the Malkmus–Voigt model with SFB to the combined set of self- and H_2-broadened CH_4 spectra, using the Malkmus–Voigt fit to the self-broadened CH_4 spectra [see Fig. 5(f)] to initialize the parameters. With this alternative method of initialization, the convergence of the fit improved in both the 3000 and 4300 cm^{-1} bands, as seen in Fig. 10(b).

This same method of initialization was also tested for the Goody–Voigt model, using the Goody–Voigt parameters fitted to the self-broadened CH_4 spectra to initialize the parameters in the Goody–Voigt model with SFB. However, in this case, the resulting r.m.s. residual error differed little from that for the Goody–Voigt model fitted using the progression, in fact being slightly worse (by <0.02) in the 3000 cm^{-1} region. The two best fits to the combined set of self- and H_2-broadened CH_4 spectra were therefore obtained with the Goody–Voigt model fitted using the progression of models, and with the Malkmus–Voigt model refitted from the Malkmus–Voigt fit to the self-broadened CH_4 spectra. As was the case for the self-broadened CH_4 spectra, σ is generally similar for these two models, except in the 3000 cm^{-1} band, where the Goody–Voigt model provides a closer fit to the original spectra. Elsewhere throughout the 2000–9500 cm^{-1} range, σ for the two fits agrees to within 0.005 except for a few scattered points. Given these results, the fit with the Goody–Voigt model was considered marginally better, and is therefore used in subsequent calculations.

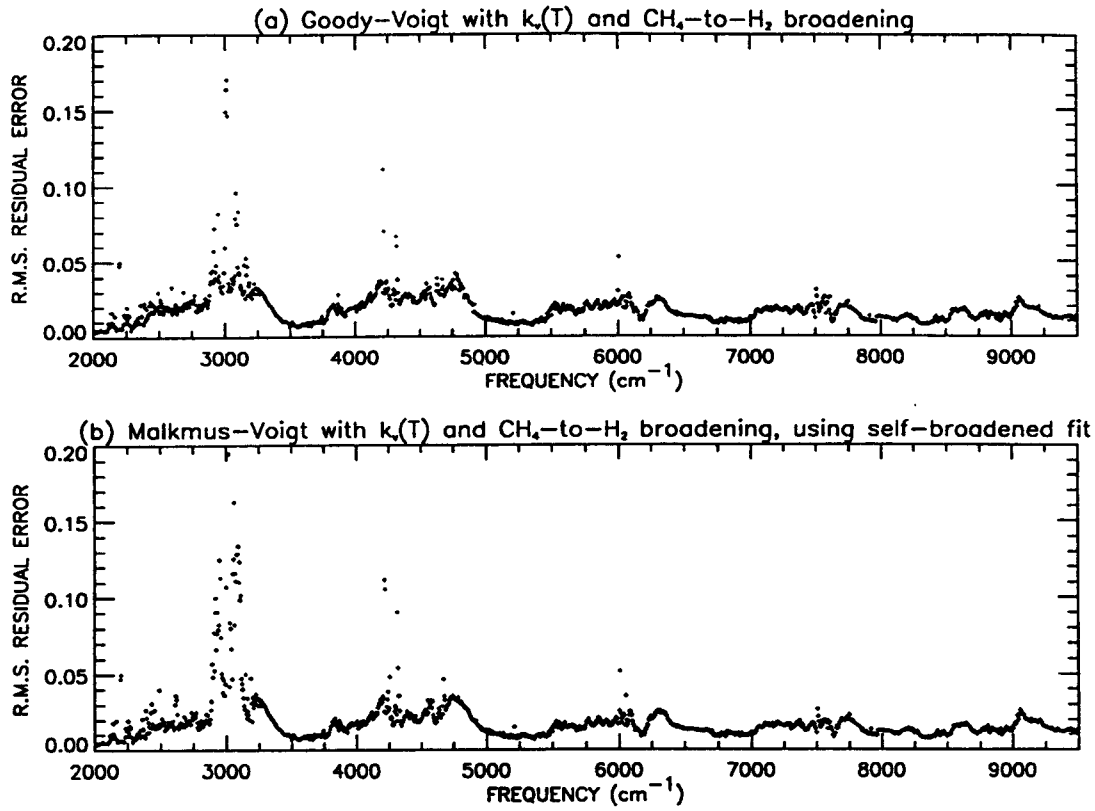

Fig. 10. The r.m.s. residual error in transmittance for the best (a) Goody–Voigt and (b) Malkmus–Voigt fits to all of the self- and H_2-broadened CH_4 spectra.

A further assessment of the quality of the Goody–Voigt fit to all of the spectra was made by comparing σ for this fit with that of the Goody–Voigt fit to the self-broadened spectra. This revealed that σ agrees to within 0.01 between the two fits except in the 3000 and 4300 cm^{-1} bands where σ is as much as 0.03 larger for the Goody–Voigt fit to all of the spectra. Thus, in these two bands, both the Goody–Voigt and the Malkmus–Voigt models are unable to provide as good a fit to all of the spectra as they do to only the self-broadened spectra. The poorer fits in these bands appear to be partly caused by contaminating absorptions, pump oil and ice absorption in the 3000 cm^{-1} band, and by H_2 absorption in the 4300 cm^{-1} band. The latter is seen in Fig. 11, where a synthetic spectrum calculated with the Goody–Voigt fit to all of the spectra is overlaid on a weakly absorbing quartz–halogen H_2-broadened CH_4 spectrum. This spectrum is for a total pressure of 0.8030 bar and a pathlength of 512.75 m, clearly showing the H_2 absorption which contributes to the poor quality of the fit in the region from 3700 to 5600 cm^{-1}. Similar figures, plotted for all of the H_2-broadened spectra fitted with the Goody–Voigt model, also suggest that in both the 3000 and 4300 cm^{-1} bands, the discrepancy between the fitted and measured transmittances is partly caused by the limitations of the band models, which have difficulty fitting the rapidly varying values of transmittance present in these regions.

Thus, although the introduction of the self-to-foreign broadening ratio accounted for the effects of H_2-broadening over most of the 2000–9500 cm^{-1} spectral range, it was unable to fully account for the strong absorptions in the 3000 and 4300 cm^{-1} bands. This may partly be due to the implicit assumption that the exponent of temperature dependence of the Lorentz half-width, n, is the same for both self- and H_2-broadened CH_4 lines, which implies that SFB, as defined in Eq. (22), is weakly temperature dependent. This has been demonstrated by Varanasi et al,[75] whose measurements of self- and H_2-broadened CH_4 line widths yielded values of 1.11, 1.27, and 1.52 for SFB at 295, 250, and 190 K. However, with temperature dependence fitted elsewhere in the model and the number of fitted parameters already being five, no attempt was made to fit n or any temperature dependence of SFB. In conclusion, despite the difficulty in fitting the 3000 and 4300 cm^{-1} bands, σ for the

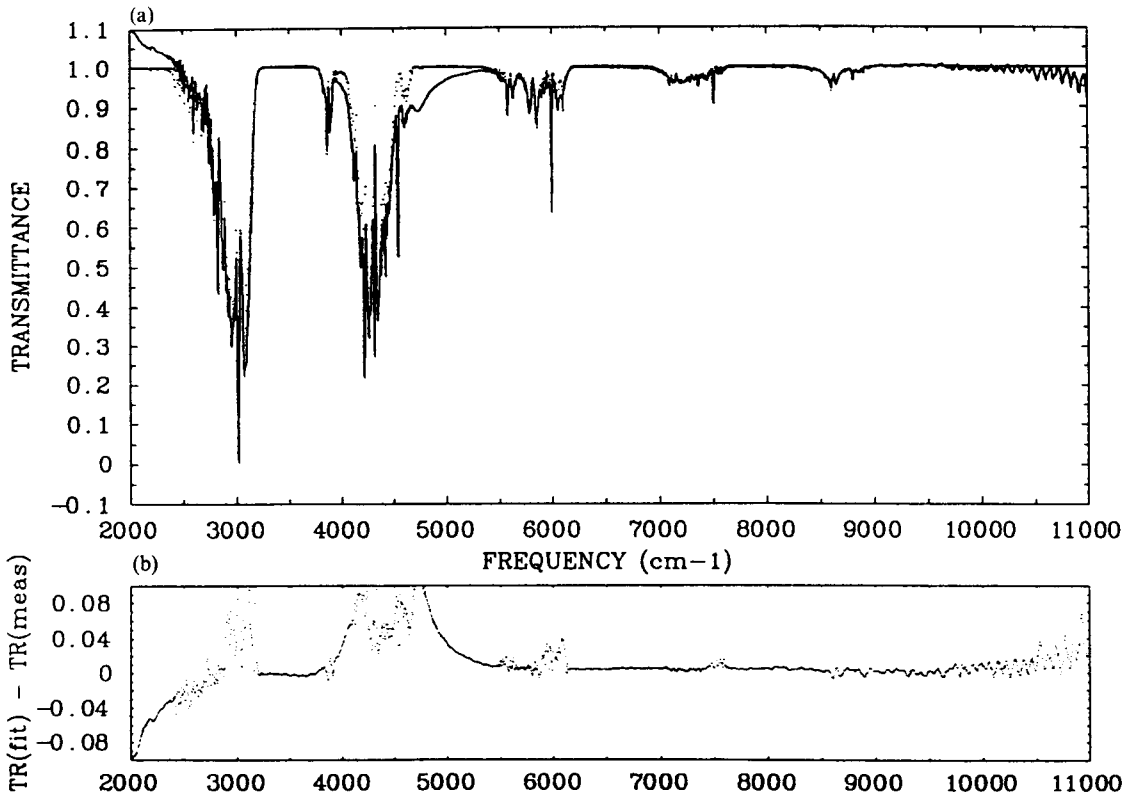

Fig. 11. (a) A H_2-broadened CH_4 spectrum recorded at 240.6 K, 0.8033 bar total pressure, 512.75 m, 0.1552 m-amagat CH_4, and a mixing ratio of 3.362×10^{-4} (——) and the Goody–Voigt fit [with $k_\nu(T)$ and SFB] to this spectrum (· · · ·). (b) The difference between these two spectra.

Goody–Voigt fit to the combined set of self- and H_2-broadened spectra is less than 0.04 for all but a few points, even in these two bands, and lies between 0.005 and 0.03 for all frequencies outside these regions.

Figure 12 shows the parameters that were obtained with the Goody–Voigt fit to the combined set of self- and H_2-broadened CH_4 spectra. In Figs. 12(a)–12(e), the five fitted parameters, $k_\nu(T_0)$, E_l, δ/α_D^0, α_L^0/α_D^0, and SFB, are plotted, while Figs. 12(f)–12(h) show the three derived parameters, δ, α_L^0, and y_ν. Similar plots and discussion of the parameters obtained with the Goody–Voigt and Malkmus–Voigt fits to the self-broadened CH_4 spectra can be found in Ref. 13. Because the Goody and Malkmus random band models are physically based, the parameters fitted with these models have a more meaningful physical interpretation than do the parameters fitted by the generalized and empirical models. However, even when a parameter has a physical definition, some caution is necessary in its interpretation, since in practice, it is simply a variable used to optimize a fit. Even the physically based models are unlikely to provide a completely accurate representation of the CH_4 transmittance, and to compensate for this fact while attempting to obtain the closest match to the measured transmittances, the parameters may vary in a physically unrealistic manner.

For the Goody–Voigt fit to all of the spectra, the absorption coefficient, $k_\nu(T_0)$, ranges between 1.5×10^{-5} and 12.5 m-amagat, and as expected, is largest in the CH_4 band centres. The lower state energy, E_l, is seen to have a jagged appearance on a finer scale than the band structure, probably indicative of the differing temperature dependence of rotational lines within the bands. The values of E_l, ranging from 84 to 1280 cm^{-1}, are physically reasonable, as the HITRAN 1991 database lists values between 10 and 2200 cm^{-1} for CH_4. The next parameter to be plotted is δ/α_D^0, from which the mean line spacing, δ, can be derived for each frequency interval using Eq. (12). The result of this calculation is presented in Fig. 12(f). The values of δ vary between approx. 0.001 and 10 cm^{-1} for the Goody–Voigt fit to all of the spectra, decreasing in the band centres where the lines are more closely spaced. The fitted parameter α_L^0/α_D^0 can be used to derive the self-broadened Lorentz half-width, α_L^0, (at $T_0 = 296$ K, $P_0 = 1.01325$ bar). This is plotted in Fig. 12(g), where it is seen to

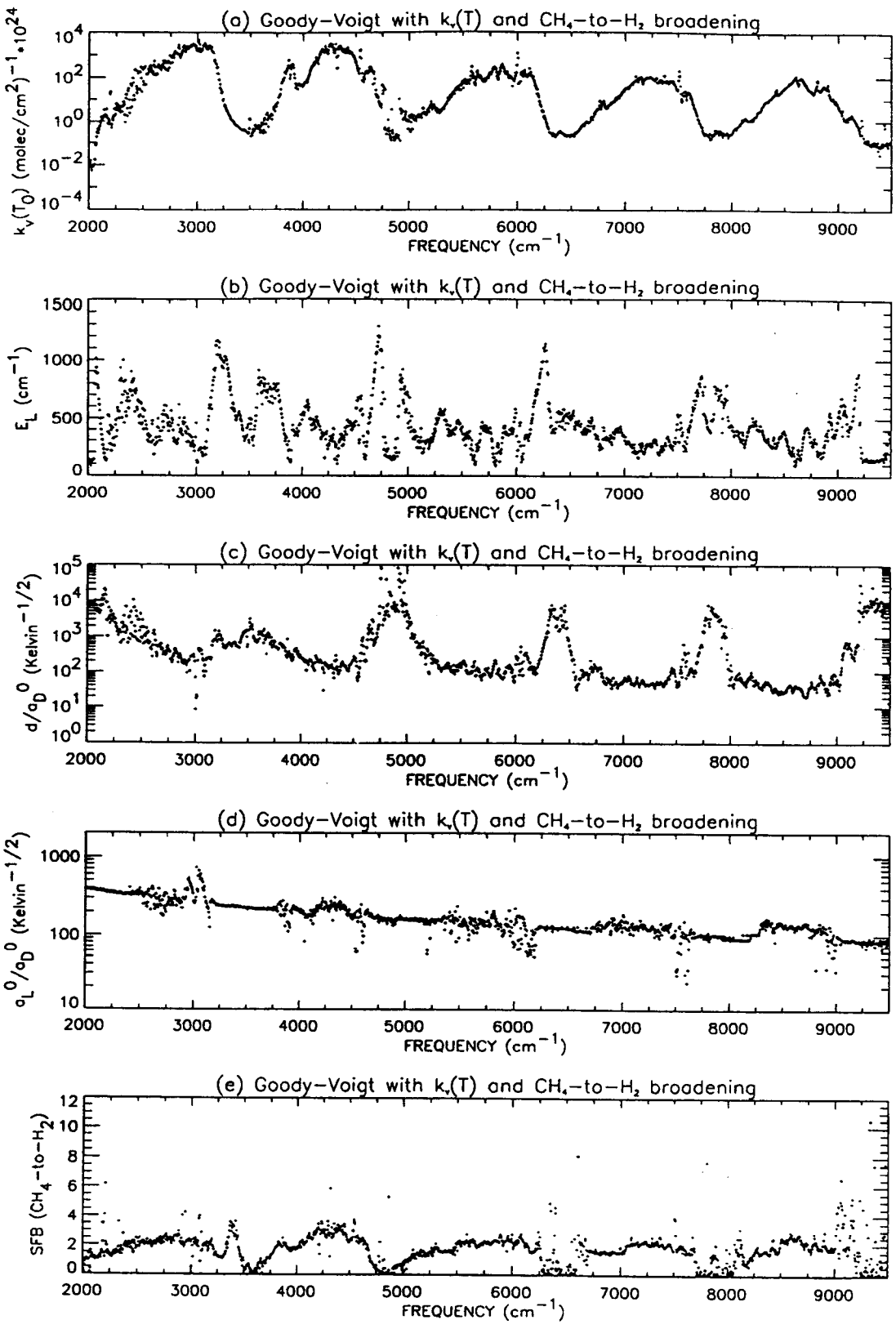

Fig. 12. *Caption on opposite page.*

Table 2. The average self- and H_2-broadened CH_4 Lorentz half-widths at 295 K and 1.01325 bar, along with the resulting self-to-foreign broadening ratio for H_2, as derived from measurements by Ballard and Johnston,[76] Varanasi and Chudamani,[77] Varanasi et al,[75] Rank et al,[78] Margolis,[79] and Fox and Jennings.[80]

BAND (cm^{-1})	No. of LINES in CALC.	AVG. CH_4 α_L^0 (cm^{-1})	AVG. H_2 α_L^0 (cm^{-1})	AVG. *SFB*	REFS.
ν_4 (1332–1348)	6	0.0765	0.0592	1.29	76, 77
ν_3 (3028–3049)	3	0.083	0.075	1.11	75
$2\nu_3$ (~ 6000)	4	0.0870	0.0749	1.16	78
$3\nu_3$ (9080–9130)	18	0.0804	0.0727	1.11	79, 80

a value of 0.03 cm^{-1} ± 50% for the H_2-broadened Lorentz half-width at 1 atm and 273 K using the Goody–Voigt model to fit transmittances at 100 cm^{-1} intervals over 4100–4700 cm^{-1}, equivalent to a value of 2.8 for SFB, while Calcutt[40] obtained a mean value of 1.4 ± 20% for SFB using the Goody–Lorentz model. In addition, the CH_4-to-H_2 broadening ratio has also been calculated for some specific CH_4 lines, using self- and H_2-broadened line widths available in the literature. The results, given in Table 2, show SFB to be fairly constant, varying between only 1.11 and 1.29, thus at the lower end of the fitted values.

In theory, if the effects of H_2 broadening were entirely accounted for by the self-to-foreign broadening ratio, then the other CH_4 parameters fitted to the combined set of self- and H_2-broadened spectra would have the same values of those fitted to the self-broadened CH_4 spectra only. However, this was not the case. For each frequency interval, the set of fitted parameters, $k_\nu(T_0)$, E_1, δ/α_D^0, and α_L^0/α_D^0, is not unique. Despite using the same fundamental band model and the same initialization, different values of these parameters are obtained when the H_2-broadened spectra are fitted along with the self-broadened spectra. Differences in one parameter are compensated for by differences in other parameters. As an additional test, both the Goody–Voigt and Malkmus–Voigt models were refitted to the combined set of self- and H_2-broadened CH_4 spectra, fixing the parameters to the best-fit values obtained in the respective fits to the self-broadened CH_4 spectra, and allowing only SFB to vary. In both cases, the r.m.s. residual error was significantly worse than when all of the parameters were refitted, thus indicating that the variation in SFB alone was unable to deal with the H_2-broadening. This again emphasizes the fact that a set of fitted parameters, even when obtained with a physically based random band model, is simply that which optimizes the fit to a particular set of measured transmittances. However, although the absolute magnitudes of the fitted parameters may not be strictly accurate, the band models are behaving well in the sense that the structure in the plotted parameters is as would be expected.

In order to allow calculation of CH_4 transmittance, the band model parameters fitted to the combined set of self- and H_2 broadened CH_4 spectra using the Goody–Voigt model are listed in Table 3. The equation for transmittance is Eq. (9), where y is given by Eq. (25) and the laboratory conditions T, P, and U are in units of K, bar, and molecules/cm^2, respectively. The first column of this table is ν, the midpoint of each 10 cm^{-1} fitting interval. The second column is σ, the r.m.s. residual error in transmittance. Columns three to seven are the five fitted parameters $k_\nu(T_0)$, δ/α_D^0, α_L^0/α_D^0, E_1, and SFB, which are plotted in Figs. 12(a)–12(e). Similar sets of parameters for all of the other fits performed in this work, as well as the self- and H_2-broadened CH_4 spectra, are available from the authors upon request.

8. APPLICATIONS TO JUPITER

Application of the band models to Jovian conditions involves some extrapolation in temperature, pressure, and CH_4 abundance beyond the conditions that were achievable in the laboratory. In order to obtain an estimate of the probable errors introduced by this extrapolation, three comparisons were performed. In the first, the spectra generated with the Goody–Voigt model were compared to those generated with the Malkmus–Voigt model for a variety of Jovian paths, providing a test of the extent to which the physically based band models give reliable extrapolations. In the second, the spectra generated with the Goody–Voigt model were compared with synthetic line-by-line spectra generated for the same Jovian paths in those regions where line data were available, allowing an estimate of how well the best of the models compares to an exact calculation of

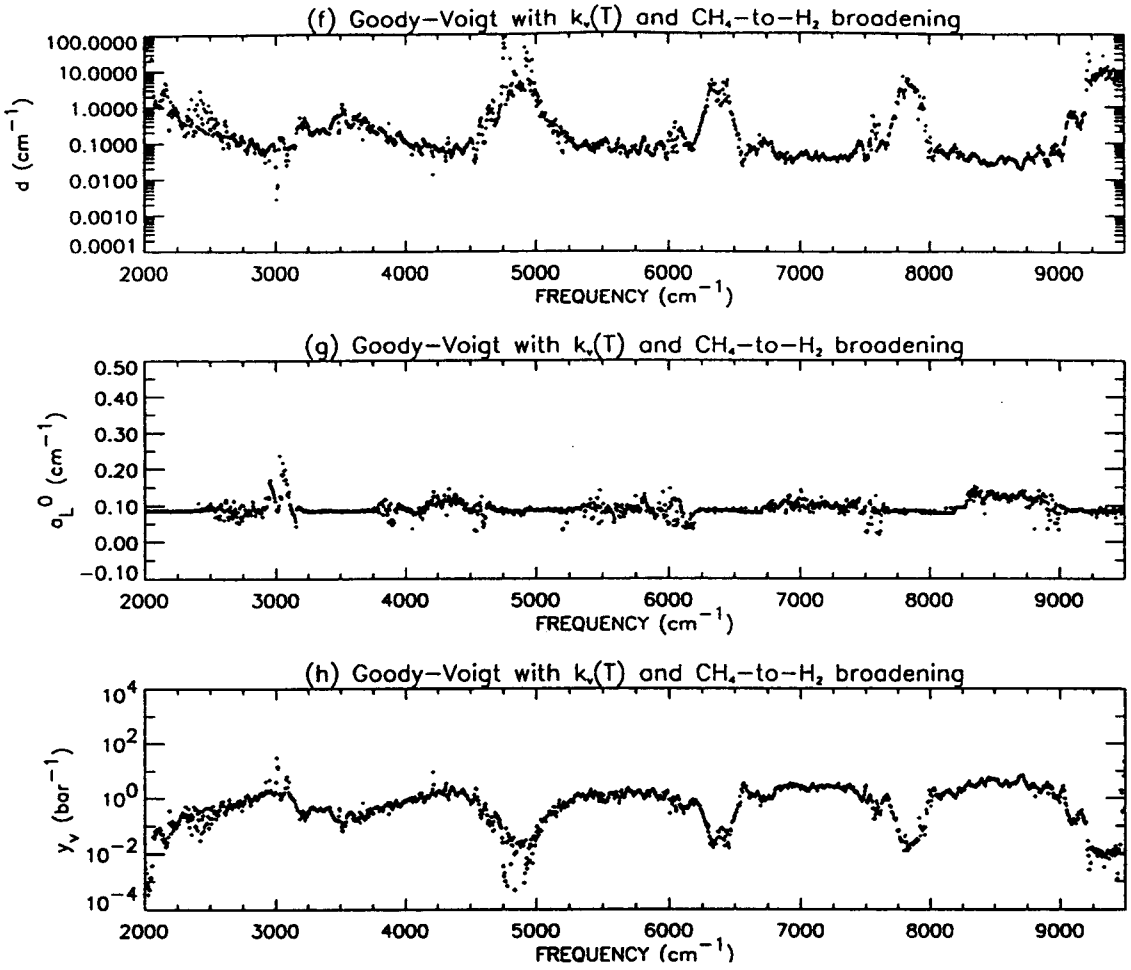

Fig. 12. The parameters fitted to all of the self- and H_2-broadened CH_4 spectra using the Goody–Voigt model with $k_v(T)$ and SFB.

vary little from its initial value of 0.085 cm^{-1} in the window regions, and to vary between 0.019 and 0.24 cm^{-1} in the bands. The pressure coefficient, y_v, plotted in Fig. 12(h), has been derived using the relation

$$y_v = \frac{\alpha_L^0}{P_0 \delta} = \frac{1}{P_0} \frac{\alpha_L^0}{\alpha_D^0} \frac{\alpha_D^0}{\delta}. \tag{26}$$

The values of y_v generally lie between 0.01 and 10 bar^{-1}, with $y_v > 1$, as found in the band centres, implying that the line half-width is greater than the mean line spacing, resulting in considerable line overlap and a pseudo-continuous appearance. A larger pressure coefficient implies that the transmittance is only weakly dependent on pressure, and so it is in the window regions that the pressure dependence is greatest.

The self-to-foreign broadening ratio fitted by the Goody–Voigt model is plotted in Fig. 12(e). It varies between extremes of 0.125×10^{-4} and 10.5, but lies predominantly in the range from 1 to 3, and is smallest in the window regions where there is minimal absorption due to the smaller CH_4 abundances of the H_2-broadened spectra (less than 78 m-amagat). As SFB tends towards 0, the expression for the transmittance [e.g., Eq. (23)] tends towards the expression for the weak limit of absorption. The lowest values of SFB are therefore more a reflection of the random noise on the data than they are physically meaningful values. This may introduce systematic errors into the other fit parameters in these regions and so ideally, it might be better to fit regions of weak absorption with a smaller number of parameters. However, in this work the same set of parameters was used in all regions. In comparison with the values of SFB fitted in this work, Silvaggio[39] derived

Table 3. The band model parameters fitted to the combined set of self- and H_2-broadened CH_4 spectra using the Goody–Voigt random band model.

ν (cm^{-1})	RMS ERROR σ	$k_\nu(T_0) \times 10^{24}$ $(molec/cm^2)^{-1}$	δ/α_D^0 $(K^{1/2})$	α_L^0/α_D^0 $(K^{1/2})$	E_l (cm^{-1})	*SFB*
2000.00	0.42102E-02	0.99287E-02	0.16243E+05	0.39578E+03	0.14040E+03	0.26620E+00
2005.00	0.45869E-02	0.12914E-01	0.76221E+05	0.39480E+03	0.13071E+03	0.98872E-01
2010.00	0.42509E-02	0.12206E-01	0.12728E+06	0.39381E+03	0.13076E+03	0.11428E+00
2015.00	0.38466E-02	0.96938E-02	0.41661E+06	0.39284E+03	0.13010E+03	0.59322E+00
2020.00	0.40933E-02	0.15260E-01	0.19317E+06	0.39187E+03	0.13000E+03	0.83532E+00
2025.00	0.40477E-02	0.74267E-02	0.52172E+06	0.39090E+03	0.11007E+03	0.93997E+00
2030.00	0.41470E-02	0.54166E-02	0.11486E+07	0.38993E+03	0.84056E+02	0.93675E+00
2035.00	0.43818E-02	0.84263E-02	0.66031E+06	0.38898E+03	0.11534E+03	0.10721E+01
2040.00	0.45015E-02	0.79847E-02	0.75680E+06	0.38802E+03	0.12179E+03	0.99312E+00
2045.00	0.47248E-02	0.95874E-02	0.28894E+06	0.38707E+03	0.13133E+03	0.97990E+00
2050.00	0.47868E-02	0.10388E-01	0.27414E+06	0.38613E+03	0.13024E+03	0.92488E+00
2055.00	0.56364E-02	0.17142E-01	0.10271E+06	0.38519E+03	0.14010E+03	0.13664E+01
2060.00	0.56168E-02	0.16133E-01	0.99070E+05	0.38426E+03	0.13559E+03	0.13969E+01
2065.00	0.48436E-02	0.74760E-01	0.89470E+04	0.38476E+03	0.79000E+03	0.12261E+00
2070.00	0.46289E-02	0.89074E-01	0.94037E+04	0.38240E+03	0.89020E+03	0.38026E+00
2075.00	0.45654E-02	0.18796E+00	0.10099E+05	0.38534E+03	0.10153E+04	0.15744E+01
2080.00	0.47181E-02	0.31728E+00	0.56816E+04	0.38443E+03	0.93169E+03	0.11490E+01
2085.00	0.45234E-02	0.27966E+00	0.71945E+04	0.38315E+03	0.88331E+03	0.13544E+01
2090.00	0.47063E-02	0.44411E+00	0.48384E+04	0.37805E+03	0.78315E+03	0.12051E+01
2095.00	0.45976E-02	0.40775E+00	0.56714E+04	0.38325E+03	0.75504E+03	0.10687E+01
2100.00	0.50798E-02	0.60171E+00	0.51994E+04	0.37637E+03	0.65894E+03	0.10431E+01
2105.00	0.44654E-02	0.60588E+00	0.48159E+04	0.37551E+03	0.61346E+03	0.12171E+01
2110.00	0.59136E-02	0.83854E+00	0.52677E+04	0.37614E+03	0.56315E+03	0.10333E+01
2115.00	0.95479E-02	0.15848E+01	0.43433E+04	0.37300E+03	0.49589E+03	0.93817E+00
2120.00	0.70859E-02	0.10857E+01	0.70126E+04	0.37341E+03	0.44732E+03	0.10201E+01
2125.00	0.78116E-02	0.14852E+01	0.49307E+04	0.37227E+03	0.39718E+03	0.10737E+01
2130.00	0.76078E-02	0.13402E+01	0.70537E+04	0.37167E+03	0.35049E+03	0.11022E+01
2135.00	0.97270E-02	0.16981E+01	0.10866E+05	0.37815E+03	0.30441E+03	0.10459E+01
2140.00	0.16516E-01	0.33352E+01	0.73861E+04	0.37001E+03	0.26030E+03	0.97802E+00
2145.00	0.10131E-01	0.19862E+01	0.13656E+05	0.36966E+03	0.22657E+03	0.10985E+01
2150.00	0.91930E-02	0.18833E+01	0.10117E+05	0.36932E+03	0.18816E+03	0.12010E+01
2155.00	0.80645E-02	0.16563E+01	0.10844E+05	0.36749E+03	0.15215E+03	0.12674E+01
2160.00	0.83295E-02	0.19036E+01	0.20635E+05	0.36962E+03	0.13648E+03	0.12226E+01
2165.00	0.14109E-01	0.36398E+01	0.14582E+05	0.37114E+03	0.13279E+03	0.10838E+01
2170.00	0.71262E-02	0.14699E+01	0.19232E+05	0.37424E+03	0.12363E+03	0.13537E+01
2175.00	0.52331E-02	0.78330E+00	0.13749E+05	0.36441E+03	0.14141E+03	0.15990E+01
2180.00	0.64817E-02	0.13515E+01	0.88591E+04	0.36372E+03	0.21953E+03	0.14593E+01
2185.00	0.59425E-02	0.71564E+00	0.27566E+04	0.36092E+03	0.37516E+03	0.21747E+01
2190.00	0.58215E-02	0.10495E+01	0.10029E+04	0.35803E+03	0.52159E+03	0.34756E+01
2195.00	0.47681E-01	0.17510E+02	0.30575E+04	0.36114E+03	0.51125E+03	0.13834E+01
2200.00	0.49770E-01	0.21709E+02	0.62313E+04	0.35413E+03	0.35425E+03	0.11369E+01
2205.00	0.66355E-02	0.72417E+00	0.35568E+04	0.36139E+03	0.27162E+03	0.40747E+01
2210.00	0.62679E-02	0.48847E+00	0.22946E+04	0.35676E+03	0.43261E+03	0.61604E+01
2215.00	0.55486E-02	0.68552E+00	0.36576E+04	0.35645E+03	0.39190E+03	0.21342E+01
2220.00	0.65144E-02	0.13380E+01	0.49219E+04	0.35541E+03	0.21123E+03	0.14556E+01
2225.00	0.58727E-02	0.11199E+01	0.29985E+04	0.35681E+03	0.26225E+03	0.19275E+01
2230.00	0.92401E-02	0.17351E+01	0.26728E+04	0.35390E+03	0.41351E+03	0.15549E+01
2235.00	0.15287E-01	0.37846E+01	0.39278E+04	0.35474E+03	0.31821E+03	0.13366E+01
2240.00	0.13621E-01	0.33964E+01	0.40115E+04	0.35320E+03	0.25312E+03	0.14123E+01
2245.00	0.98133E-02	0.20203E+01	0.33885E+04	0.35681E+03	0.25525E+03	0.13855E+01
2250.00	0.15241E-01	0.40315E+01	0.30718E+04	0.35099E+03	0.32424E+03	0.12233E+01
2255.00	0.20060E-01	0.63038E+01	0.23875E+04	0.34994E+03	0.43813E+03	0.12562E+01
2260.00	0.12178E-01	0.34463E+01	0.30482E+04	0.35776E+03	0.48425E+03	0.13034E+01
2265.00	0.99050E-02	0.31092E+01	0.22233E+04	0.34837E+03	0.33228E+03	0.12588E+01
2270.00	0.14936E-01	0.50571E+01	0.18856E+04	0.34686E+03	0.38445E+03	0.11559E+01
2275.00	0.14279E-01	0.52761E+01	0.17055E+04	0.35556E+03	0.58563E+03	0.12001E+01
2280.00	0.87053E-02	0.35606E+01	0.13469E+04	0.34565E+03	0.55718E+03	0.13840E+01
2285.00	0.48418E-02	0.25976E+01	0.10675E+04	0.34167E+03	0.49692E+03	0.15543E+01
2290.00	0.62132E-02	0.27297E+01	0.12451E+04	0.34137E+03	0.55577E+03	0.13943E+01
2295.00	0.72198E-02	0.46338E+01	0.15145E+04	0.34315E+03	0.82077E+03	0.13201E+01

continued overleaf

Table 3—*continued*

2300.00	0.75760E-02	0.47439E+01	0.15420E+04	0.34252E+03	0.92997E+03	0.13412E+01
2305.00	0.74235E-02	0.28059E+01	0.12718E+04	0.34613E+03	0.83908E+03	0.15001E+01
2310.00	0.74317E-02	0.27914E+01	0.64883E+03	0.33813E+03	0.62775E+03	0.16336E+01
2315.00	0.99125E-02	0.49089E+01	0.66381E+03	0.33859E+03	0.50105E+03	0.14757E+01
2320.00	0.11400E-01	0.78185E+01	0.12921E+04	0.34529E+03	0.69927E+03	0.14136E+01
2325.00	0.92198E-02	0.58732E+01	0.23507E+04	0.34731E+03	0.99832E+03	0.14727E+01
2330.00	0.10105E-01	0.19872E+01	0.17745E+04	0.34187E+03	0.81319E+03	0.18140E+01
2335.00	0.11670E-01	0.90323E+00	0.79128E+03	0.33537E+03	0.45926E+03	0.35800E+01
2340.00	0.13521E-01	0.11055E+02	0.36613E+04	0.33902E+03	0.72754E+03	0.13589E+01
2345.00	0.97904E-02	0.16928E+02	0.20044E+04	0.33495E+03	0.82601E+03	0.15475E+01
2350.00	0.97289E-02	0.39553E+01	0.12656E+04	0.33478E+03	0.55144E+03	0.16249E+01
2355.00	0.98616E-02	0.17532E+01	0.12092E+04	0.33199E+03	0.51304E+03	0.18651E+01
2360.00	0.21997E-01	0.24352E+02	0.66975E+04	0.33701E+03	0.64542E+03	0.13286E+01
2365.00	0.14304E-01	0.31421E+02	0.17873E+04	0.33452E+03	0.70847E+03	0.16384E+01
2370.00	0.14314E-01	0.96262E+01	0.14854E+04	0.33301E+03	0.67599E+03	0.15800E+01
2375.00	0.93231E-02	0.23822E+01	0.65408E+03	0.33851E+03	0.58390E+03	0.27553E+01
2380.00	0.86580E-02	0.40747E+01	0.86802E+03	0.33846E+03	0.64488E+03	0.19834E+01
2385.00	0.23089E-01	0.50249E+02	0.32959E+04	0.33633E+03	0.74195E+03	0.18723E+01
2390.00	0.20211E-01	0.41291E+02	0.35938E+04	0.34056E+03	0.72684E+03	0.18097E+01
2395.00	0.11417E-01	0.46149E+01	0.81568E+03	0.33580E+03	0.73669E+03	0.21576E+01
2400.00	0.12395E-01	0.92372E+01	0.11539E+04	0.33349E+03	0.89569E+03	0.18476E+01
2405.00	0.18753E-01	0.93498E+02	0.47791E+04	0.34051E+03	0.80334E+03	0.19430E+01
2410.00	0.13972E-01	0.57940E+02	0.23756E+04	0.40800E+03	0.69207E+03	0.17782E+01
2415.00	0.13076E-01	0.14895E+02	0.10741E+04	0.32643E+03	0.81870E+03	0.17913E+01
2420.00	0.15820E-01	0.97354E+01	0.95432E+03	0.33059E+03	0.83915E+03	0.19980E+01
2425.00	0.21463E-01	0.22202E+03	0.10621E+05	0.32832E+03	0.73627E+03	0.21713E+01
2430.00	0.24277E-01	0.21189E+03	0.63360E+04	0.35726E+03	0.55100E+03	0.20106E+01
2435.00	0.17246E-01	0.38833E+02	0.19155E+04	0.34121E+03	0.71422E+03	0.19814E+01
2440.00	0.16405E-01	0.19582E+02	0.93144E+03	0.32828E+03	0.75174E+03	0.17603E+01
2445.00	0.16206E-01	0.28105E+02	0.13575E+04	0.33707E+03	0.73694E+03	0.17913E+01
2450.00	0.22640E-01	0.15379E+03	0.49723E+04	0.33358E+03	0.59004E+03	0.20312E+01
2455.00	0.21467E-01	0.18622E+03	0.35943E+04	0.34868E+03	0.56985E+03	0.22454E+01
2460.00	0.16085E-01	0.29818E+02	0.80446E+03	0.33688E+03	0.65520E+03	0.16305E+01
2465.00	0.17549E-01	0.28457E+02	0.73378E+03	0.33209E+03	0.63833E+03	0.14477E+01
2470.00	0.18840E-01	0.17978E+03	0.28677E+04	0.33984E+03	0.51225E+03	0.21129E+01
2475.00	0.20124E-01	0.30400E+03	0.28724E+04	0.36984E+03	0.45420E+03	0.22251E+01
2480.00	0.18294E-01	0.92202E+02	0.14568E+04	0.33842E+03	0.52650E+03	0.19815E+01
2485.00	0.18964E-01	0.22391E+02	0.68736E+03	0.32375E+03	0.63379E+03	0.16981E+01
2490.00	0.30146E-01	0.26796E+03	0.42360E+04	0.36105E+03	0.61962E+03	0.24665E+01
2495.00	0.21429E-01	0.23172E+03	0.18022E+04	0.34057E+03	0.44172E+03	0.24466E+01
2500.00	0.16189E-01	0.65186E+02	0.93436E+03	0.39518E+03	0.45876E+03	0.18598E+01
2505.00	0.18046E-01	0.44198E+02	0.87469E+03	0.33672E+03	0.57917E+03	0.18371E+01
2510.00	0.25860E-01	0.26115E+03	0.28384E+04	0.35337E+03	0.50538E+03	0.23829E+01
2515.00	0.23740E-01	0.32437E+03	0.18376E+04	0.35764E+03	0.40016E+03	0.21437E+01
2520.00	0.20898E-01	0.46744E+02	0.60887E+03	0.33648E+03	0.56456E+03	0.18526E+01
2525.00	0.21298E-01	0.14267E+03	0.10548E+04	0.31298E+03	0.47559E+03	0.24894E+01
2530.00	0.15842E-01	0.13533E+03	0.67419E+03	0.25023E+03	0.40424E+03	0.20241E+01
2535.00	0.18334E-01	0.13857E+03	0.99926E+03	0.30815E+03	0.43770E+03	0.21556E+01
2540.00	0.18108E-01	0.15085E+03	0.12178E+04	0.32921E+03	0.40049E+03	0.20793E+01
2545.00	0.20520E-01	0.24179E+03	0.17567E+04	0.32506E+03	0.30721E+03	0.21223E+01
2550.00	0.20080E-01	0.25027E+03	0.11821E+04	0.34410E+03	0.34618E+03	0.21040E+01
2555.00	0.20921E-01	0.20052E+03	0.75858E+03	0.25392E+03	0.36161E+03	0.22624E+01
2560.00	0.20759E-01	0.34564E+03	0.13444E+04	0.34089E+03	0.28526E+03	0.22276E+01
2565.00	0.20460E-01	0.28181E+03	0.61249E+03	0.22984E+03	0.32840E+03	0.19771E+01
2570.00	0.18122E-01	0.21855E+03	0.68164E+03	0.25945E+03	0.34109E+03	0.20474E+01
2575.00	0.18748E-01	0.16862E+03	0.67634E+03	0.37724E+03	0.33666E+03	0.20151E+01
2580.00	0.18467E-01	0.19519E+03	0.46568E+03	0.36361E+03	0.28030E+03	0.20756E+01
2585.00	0.18586E-01	0.18026E+03	0.44332E+03	0.32542E+03	0.28067E+03	0.21507E+01
2590.00	0.19326E-01	0.13079E+03	0.41501E+03	0.31959E+03	0.44772E+03	0.20438E+01
2595.00	0.33403E-01	0.36737E+03	0.54625E+03	0.31245E+03	0.47989E+03	0.23512E+01

continued opposite

Table 3—*continued*

2600.00	0.15841E-01	0.56154E+03	0.26544E+03	0.21124E+03	0.30008E+03	0.19723E+01
2605.00	0.16014E-01	0.29703E+03	0.56235E+03	0.30146E+03	0.18117E+03	0.19978E+01
2610.00	0.17866E-01	0.12348E+03	0.12174E+04	0.39066E+03	0.17980E+03	0.20506E+01
2615.00	0.19708E-01	0.14533E+03	0.15071E+04	0.41326E+03	0.26166E+03	0.21431E+01
2620.00	0.22747E-01	0.14992E+03	0.10933E+04	0.38252E+03	0.32573E+03	0.22316E+01
2625.00	0.21837E-01	0.13961E+03	0.76912E+03	0.31926E+03	0.32472E+03	0.21332E+01
2630.00	0.17599E-01	0.29008E+03	0.54247E+03	0.24599E+03	0.27814E+03	0.19663E+01
2635.00	0.15653E-01	0.37825E+03	0.35504E+03	0.21402E+03	0.28518E+03	0.18340E+01
2640.00	0.17510E-01	0.32382E+03	0.26785E+03	0.23640E+03	0.42322E+03	0.19520E+01
2645.00	0.20356E-01	0.28007E+03	0.31140E+03	0.29711E+03	0.49651E+03	0.21156E+01
2650.00	0.20081E-01	0.27567E+03	0.49753E+03	0.33679E+03	0.41160E+03	0.21162E+01
2655.00	0.18747E-01	0.28996E+03	0.54490E+03	0.29060E+03	0.33264E+03	0.20136E+01
2660.00	0.20041E-01	0.23097E+03	0.54926E+03	0.24367E+03	0.30305E+03	0.22135E+01
2665.00	0.18503E-01	0.31175E+03	0.51539E+03	0.22523E+03	0.38272E+03	0.20983E+01
2670.00	0.18586E-01	0.36566E+03	0.50283E+03	0.29744E+03	0.38530E+03	0.19928E+01
2675.00	0.21106E-01	0.30525E+03	0.62598E+03	0.38775E+03	0.29652E+03	0.20531E+01
2680.00	0.18085E-01	0.57623E+03	0.40890E+03	0.27232E+03	0.38482E+03	0.21758E+01
2685.00	0.30321E-01	0.45520E+03	0.60860E+03	0.31383E+03	0.52917E+03	0.23750E+01
2690.00	0.23106E-01	0.28403E+03	0.44758E+03	0.24800E+03	0.46859E+03	0.22119E+01
2695.00	0.20246E-01	0.58263E+03	0.44190E+03	0.23657E+03	0.41814E+03	0.22298E+01
2700.00	0.21211E-01	0.45859E+03	0.29917E+03	0.18529E+03	0.56371E+03	0.23036E+01
2705.00	0.20131E-01	0.23014E+03	0.35434E+03	0.28155E+03	0.60688E+03	0.21072E+01
2710.00	0.23378E-01	0.50443E+03	0.35802E+03	0.17944E+03	0.52535E+03	0.24593E+01
2715.00	0.23789E-01	0.46352E+03	0.29227E+03	0.17692E+03	0.52223E+03	0.25227E+01
2720.00	0.21462E-01	0.20993E+03	0.35771E+03	0.31721E+03	0.60253E+03	0.20004E+01
2725.00	0.20362E-01	0.53795E+03	0.38177E+03	0.23440E+03	0.51701E+03	0.22429E+01
2730.00	0.20762E-01	0.49904E+03	0.31934E+03	0.21424E+03	0.45469E+03	0.23322E+01
2735.00	0.24031E-01	0.27953E+03	0.48358E+03	0.34518E+03	0.49832E+03	0.21075E+01
2740.00	0.24940E-01	0.95974E+03	0.53342E+03	0.19708E+03	0.43041E+03	0.24096E+01
2745.00	0.23438E-01	0.93725E+03	0.44443E+03	0.23712E+03	0.38403E+03	0.24449E+01
2750.00	0.23028E-01	0.43165E+03	0.42170E+03	0.33818E+03	0.46644E+03	0.21156E+01
2755.00	0.24653E-01	0.82401E+03	0.37979E+03	0.24992E+03	0.42988E+03	0.25581E+01
2760.00	0.25613E-01	0.79056E+03	0.35999E+03	0.30442E+03	0.42635E+03	0.26721E+01
2765.00	0.25237E-01	0.47647E+03	0.22459E+03	0.26982E+03	0.56181E+03	0.23055E+01
2770.00	0.28601E-01	0.94491E+03	0.21702E+03	0.28473E+03	0.49833E+03	0.27042E+01
2775.00	0.22374E-01	0.99199E+03	0.21229E+03	0.28443E+03	0.45443E+03	0.25115E+01
2780.00	0.18077E-01	0.76681E+03	0.17844E+03	0.24099E+03	0.48377E+03	0.22201E+01
2785.00	0.17121E-01	0.11619E+04	0.21125E+03	0.27266E+03	0.39253E+03	0.22966E+01
2790.00	0.17400E-01	0.15055E+04	0.26925E+03	0.29662E+03	0.32005E+03	0.23407E+01
2795.00	0.17564E-01	0.13308E+04	0.27204E+03	0.28389E+03	0.28897E+03	0.23482E+01
2800.00	0.20403E-01	0.11777E+04	0.31614E+03	0.26231E+03	0.29112E+03	0.24986E+01
2805.00	0.22057E-01	0.12177E+04	0.43032E+03	0.24309E+03	0.29195E+03	0.24665E+01
2810.00	0.19197E-01	0.10716E+04	0.38713E+03	0.29317E+03	0.29211E+03	0.22724E+01
2815.00	0.19928E-01	0.11572E+04	0.44125E+03	0.37257E+03	0.27081E+03	0.20602E+01
2820.00	0.18552E-01	0.21698E+04	0.38818E+03	0.32976E+03	0.27876E+03	0.22286E+01
2825.00	0.19477E-01	0.28562E+04	0.35522E+03	0.36120E+03	0.27799E+03	0.23078E+01
2830.00	0.21787E-01	0.19213E+04	0.31842E+03	0.30430E+03	0.31524E+03	0.24594E+01
2835.00	0.23067E-01	0.10248E+04	0.25958E+03	0.28891E+03	0.43946E+03	0.24215E+01
2840.00	0.21469E-01	0.76450E+03	0.17933E+03	0.23853E+03	0.61684E+03	0.22469E+01
2845.00	0.23292E-01	0.80564E+03	0.24128E+03	0.27293E+03	0.50277E+03	0.22013E+01
2850.00	0.26537E-01	0.98769E+03	0.31272E+03	0.27849E+03	0.37357E+03	0.26291E+01
2855.00	0.25908E-01	0.12519E+04	0.32192E+03	0.28922E+03	0.40568E+03	0.26295E+01
2860.00	0.23251E-01	0.15119E+04	0.29589E+03	0.29732E+03	0.38932E+03	0.25503E+01
2865.00	0.22059E-01	0.22240E+04	0.24860E+03	0.27080E+03	0.35584E+03	0.26252E+01
2870.00	0.19941E-01	0.24394E+04	0.21142E+03	0.25579E+03	0.34756E+03	0.25831E+01
2875.00	0.22232E-01	0.26519E+04	0.17780E+03	0.26622E+03	0.46917E+03	0.25309E+01
2880.00	0.24953E-01	0.21504E+04	0.17353E+03	0.27778E+03	0.44779E+03	0.26368E+01
2885.00	0.28630E-01	0.20709E+04	0.16161E+03	0.25912E+03	0.45000E+03	0.27189E+01
2890.00	0.35934E-01	0.13756E+04	0.16306E+03	0.26623E+03	0.50452E+03	0.29321E+01
2895.00	0.43360E-01	0.17351E+04	0.16550E+03	0.22332E+03	0.46214E+03	0.26378E+01

continued overleaf

Table 3—*continued*

2900.00	0.37714E-01	0.22966E+04	0.21609E+03	0.30340E+03	0.38218E+03	0.21657E+01
2905.00	0.44389E-01	0.21508E+04	0.18775E+03	0.29522E+03	0.36352E+03	0.20880E+01
2910.00	0.36933E-01	0.22818E+04	0.19478E+03	0.28752E+03	0.42486E+03	0.24312E+01
2915.00	0.57441E-01	0.18217E+04	0.14710E+03	0.29259E+03	0.28553E+03	0.19586E+01
2920.00	0.72833E-01	0.19870E+04	0.93843E+02	0.38235E+03	0.29188E+03	0.40355E+01
2925.00	0.39570E-01	0.23154E+04	0.17438E+03	0.29474E+03	0.40335E+03	0.21689E+01
2930.00	0.43619E-01	0.21976E+04	0.18827E+03	0.30943E+03	0.35363E+03	0.19850E+01
2935.00	0.47915E-01	0.21622E+04	0.19732E+03	0.38052E+03	0.29018E+03	0.18149E+01
2940.00	0.38364E-01	0.26600E+04	0.21937E+03	0.39332E+03	0.34823E+03	0.19293E+01
2945.00	0.39282E-01	0.27414E+04	0.20751E+03	0.37660E+03	0.33708E+03	0.20407E+01
2950.00	0.82470E-01	0.24560E+04	0.10634E+03	0.51017E+03	0.25299E+03	0.42494E+01
2955.00	0.41335E-01	0.30392E+04	0.26498E+03	0.53530E+03	0.27302E+03	0.20954E+01
2960.00	0.37234E-01	0.29557E+04	0.26741E+03	0.48272E+03	0.33086E+03	0.22287E+01
2965.00	0.33439E-01	0.29470E+04	0.28504E+03	0.46430E+03	0.27963E+03	0.21749E+01
2970.00	0.34043E-01	0.28193E+04	0.27759E+03	0.45613E+03	0.29732E+03	0.21979E+01
2975.00	0.30724E-01	0.26488E+04	0.28619E+03	0.42639E+03	0.27028E+03	0.22384E+01
2980.00	0.29989E-01	0.28524E+04	0.28986E+03	0.44271E+03	0.24625E+03	0.23629E+01
2985.00	0.29729E-01	0.25265E+04	0.30812E+03	0.40335E+03	0.21124E+03	0.22529E+01
2990.00	0.34392E-01	0.20332E+04	0.26085E+03	0.38039E+03	0.25722E+03	0.23668E+01
2995.00	0.43457E-01	0.15879E+04	0.19690E+03	0.34512E+03	0.33091E+03	0.23072E+01
3000.00	0.59649E-01	0.19228E+04	0.68541E+02	0.27496E+03	0.45822E+03	0.21753E+01
3005.00	0.14946E+00	0.15223E+04	0.87352E+01	0.26743E+03	0.13375E+03	0.50773E+00
3010.00	0.16402E+00	0.36184E+04	0.17775E+02	0.25804E+03	0.10795E+03	0.42128E-01
3015.00	0.17064E+00	0.46352E+04	0.22041E+02	0.26904E+03	0.11931E+03	0.19179E+01
3020.00	0.14683E+00	0.19670E+04	0.19772E+02	0.27728E+03	0.11240E+03	0.11663E+01
3025.00	0.31087E-01	0.29634E+04	0.20847E+03	0.30522E+03	0.21436E+03	0.23457E+01
3030.00	0.36175E-01	0.13552E+04	0.45752E+03	0.72713E+03	0.22909E+03	0.24055E+01
3035.00	0.33705E-01	0.15115E+04	0.40247E+03	0.38330E+03	0.22067E+03	0.21424E+01
3040.00	0.33540E-01	0.15230E+04	0.37196E+03	0.36285E+03	0.24165E+03	0.20505E+01
3045.00	0.31171E-01	0.17956E+04	0.44012E+03	0.56334E+03	0.23475E+03	0.24541E+01
3050.00	0.39428E-01	0.17796E+04	0.43415E+03	0.66345E+03	0.19994E+03	0.22898E+01
3055.00	0.32893E-01	0.25961E+04	0.41653E+03	0.56337E+03	0.19873E+03	0.21750E+01
3060.00	0.39206E-01	0.28388E+04	0.40440E+03	0.59857E+03	0.16364E+03	0.19264E+01
3065.00	0.36153E-01	0.30932E+04	0.30831E+03	0.51327E+03	0.16741E+03	0.20674E+01
3070.00	0.37820E-01	0.33172E+04	0.23357E+03	0.60052E+03	0.17512E+03	0.22469E+01
3075.00	0.41521E-01	0.30219E+04	0.20488E+03	0.52193E+03	0.23517E+03	0.18601E+01
3080.00	0.79165E-01	0.24307E+04	0.10210E+03	0.51847E+03	0.24355E+03	0.37978E+01
3085.00	0.96018E-01	0.21214E+04	0.73740E+02	0.47794E+03	0.23352E+03	0.40058E+01
3090.00	0.75518E-01	0.18584E+04	0.14929E+03	0.39449E+03	0.17867E+03	0.85258E+00
3095.00	0.46851E-01	0.24314E+04	0.20860E+03	0.37035E+03	0.29126E+03	0.15673E+01
3100.00	0.83881E-01	0.18288E+04	0.10066E+03	0.41672E+03	0.23885E+03	0.28593E+01
3105.00	0.43203E-01	0.23597E+04	0.24027E+03	0.30890E+03	0.40174E+03	0.15556E+01
3110.00	0.42363E-01	0.25096E+04	0.21220E+03	0.30687E+03	0.38963E+03	0.16635E+01
3115.00	0.33452E-01	0.25743E+04	0.23879E+03	0.27029E+03	0.48195E+03	0.19082E+01
3120.00	0.35266E-01	0.23828E+04	0.23128E+03	0.27319E+03	0.51468E+03	0.20301E+01
3125.00	0.33470E-01	0.22826E+04	0.24290E+03	0.25360E+03	0.58370E+03	0.19082E+01
3130.00	0.31717E-01	0.19137E+04	0.24877E+03	0.22730E+03	0.61370E+03	0.19895E+01
3135.00	0.28766E-01	0.21775E+04	0.23662E+03	0.22949E+03	0.61650E+03	0.20763E+01
3140.00	0.30474E-01	0.14786E+04	0.25837E+03	0.21851E+03	0.67746E+03	0.20249E+01
3145.00	0.48268E-01	0.13367E+04	0.21414E+03	0.19297E+03	0.57712E+03	0.19099E+01
3150.00	0.31011E-01	0.12801E+04	0.24828E+03	0.16684E+03	0.73569E+03	0.21780E+01
3155.00	0.26021E-01	0.12156E+04	0.24143E+03	0.12558E+03	0.78504E+03	0.21299E+01
3160.00	0.52678E-01	0.60764E+03	0.55077E+03	0.26110E+03	0.82477E+03	0.15686E+01
3165.00	0.41891E-01	0.53531E+03	0.72738E+03	0.27306E+03	0.91183E+03	0.18107E+01
3170.00	0.47091E-01	0.58385E+03	0.71173E+03	0.27829E+03	0.85267E+03	0.16868E+01
3175.00	0.28313E-01	0.40199E+03	0.81014E+03	0.28680E+03	0.90750E+03	0.21283E+01
3180.00	0.34447E-01	0.40350E+03	0.83915E+03	0.26665E+03	0.92999E+03	0.19953E+01
3185.00	0.36793E-01	0.27714E+03	0.14981E+04	0.27720E+03	0.11207E+04	0.21267E+01
3190.00	0.27919E-01	0.15482E+03	0.83835E+03	0.26028E+03	0.11586E+04	0.21979E+01
3195.00	0.30209E-01	0.29177E+03	0.79329E+03	0.26882E+03	0.10438E+04	0.22789E+01

continued opposite

Table 3—*continued*

3200.00	0.30199E-01	0.14436E+03	0.10198E+04	0.25513E+03	0.11626E+04	0.23956E+01
3205.00	0.26014E-01	0.77701E+02	0.69728E+03	0.24968E+03	0.11590E+04	0.19383E+01
3210.00	0.29736E-01	0.77126E+02	0.11498E+04	0.24989E+03	0.10417E+04	0.18434E+01
3215.00	0.31929E-01	0.33338E+02	0.10180E+04	0.24052E+03	0.11015E+04	0.16668E+01
3220.00	0.29492E-01	0.48425E+02	0.80515E+03	0.24935E+03	0.11482E+04	0.16821E+01
3225.00	0.35857E-01	0.28445E+02	0.14381E+04	0.24358E+03	0.10404E+04	0.12605E+01
3230.00	0.32768E-01	0.19023E+02	0.11542E+04	0.25166E+03	0.10157E+04	0.14118E+01
3235.00	0.28890E-01	0.22226E+02	0.78520E+03	0.24164E+03	0.10105E+04	0.14854E+01
3240.00	0.33069E-01	0.89748E+01	0.10797E+04	0.24231E+03	0.94365E+03	0.12845E+01
3245.00	0.32077E-01	0.92433E+01	0.87480E+03	0.24198E+03	0.99465E+03	0.12755E+01
3250.00	0.28789E-01	0.10686E+02	0.75541E+03	0.24143E+03	0.99025E+03	0.13143E+01
3255.00	0.31804E-01	0.55560E+01	0.84806E+03	0.24050E+03	0.92537E+03	0.12295E+01
3260.00	0.32335E-01	0.45969E+01	0.60591E+03	0.23905E+03	0.97253E+03	0.11511E+01
3265.00	0.28992E-01	0.56342E+01	0.48122E+03	0.23805E+03	0.10308E+04	0.12181E+01
3270.00	0.29205E-01	0.48135E+01	0.51586E+03	0.23731E+03	0.10302E+04	0.11849E+01
3275.00	0.30629E-01	0.36410E+01	0.53191E+03	0.23967E+03	0.10246E+04	0.11787E+01
3280.00	0.29865E-01	0.30759E+01	0.46731E+03	0.24179E+03	0.99603E+03	0.11482E+01
3285.00	0.29173E-01	0.29604E+01	0.45669E+03	0.23634E+03	0.10001E+04	0.11420E+01
3290.00	0.29030E-01	0.25077E+01	0.54062E+03	0.23653E+03	0.96032E+03	0.10947E+01
3295.00	0.28859E-01	0.20503E+01	0.57354E+03	0.23640E+03	0.91565E+03	0.11729E+01
3300.00	0.27688E-01	0.20140E+01	0.50754E+03	0.23552E+03	0.93033E+03	0.10935E+01
3305.00	0.26799E-01	0.17565E+01	0.59301E+03	0.23579E+03	0.88507E+03	0.11573E+01
3310.00	0.25645E-01	0.16024E+01	0.60282E+03	0.23553E+03	0.85888E+03	0.12181E+01
3315.00	0.24885E-01	0.14085E+01	0.65037E+03	0.23535E+03	0.81075E+03	0.12294E+01
3320.00	0.24069E-01	0.12003E+01	0.66587E+03	0.23481E+03	0.74082E+03	0.13083E+01
3325.00	0.23291E-01	0.12176E+01	0.60448E+03	0.23871E+03	0.76678E+03	0.13753E+01
3330.00	0.22999E-01	0.10416E+01	0.61774E+03	0.23486E+03	0.70064E+03	0.15279E+01
3335.00	0.21591E-01	0.98573E+00	0.56039E+03	0.23296E+03	0.58588E+03	0.20220E+01
3340.00	0.21018E-01	0.10072E+01	0.50756E+03	0.23296E+03	0.57792E+03	0.21802E+01
3345.00	0.20988E-01	0.92800E+00	0.52093E+03	0.23227E+03	0.62986E+03	0.17692E+01
3350.00	0.20665E-01	0.78276E+00	0.61026E+03	0.24049E+03	0.62064E+03	0.20483E+01
3355.00	0.19914E-01	0.68948E+00	0.64971E+03	0.23259E+03	0.58119E+03	0.24759E+01
3360.00	0.19642E-01	0.62918E+00	0.66302E+03	0.23923E+03	0.55446E+03	0.25261E+01
3365.00	0.18669E-01	0.64031E+00	0.64308E+03	0.23861E+03	0.55837E+03	0.29354E+01
3370.00	0.17615E-01	0.65032E+00	0.63965E+03	0.23702E+03	0.51969E+03	0.32981E+01
3375.00	0.16646E-01	0.59850E+00	0.67378E+03	0.24275E+03	0.48136E+03	0.35896E+01
3380.00	0.15468E-01	0.59327E+00	0.52673E+03	0.23069E+03	0.49905E+03	0.35357E+01
3385.00	0.15185E-01	0.54834E+00	0.56527E+03	0.23804E+03	0.51506E+03	0.29139E+01
3390.00	0.14673E-01	0.51928E+00	0.53960E+03	0.22944E+03	0.51844E+03	0.31425E+01
3395.00	0.14051E-01	0.49552E+00	0.51623E+03	0.22909E+03	0.52227E+03	0.32623E+01
3400.00	0.14061E-01	0.48653E+00	0.50770E+03	0.23704E+03	0.54443E+03	0.33940E+01
3405.00	0.13962E-01	0.45759E+00	0.51160E+03	0.22850E+03	0.55807E+03	0.27953E+01
3410.00	0.13490E-01	0.44375E+00	0.49215E+03	0.23652E+03	0.54018E+03	0.32742E+01
3415.00	0.13107E-01	0.40301E+00	0.48217E+03	0.23795E+03	0.52017E+03	0.25648E+01
3420.00	0.12342E-01	0.40539E+00	0.68069E+03	0.23474E+03	0.48943E+03	0.26876E+01
3425.00	0.11789E-01	0.39045E+00	0.70192E+03	0.23435E+03	0.47350E+03	0.36452E+01
3430.00	0.11113E-01	0.39544E+00	0.83119E+03	0.22817E+03	0.43784E+03	0.29819E+01
3435.00	0.10441E-01	0.42846E+00	0.94329E+03	0.22913E+03	0.41029E+03	0.23314E+01
3440.00	0.10474E-01	0.38988E+00	0.10012E+04	0.23249E+03	0.38927E+03	0.25052E+01
3445.00	0.10344E-01	0.40974E+00	0.10992E+04	0.23165E+03	0.33918E+03	0.26087E+01
3450.00	0.10167E-01	0.36342E+00	0.12725E+04	0.23098E+03	0.33377E+03	0.18458E+01
3455.00	0.10090E-01	0.38838E+00	0.13011E+04	0.22758E+03	0.29908E+03	0.17544E+01
3460.00	0.10316E-01	0.32749E+00	0.14272E+04	0.22725E+03	0.32784E+03	0.15864E+01
3465.00	0.10282E-01	0.31150E+00	0.12918E+04	0.22628E+03	0.31829E+03	0.13679E+01
3470.00	0.10157E-01	0.30045E+00	0.13992E+04	0.22894E+03	0.33199E+03	0.12051E+01
3475.00	0.10250E-01	0.25879E+00	0.15377E+04	0.22942E+03	0.40964E+03	0.95045E+00
3480.00	0.93353E-02	0.31172E+00	0.14135E+04	0.22901E+03	0.34921E+03	0.90274E+00
3485.00	0.94401E-02	0.27517E+00	0.97624E+03	0.22527E+03	0.42278E+03	0.56661E+00
3490.00	0.83942E-02	0.45900E+00	0.50350E+03	0.22354E+03	0.44560E+03	0.98046E+00
3495.00	0.66875E-02	0.12966E+01	0.59919E+03	0.22310E+03	0.30656E+03	0.11168E+01

continued overleaf

Table 3—*continued*

3500.00	0.78786E-02	0.11314E+01	0.14866E+04	0.22481E+03	0.28207E+03	0.92481E+00
3505.00	0.98427E-02	0.19528E+00	0.15712E+04	0.21628E+03	0.49671E+03	0.43836E+00
3510.00	0.87682E-02	0.20467E+00	0.24336E+04	0.22846E+03	0.39756E+03	0.28514E+00
3515.00	0.99820E-02	0.21100E+00	0.31856E+04	0.21853E+03	0.44940E+03	0.42527E+00
3520.00	0.89021E-02	0.28796E+00	0.19127E+04	0.22366E+03	0.49087E+03	0.34019E+00
3525.00	0.80573E-02	0.42013E+00	0.16567E+04	0.22596E+03	0.32820E+03	0.62884E+00
3530.00	0.79016E-02	0.42513E+00	0.18893E+04	0.22525E+03	0.30311E+03	0.63698E+00
3535.00	0.80930E-02	0.34997E+00	0.21452E+04	0.22269E+03	0.32480E+03	0.58158E+00
3540.00	0.74619E-02	0.41622E+00	0.15968E+04	0.22231E+03	0.25663E+03	0.71036E+00
3545.00	0.70168E-02	0.62807E+00	0.10483E+04	0.22237E+03	0.33729E+03	0.70531E+00
3550.00	0.70272E-02	0.64718E+00	0.92043E+03	0.22550E+03	0.39883E+03	0.63126E+00
3555.00	0.69063E-02	0.64270E+00	0.87228E+03	0.22023E+03	0.42984E+03	0.46902E+00
3560.00	0.71204E-02	0.57990E+00	0.83870E+03	0.21970E+03	0.47538E+03	0.32477E+00
3565.00	0.74753E-02	0.46778E+00	0.71216E+03	0.21911E+03	0.51922E+03	0.14423E+00
3570.00	0.75646E-02	0.42752E+00	0.71035E+03	0.21881E+03	0.58608E+03	0.72707E-01
3575.00	0.74923E-02	0.55452E+00	0.69817E+03	0.21859E+03	0.70772E+03	0.17299E+00
3580.00	0.75629E-02	0.62993E+00	0.67301E+03	0.21806E+03	0.78938E+03	0.18950E+00
3585.00	0.82687E-02	0.45863E+00	0.78748E+03	0.21797E+03	0.84482E+03	0.30651E-01
3590.00	0.86518E-02	0.40320E+00	0.72720E+03	0.21807E+03	0.90976E+03	0.29285E-02
3595.00	0.89112E-02	0.29333E+00	0.11304E+04	0.21825E+03	0.84796E+03	0.21294E-02
3600.00	0.86925E-02	0.37367E+00	0.13939E+04	0.21822E+03	0.78007E+03	0.85988E-02
3605.00	0.82882E-02	0.56791E+00	0.85915E+03	0.21733E+03	0.80528E+03	0.22675E+00
3610.00	0.82302E-02	0.84896E+00	0.12368E+04	0.21759E+03	0.81602E+03	0.38895E+00
3615.00	0.86353E-02	0.71854E+00	0.13761E+04	0.21730E+03	0.71765E+03	0.30693E+00
3620.00	0.91457E-02	0.27749E+00	0.11199E+04	0.21634E+03	0.61587E+03	0.16177E+00
3625.00	0.92244E-02	0.37528E+00	0.11502E+04	0.21630E+03	0.84803E+03	0.37379E-03
3630.00	0.81224E-02	0.11040E+01	0.11706E+04	0.21792E+03	0.79579E+03	0.59289E+00
3635.00	0.73196E-02	0.13790E+01	0.10433E+04	0.21842E+03	0.73741E+03	0.74524E+00
3640.00	0.82857E-02	0.69704E+00	0.14681E+04	0.21603E+03	0.76992E+03	0.44386E+00
3645.00	0.96190E-02	0.30309E+00	0.64656E+03	0.21389E+03	0.83510E+03	0.15407E-03
3650.00	0.92477E-02	0.72486E+00	0.16461E+04	0.21567E+03	0.79629E+03	0.37407E+00
3655.00	0.82068E-02	0.20224E+01	0.10538E+04	0.21588E+03	0.73426E+03	0.83346E+00
3660.00	0.73810E-02	0.23618E+01	0.82040E+03	0.22455E+03	0.67643E+03	0.10416E+01
3665.00	0.85317E-02	0.11584E+01	0.10385E+04	0.21860E+03	0.67563E+03	0.71804E+00
3670.00	0.10029E-01	0.54174E+00	0.31669E+03	0.22147E+03	0.71882E+03	0.10492E+00
3675.00	0.99766E-02	0.14970E+01	0.10431E+04	0.21343E+03	0.74469E+03	0.53728E+00
3680.00	0.99744E-02	0.14665E+01	0.12459E+04	0.21352E+03	0.79702E+03	0.53485E+00
3685.00	0.96111E-02	0.16155E+01	0.12881E+04	0.21347E+03	0.64342E+03	0.78901E+00
3690.00	0.93243E-02	0.17943E+01	0.90865E+03	0.21342E+03	0.63439E+03	0.87002E+00
3695.00	0.98223E-02	0.17473E+01	0.10271E+04	0.21416E+03	0.76723E+03	0.76417E+00
3700.00	0.98974E-02	0.21434E+01	0.11275E+04	0.21287E+03	0.74792E+03	0.89430E+00
3705.00	0.99441E-02	0.11841E+01	0.59543E+03	0.22523E+03	0.74329E+03	0.76378E+00
3710.00	0.10161E-01	0.18884E+01	0.70241E+03	0.21328E+03	0.68611E+03	0.94630E+00
3715.00	0.10144E-01	0.35711E+01	0.95367E+03	0.21411E+03	0.62811E+03	0.11489E+01
3720.00	0.99912E-02	0.45689E+01	0.72826E+03	0.21784E+03	0.62447E+03	0.11440E+01
3725.00	0.93485E-02	0.39256E+01	0.48720E+03	0.21724E+03	0.75098E+03	0.11438E+01
3730.00	0.10140E-01	0.29415E+01	0.54006E+03	0.21642E+03	0.79470E+03	0.10888E+01
3735.00	0.10863E-01	0.27467E+01	0.53292E+03	0.21582E+03	0.75417E+03	0.11249E+01
3740.00	0.11934E-01	0.54901E+01	0.59329E+03	0.21123E+03	0.66836E+03	0.11051E+01
3745.00	0.13618E-01	0.51315E+01	0.75678E+03	0.21198E+03	0.66848E+03	0.10366E+01
3750.00	0.11432E-01	0.45426E+01	0.72011E+03	0.20862E+03	0.76750E+03	0.11506E+01
3755.00	0.90682E-02	0.69372E+01	0.49047E+03	0.22950E+03	0.73171E+03	0.13265E+01
3760.00	0.10335E-01	0.67898E+01	0.49737E+03	0.22111E+03	0.79449E+03	0.13111E+01
3765.00	0.11225E-01	0.11726E+02	0.51196E+03	0.22224E+03	0.73096E+03	0.13249E+01
3770.00	0.10460E-01	0.13080E+02	0.45186E+03	0.22424E+03	0.73846E+03	0.13786E+01
3775.00	0.12241E-01	0.13575E+02	0.45857E+03	0.21005E+03	0.79816E+03	0.14409E+01
3780.00	0.11515E-01	0.14405E+02	0.43032E+03	0.23358E+03	0.69353E+03	0.15424E+01
3785.00	0.11881E-01	0.16965E+02	0.45885E+03	0.22503E+03	0.63763E+03	0.15588E+01
3790.00	0.14446E-01	0.28478E+02	0.44753E+03	0.19859E+03	0.65198E+03	0.16637E+01
3795.00	0.16611E-01	0.51747E+02	0.60693E+03	0.20237E+03	0.65117E+03	0.17551E+01

continued opposite

Table 3—*continued*

3800.00	0.18077E-01	0.52958E+02	0.63997E+03	0.25045E+03	0.57743E+03	0.17885E+01
3805.00	0.18213E-01	0.64348E+02	0.59279E+03	0.25851E+03	0.53580E+03	0.18809E+01
3810.00	0.19037E-01	0.81332E+02	0.55836E+03	0.26711E+03	0.50448E+03	0.19390E+01
3815.00	0.20251E-01	0.72148E+02	0.61511E+03	0.25345E+03	0.45407E+03	0.18839E+01
3820.00	0.19826E-01	0.98710E+02	0.52539E+03	0.18300E+03	0.43474E+03	0.19445E+01
3825.00	0.21539E-01	0.17308E+03	0.48609E+03	0.17572E+03	0.39580E+03	0.22226E+01
3830.00	0.21771E-01	0.16249E+03	0.55129E+03	0.23566E+03	0.36033E+03	0.21266E+01
3835.00	0.21599E-01	0.14831E+03	0.51880E+03	0.27728E+03	0.35341E+03	0.21084E+01
3840.00	0.20403E-01	0.18935E+03	0.48209E+03	0.27803E+03	0.29545E+03	0.21181E+01
3845.00	0.19250E-01	0.20273E+03	0.48443E+03	0.28020E+03	0.31850E+03	0.19790E+01
3850.00	0.17857E-01	0.25228E+03	0.38374E+03	0.21183E+03	0.33779E+03	0.19574E+01
3855.00	0.16327E-01	0.34943E+03	0.28670E+03	0.17593E+03	0.32257E+03	0.18704E+01
3860.00	0.14844E-01	0.58146E+03	0.25831E+03	0.18438E+03	0.26349E+03	0.18432E+01
3865.00	0.22188E-01	0.59849E+03	0.25121E+03	0.12933E+03	0.14865E+03	0.18903E+01
3870.00	0.28053E-01	0.30788E+03	0.84939E+03	0.23425E+03	0.21449E+03	0.24944E+01
3875.00	0.20449E-01	0.89219E+02	0.31940E+03	0.20996E+03	0.29342E+03	0.21506E+01
3880.00	0.18788E-01	0.13356E+03	0.33626E+03	0.24433E+03	0.22288E+03	0.21295E+01
3885.00	0.17330E-01	0.24479E+03	0.37214E+03	0.25164E+03	0.12936E+03	0.20390E+01
3890.00	0.18397E-01	0.38283E+03	0.30886E+03	0.14667E+03	0.11472E+03	0.20904E+01
3895.00	0.19253E-01	0.38061E+03	0.26453E+03	0.10941E+03	0.13652E+03	0.21059E+01
3900.00	0.15416E-01	0.36040E+03	0.30849E+03	0.14181E+03	0.21817E+03	0.19331E+01
3905.00	0.16284E-01	0.39063E+03	0.23057E+03	0.13306E+03	0.39402E+03	0.18430E+01
3910.00	0.14699E-01	0.27710E+03	0.20236E+03	0.12327E+03	0.43749E+03	0.17988E+01
3915.00	0.13665E-01	0.14282E+03	0.30762E+03	0.20185E+03	0.38504E+03	0.17315E+01
3920.00	0.14200E-01	0.91305E+02	0.26655E+03	0.20838E+03	0.39448E+03	0.17496E+01
3925.00	0.14552E-01	0.52368E+02	0.21878E+03	0.19042E+03	0.37981E+03	0.18134E+01
3930.00	0.13753E-01	0.33603E+02	0.25516E+03	0.19138E+03	0.34090E+03	0.16585E+01
3935.00	0.16671E-01	0.31728E+02	0.38785E+03	0.21799E+03	0.37209E+03	0.15525E+01
3940.00	0.17127E-01	0.50813E+02	0.43297E+03	0.22580E+03	0.37109E+03	0.17491E+01
3945.00	0.18066E-01	0.45761E+02	0.41823E+03	0.24130E+03	0.36778E+03	0.17904E+01
3950.00	0.18582E-01	0.28906E+02	0.37754E+03	0.21361E+03	0.40982E+03	0.15729E+01
3955.00	0.18317E-01	0.47423E+02	0.46320E+03	0.23410E+03	0.35919E+03	0.18173E+01
3960.00	0.18905E-01	0.50173E+02	0.36145E+03	0.21623E+03	0.33976E+03	0.18094E+01
3965.00	0.18931E-01	0.39886E+02	0.31534E+03	0.21173E+03	0.37970E+03	0.16800E+01
3970.00	0.18789E-01	0.45346E+02	0.38869E+03	0.22864E+03	0.38428E+03	0.17525E+01
3975.00	0.18828E-01	0.45838E+02	0.34091E+03	0.22534E+03	0.43586E+03	0.18393E+01
3980.00	0.19194E-01	0.41623E+02	0.26205E+03	0.21507E+03	0.45464E+03	0.17372E+01
3985.00	0.19103E-01	0.43405E+02	0.27508E+03	0.20723E+03	0.44189E+03	0.17102E+01
3990.00	0.19412E-01	0.41874E+02	0.29896E+03	0.21553E+03	0.52826E+03	0.18260E+01
3995.00	0.19770E-01	0.36494E+02	0.24316E+03	0.20695E+03	0.52596E+03	0.16886E+01
4000.00	0.20723E-01	0.45511E+02	0.25477E+03	0.21134E+03	0.48733E+03	0.17783E+01
4005.00	0.19929E-01	0.43658E+02	0.24799E+03	0.19359E+03	0.53693E+03	0.18473E+01
4010.00	0.16580E-01	0.44451E+02	0.22776E+03	0.21294E+03	0.55177E+03	0.17563E+01
4015.00	0.18527E-01	0.59565E+02	0.24242E+03	0.21358E+03	0.52502E+03	0.18358E+01
4020.00	0.19595E-01	0.56198E+02	0.22505E+03	0.21008E+03	0.51914E+03	0.18502E+01
4025.00	0.20525E-01	0.53916E+02	0.20636E+03	0.19183E+03	0.54552E+03	0.19498E+01
4030.00	0.21842E-01	0.66862E+02	0.22134E+03	0.19022E+03	0.59758E+03	0.21405E+01
4035.00	0.18541E-01	0.64285E+02	0.18545E+03	0.18857E+03	0.59212E+03	0.19265E+01
4040.00	0.19639E-01	0.55951E+02	0.18997E+03	0.20284E+03	0.59148E+03	0.18336E+01
4045.00	0.23010E-01	0.82213E+02	0.21278E+03	0.18734E+03	0.60901E+03	0.22588E+01
4050.00	0.23224E-01	0.10428E+03	0.11030E+03	0.81412E+02	0.64051E+03	0.23015E+01
4055.00	0.22314E-01	0.11962E+03	0.17195E+03	0.16560E+03	0.65654E+03	0.23444E+01
4060.00	0.20434E-01	0.12888E+03	0.18417E+03	0.18646E+03	0.56594E+03	0.21459E+01
4065.00	0.19836E-01	0.15153E+03	0.16675E+03	0.17906E+03	0.61939E+03	0.20667E+01
4070.00	0.19605E-01	0.20023E+03	0.15166E+03	0.17785E+03	0.59162E+03	0.19928E+01
4075.00	0.20443E-01	0.22511E+03	0.19048E+03	0.16909E+03	0.49181E+03	0.21627E+01
4080.00	0.21537E-01	0.26747E+03	0.21916E+03	0.16860E+03	0.49953E+03	0.21310E+01
4085.00	0.22373E-01	0.31246E+03	0.22272E+03	0.18164E+03	0.49043E+03	0.21104E+01
4090.00	0.23724E-01	0.31979E+03	0.21470E+03	0.18318E+03	0.43799E+03	0.21346E+01
4095.00	0.25161E-01	0.31560E+03	0.20985E+03	0.17859E+03	0.39350E+03	0.22231E+01

continued overleaf

Table 3—*continued*

4100.00	0.26827E-01	0.42114E+03	0.19111E+03	0.18551E+03	0.45174E+03	0.24879E+01
4105.00	0.26959E-01	0.50322E+03	0.14062E+03	0.21056E+03	0.49014E+03	0.25749E+01
4110.00	0.27885E-01	0.37744E+03	0.13851E+03	0.15498E+03	0.44702E+03	0.24304E+01
4115.00	0.29403E-01	0.46217E+03	0.16235E+03	0.17465E+03	0.46879E+03	0.26532E+01
4120.00	0.25730E-01	0.79185E+03	0.12729E+03	0.20248E+03	0.44272E+03	0.28054E+01
4125.00	0.23672E-01	0.77715E+03	0.10945E+03	0.17365E+03	0.40799E+03	0.26829E+01
4130.00	0.25121E-01	0.59021E+03	0.10949E+03	0.13978E+03	0.41974E+03	0.24708E+01
4135.00	0.25690E-01	0.67356E+03	0.18113E+03	0.18447E+03	0.48218E+03	0.24723E+01
4140.00	0.26874E-01	0.59285E+03	0.28384E+03	0.21134E+03	0.51164E+03	0.25018E+01
4145.00	0.27466E-01	0.40703E+03	0.24556E+03	0.17871E+03	0.46627E+03	0.23517E+01
4150.00	0.27384E-01	0.75945E+03	0.24624E+03	0.19273E+03	0.47840E+03	0.24196E+01
4155.00	0.27009E-01	0.11076E+04	0.21902E+03	0.20921E+03	0.45260E+03	0.24532E+01
4160.00	0.28672E-01	0.99155E+03	0.20788E+03	0.21953E+03	0.43406E+03	0.26911E+01
4165.00	0.31835E-01	0.10709E+04	0.19054E+03	0.24212E+03	0.43362E+03	0.28519E+01
4170.00	0.33642E-01	0.14126E+04	0.17687E+03	0.21546E+03	0.42712E+03	0.29272E+01
4175.00	0.34798E-01	0.14887E+04	0.18764E+03	0.20208E+03	0.39531E+03	0.26662E+01
4180.00	0.33346E-01	0.18301E+04	0.21371E+03	0.22296E+03	0.31536E+03	0.27417E+01
4185.00	0.37005E-01	0.14458E+04	0.19832E+03	0.24327E+03	0.33031E+03	0.28468E+01
4190.00	0.35136E-01	0.13450E+04	0.17893E+03	0.23943E+03	0.37525E+03	0.30002E+01
4195.00	0.34817E-01	0.14436E+04	0.17614E+03	0.24890E+03	0.35989E+03	0.31234E+01
4200.00	0.36868E-01	0.13146E+04	0.17638E+03	0.24546E+03	0.37062E+03	0.31567E+01
4205.00	0.34998E-01	0.16334E+04	0.12995E+03	0.22209E+03	0.34249E+03	0.34531E+01
4210.00	0.29200E-01	0.24738E+04	0.11530E+03	0.24731E+03	0.35400E+03	0.31511E+01
4215.00	0.11112E+00	0.17200E+04	0.29762E+02	0.27384E+03	0.14890E+03	0.19954E+01
4220.00	0.70183E-01	0.18451E+04	0.92253E+02	0.30245E+03	0.15453E+03	0.13646E+01
4225.00	0.28383E-01	0.15524E+04	0.18611E+03	0.27289E+03	0.30905E+03	0.27523E+01
4230.00	0.31531E-01	0.11853E+04	0.16961E+03	0.21796E+03	0.35687E+03	0.30141E+01
4235.00	0.35605E-01	0.11283E+04	0.14787E+03	0.21378E+03	0.38130E+03	0.36218E+01
4240.00	0.37026E-01	0.16406E+04	0.14901E+03	0.22908E+03	0.26124E+03	0.34616E+01
4245.00	0.30300E-01	0.24263E+04	0.15687E+03	0.27333E+03	0.23043E+03	0.28491E+01
4250.00	0.31623E-01	0.24606E+04	0.14093E+03	0.26037E+03	0.27129E+03	0.30458E+01
4255.00	0.32197E-01	0.28923E+04	0.12944E+03	0.23025E+03	0.25795E+03	0.30826E+01
4260.00	0.27293E-01	0.32285E+04	0.12478E+03	0.24109E+03	0.27141E+03	0.27983E+01
4265.00	0.25308E-01	0.27329E+04	0.13999E+03	0.22854E+03	0.33793E+03	0.29843E+01
4270.00	0.24996E-01	0.29035E+04	0.14739E+03	0.23974E+03	0.30275E+03	0.30561E+01
4275.00	0.21178E-01	0.29214E+04	0.13043E+03	0.20538E+03	0.30910E+03	0.26140E+01
4280.00	0.20233E-01	0.22300E+04	0.12974E+03	0.20224E+03	0.33883E+03	0.25070E+01
4285.00	0.21576E-01	0.19698E+04	0.14225E+03	0.21668E+03	0.29337E+03	0.26975E+01
4290.00	0.28032E-01	0.16108E+04	0.15686E+03	0.22213E+03	0.31983E+03	0.30491E+01
4295.00	0.31715E-01	0.13008E+04	0.13394E+03	0.24816E+03	0.35185E+03	0.36414E+01
4300.00	0.30659E-01	0.12351E+04	0.12914E+03	0.27449E+03	0.40983E+03	0.33260E+01
4305.00	0.28024E-01	0.17055E+04	0.12248E+03	0.24706E+03	0.40122E+03	0.28435E+01
4310.00	0.24613E-01	0.30615E+04	0.91458E+02	0.24560E+03	0.28954E+03	0.26310E+01
4315.00	0.66790E-01	0.17583E+04	0.66928E+02	0.23704E+03	0.14262E+03	0.12092E+01
4320.00	0.60041E-01	0.79214E+03	0.11964E+03	0.15530E+03	0.24699E+03	0.58643E+01
4325.00	0.38080E-01	0.25592E+03	0.20443E+03	0.23819E+03	0.26559E+03	0.27928E+01
4330.00	0.29237E-01	0.91519E+03	0.29543E+03	0.26479E+03	0.13154E+03	0.32063E+01
4335.00	0.24119E-01	0.17599E+04	0.21568E+03	0.30903E+03	0.10012E+03	0.24689E+01
4340.00	0.22053E-01	0.22498E+04	0.13658E+03	0.25245E+03	0.16600E+03	0.25168E+01
4345.00	0.21514E-01	0.25512E+04	0.10951E+03	0.21649E+03	0.17055E+03	0.25456E+01
4350.00	0.23030E-01	0.24820E+04	0.10798E+03	0.20863E+03	0.23206E+03	0.27350E+01
4355.00	0.24884E-01	0.24523E+04	0.85239E+02	0.22904E+03	0.28717E+03	0.34651E+01
4360.00	0.24716E-01	0.21785E+04	0.90988E+02	0.23643E+03	0.30556E+03	0.30423E+01
4365.00	0.26675E-01	0.18667E+04	0.10474E+03	0.24104E+03	0.31412E+03	0.30871E+01
4370.00	0.26964E-01	0.15140E+04	0.10997E+03	0.23217E+03	0.35899E+03	0.31325E+01
4375.00	0.26881E-01	0.14017E+04	0.13998E+03	0.25726E+03	0.32198E+03	0.28622E+01
4380.00	0.26938E-01	0.18716E+04	0.17038E+03	0.27517E+03	0.25633E+03	0.29239E+01
4385.00	0.28864E-01	0.13109E+04	0.16357E+03	0.21432E+03	0.34013E+03	0.31324E+01
4390.00	0.27139E-01	0.15921E+04	0.18763E+03	0.24473E+03	0.30892E+03	0.33815E+01
4395.00	0.27414E-01	0.15037E+04	0.19659E+03	0.26433E+03	0.26767E+03	0.29921E+01

continued opposite

Table 3—*continued*

4400.00	0.27457E-01	0.12231E+04	0.17057E+03	0.22127E+03	0.33137E+03	0.30693E+01
4405.00	0.25732E-01	0.16760E+04	0.15452E+03	0.24133E+03	0.30728E+03	0.30290E+01
4410.00	0.26456E-01	0.13338E+04	0.14633E+03	0.23510E+03	0.38333E+03	0.32139E+01
4415.00	0.28727E-01	0.12584E+04	0.15301E+03	0.23175E+03	0.41633E+03	0.32719E+01
4420.00	0.28072E-01	0.20622E+04	0.14381E+03	0.24755E+03	0.35470E+03	0.29744E+01
4425.00	0.27191E-01	0.15366E+04	0.13251E+03	0.21897E+03	0.43030E+03	0.33009E+01
4430.00	0.26887E-01	0.11639E+04	0.12305E+03	0.21148E+03	0.48502E+03	0.30226E+01
4435.00	0.26715E-01	0.15116E+04	0.10862E+03	0.22887E+03	0.43020E+03	0.28856E+01
4440.00	0.24227E-01	0.13086E+04	0.10748E+03	0.23364E+03	0.42779E+03	0.26827E+01
4445.00	0.22655E-01	0.11566E+04	0.10774E+03	0.21212E+03	0.46179E+03	0.27922E+01
4450.00	0.24601E-01	0.12631E+04	0.10704E+03	0.18835E+03	0.46807E+03	0.34289E+01
4455.00	0.26031E-01	0.13260E+04	0.12308E+03	0.17952E+03	0.47104E+03	0.32694E+01
4460.00	0.23685E-01	0.12820E+04	0.14649E+03	0.19221E+03	0.46905E+03	0.28272E+01
4465.00	0.23133E-01	0.11047E+04	0.15489E+03	0.20706E+03	0.43891E+03	0.27235E+01
4470.00	0.22219E-01	0.90504E+03	0.16158E+03	0.21299E+03	0.39664E+03	0.25574E+01
4475.00	0.23235E-01	0.93385E+03	0.17165E+03	0.18464E+03	0.40167E+03	0.23497E+01
4480.00	0.23189E-01	0.88105E+03	0.19548E+03	0.17503E+03	0.41367E+03	0.23199E+01
4485.00	0.22484E-01	0.72929E+03	0.19753E+03	0.16537E+03	0.45620E+03	0.21869E+01
4490.00	0.23571E-01	0.63993E+03	0.20563E+03	0.18457E+03	0.45175E+03	0.22686E+01
4495.00	0.23482E-01	0.46166E+03	0.21839E+03	0.17140E+03	0.43239E+03	0.21455E+01
4500.00	0.24028E-01	0.52479E+03	0.27188E+03	0.16174E+03	0.43302E+03	0.22279E+01
4505.00	0.25097E-01	0.47613E+03	0.22706E+03	0.16134E+03	0.47477E+03	0.22958E+01
4510.00	0.26458E-01	0.33172E+03	0.24212E+03	0.18247E+03	0.47531E+03	0.23301E+01
4515.00	0.28314E-01	0.26566E+03	0.24347E+03	0.16738E+03	0.58533E+03	0.24492E+01
4520.00	0.26852E-01	0.19542E+03	0.19424E+03	0.18193E+03	0.65272E+03	0.22891E+01
4525.00	0.29867E-01	0.14425E+03	0.14248E+03	0.19439E+03	0.64707E+03	0.25263E+01
4530.00	0.30555E-01	0.25158E+03	0.65661E+02	0.64587E+02	0.67996E+03	0.30122E+01
4535.00	0.29140E-01	0.78262E+03	0.56658E+02	0.57914E+02	0.43990E+03	0.29541E+01
4540.00	0.24762E-01	0.14923E+04	0.74714E+02	0.16946E+03	0.28179E+03	0.37608E+01
4545.00	0.25852E-01	0.17343E+04	0.94257E+02	0.20569E+03	0.30982E+03	0.35845E+01
4550.00	0.35315E-01	0.71677E+03	0.73283E+02	0.59154E+02	0.56445E+03	0.34490E+01
4555.00	0.27987E-01	0.15088E+03	0.12869E+03	0.14906E+03	0.66450E+03	0.25619E+01
4560.00	0.31128E-01	0.72158E+02	0.20123E+03	0.16842E+03	0.69434E+03	0.25450E+01
4565.00	0.32206E-01	0.63368E+02	0.33819E+03	0.20185E+03	0.57887E+03	0.22338E+01
4570.00	0.31975E-01	0.58123E+02	0.58014E+03	0.21586E+03	0.52570E+03	0.21617E+01
4575.00	0.32937E-01	0.10027E+03	0.77232E+03	0.19512E+03	0.53297E+03	0.26289E+01
4580.00	0.28920E-01	0.14233E+03	0.91392E+03	0.17486E+03	0.34136E+03	0.24587E+01
4585.00	0.26248E-01	0.81729E+02	0.95143E+03	0.25150E+03	0.28676E+03	0.20921E+01
4590.00	0.25073E-01	0.18341E+03	0.53902E+03	0.14877E+03	0.18372E+03	0.24398E+01
4595.00	0.24635E-01	0.14645E+03	0.32135E+03	0.11148E+03	0.15683E+03	0.24390E+01
4600.00	0.22573E-01	0.16892E+03	0.20857E+03	0.78998E+02	0.14016E+03	0.22293E+01
4605.00	0.21315E-01	0.18859E+03	0.19474E+03	0.96199E+02	0.17375E+03	0.22409E+01
4610.00	0.20732E-01	0.15658E+03	0.21475E+03	0.13643E+03	0.25360E+03	0.22438E+01
4615.00	0.22004E-01	0.19839E+03	0.20140E+03	0.12832E+03	0.29020E+03	0.24226E+01
4620.00	0.30349E-01	0.16923E+03	0.48701E+03	0.18536E+03	0.38019E+03	0.24943E+01
4625.00	0.34882E-01	0.28317E+03	0.81204E+03	0.20053E+03	0.36461E+03	0.24592E+01
4630.00	0.38949E-01	0.29517E+03	0.17607E+04	0.20492E+03	0.45432E+03	0.20211E+01
4635.00	0.30605E-01	0.20952E+03	0.12239E+04	0.18893E+03	0.50518E+03	0.22907E+01
4640.00	0.34248E-01	0.28317E+03	0.16175E+04	0.19941E+03	0.46282E+03	0.22507E+01
4645.00	0.30461E-01	0.22488E+03	0.21461E+04	0.21384E+03	0.54137E+03	0.21626E+01
4650.00	0.28285E-01	0.23209E+03	0.13676E+04	0.19704E+03	0.51376E+03	0.20678E+01
4655.00	0.27798E-01	0.18138E+03	0.15568E+04	0.19463E+03	0.58184E+03	0.20869E+01
4660.00	0.28050E-01	0.46576E+02	0.82847E+03	0.17577E+03	0.69458E+03	0.17394E+01
4665.00	0.31987E-01	0.13792E+03	0.16818E+04	0.17795E+03	0.69964E+03	0.19933E+01
4670.00	0.38179E-01	0.17731E+03	0.29431E+04	0.18882E+03	0.75681E+03	0.18041E+01
4675.00	0.31355E-01	0.50553E+02	0.12522E+04	0.18165E+03	0.81210E+03	0.16378E+01
4680.00	0.33707E-01	0.84133E+02	0.26026E+04	0.18842E+03	0.84084E+03	0.16472E+01
4685.00	0.26415E-01	0.16563E+02	0.56034E+03	0.16938E+03	0.89442E+03	0.11780E+01
4690.00	0.26940E-01	0.25937E+02	0.79323E+03	0.17701E+03	0.91815E+03	0.12760E+01
4695.00	0.27717E-01	0.15312E+02	0.62114E+03	0.16989E+03	0.97227E+03	0.11180E+01

continued overleaf

Table 3—*continued*

4700.00	0.29198E-01	0.11761E+02	0.69233E+03	0.16686E+03	0.10485E+04	0.90139E+00
4705.00	0.30344E-01	0.12164E+02	0.84418E+03	0.16564E+03	0.10665E+04	0.84751E+00
4710.00	0.31507E-01	0.11987E+02	0.90887E+03	0.16643E+03	0.11154E+04	0.80152E+00
4715.00	0.32338E-01	0.77148E+01	0.12697E+04	0.16949E+03	0.11504E+04	0.71284E+00
4720.00	0.32772E-01	0.67423E+01	0.97375E+03	0.16609E+03	0.12011E+04	0.69954E+00
4725.00	0.33613E-01	0.58285E+01	0.16293E+04	0.16966E+03	0.12827E+04	0.63207E+00
4730.00	0.34290E-01	0.46515E+01	0.19791E+04	0.17444E+03	0.11880E+04	0.46600E+00
4735.00	0.34136E-01	0.49323E+01	0.21712E+04	0.17818E+03	0.11991E+04	0.56887E+00
4740.00	0.35857E-01	0.42086E+01	0.43766E+04	0.16751E+03	0.10821E+04	0.42922E+00
4745.00	0.34420E-01	0.57557E+01	0.69809E+04	0.17969E+03	0.10887E+04	0.48059E+00
4750.00	0.31263E-01	0.42490E+02	0.41527E+05	0.14920E+03	0.10764E+04	0.60795E+00
4755.00	0.37697E-01	0.17423E+02	0.10825E+06	0.16647E+03	0.62419E+03	0.29543E+00
4760.00	0.33215E-01	0.24634E+02	0.80298E+05	0.16630E+03	0.93353E+03	0.35985E+00
4765.00	0.32683E-01	0.34401E+02	0.16739E+06	0.16612E+03	0.72450E+03	0.30907E+00
4770.00	0.42319E-01	0.40093E+00	0.21333E+04	0.17374E+03	0.33258E+03	0.19710E-02
4775.00	0.41680E-01	0.48029E+00	0.64521E+04	0.16863E+03	0.22751E+03	0.12490E+01
4780.00	0.31601E-01	0.27190E+02	0.23872E+06	0.16560E+03	0.66516E+03	0.25904E+00
4785.00	0.40986E-01	0.40201E+00	0.28526E+04	0.15258E+03	0.33321E+03	0.84786E+00
4790.00	0.41284E-01	0.25019E+00	0.30917E+04	0.15731E+03	0.17481E+03	0.22025E+01
4795.00	0.38422E-01	0.36060E+00	0.40475E+04	0.16395E+03	0.28271E+03	0.13291E+00
4800.00	0.37164E-01	0.37162E+00	0.50632E+04	0.15988E+03	0.21050E+03	0.26886E-01
4805.00	0.30343E-01	0.11486E+01	0.39559E+05	0.16545E+03	0.16167E+03	0.19107E+00
4810.00	0.34546E-01	0.47026E+00	0.73341E+04	0.15507E+03	0.22752E+03	0.11283E+00
4815.00	0.35240E-01	0.34022E+00	0.50210E+04	0.15389E+03	0.23227E+03	0.94594E+00
4820.00	0.32205E-01	0.23242E+00	0.81070E+04	0.15650E+03	0.15971E+03	0.39873E+00
4825.00	0.33292E-01	0.17043E+00	0.40429E+04	0.15232E+03	0.15969E+03	0.40375E-02
4830.00	0.32898E-01	0.18028E+00	0.36501E+04	0.14073E+03	0.16660E+03	0.10193E+01
4835.00	0.32070E-01	0.13004E+00	0.17600E+05	0.16372E+03	0.15056E+03	0.43863E+00
4840.00	0.25874E-01	0.34328E+01	0.32830E+06	0.16355E+03	0.15134E+03	0.11827E+00
4845.00	0.27731E-01	0.36162E+00	0.14735E+05	0.15908E+03	0.15077E+03	0.98271E-01
4850.00	0.26470E-01	0.27746E+00	0.13849E+05	0.16108E+03	0.13270E+03	0.13275E+00
4855.00	0.27642E-01	0.18165E+00	0.67663E+04	0.15987E+03	0.15060E+03	0.60802E-01
4860.00	0.27225E-01	0.17093E+00	0.64661E+04	0.16246E+03	0.15245E+03	0.19314E-01
4865.00	0.27413E-01	0.12373E+00	0.59160E+04	0.14908E+03	0.14064E+03	0.53094E+01
4870.00	0.26080E-01	0.16315E+00	0.61565E+04	0.15555E+03	0.17345E+03	0.31328E+00
4875.00	0.24179E-01	0.13956E+00	0.72325E+04	0.16145E+03	0.14036E+03	0.91452E-01
4880.00	0.23186E-01	0.18150E+00	0.89635E+04	0.15241E+03	0.14896E+03	0.19564E-01
4885.00	0.23052E-01	0.24103E+00	0.60945E+04	0.13320E+03	0.24196E+03	0.12853E-01
4890.00	0.22151E-01	0.22000E+00	0.50209E+04	0.14404E+03	0.31235E+03	0.19603E-01
4895.00	0.22273E-01	0.17421E+00	0.62561E+04	0.15146E+03	0.19865E+03	0.39199E-01
4900.00	0.21915E-01	0.16095E+00	0.76376E+04	0.14727E+03	0.16377E+03	0.99695E-01
4905.00	0.20629E-01	0.21345E+00	0.54137E+04	0.13848E+03	0.32218E+03	0.64699E-01
4910.00	0.16164E-01	0.10068E+02	0.18736E+06	0.16280E+03	0.51313E+03	0.41925E+00
4915.00	0.16478E-01	0.35874E+01	0.81699E+05	0.16119E+03	0.60200E+03	0.39424E+00
4920.00	0.21528E-01	0.12213E+00	0.50337E+04	0.15402E+03	0.19965E+03	0.10814E+00
4925.00	0.15782E-01	0.36154E+01	0.38883E+05	0.15969E+03	0.82628E+03	0.57113E+00
4930.00	0.15164E-01	0.21987E+01	0.24142E+05	0.16855E+03	0.87396E+03	0.52834E+00
4935.00	0.14841E-01	0.32460E+01	0.57528E+05	0.16328E+03	0.74782E+03	0.45974E+00
4940.00	0.14853E-01	0.28371E+01	0.33856E+05	0.16240E+03	0.81088E+03	0.61811E+00
4945.00	0.14192E-01	0.11492E+01	0.10297E+05	0.16081E+03	0.84304E+03	0.46013E+00
4950.00	0.13573E-01	0.28145E+01	0.31880E+05	0.17938E+03	0.91878E+03	0.61982E+00
4955.00	0.12806E-01	0.14805E+01	0.73804E+04	0.16379E+03	0.65388E+03	0.64777E+00
4960.00	0.12862E-01	0.12415E+01	0.48463E+04	0.15972E+03	0.62649E+03	0.62875E+00
4965.00	0.12965E-01	0.14134E+01	0.87600E+04	0.16948E+03	0.74774E+03	0.59180E+00
4970.00	0.12604E-01	0.19967E+01	0.16853E+05	0.16773E+03	0.77458E+03	0.66728E+00
4975.00	0.12296E-01	0.27036E+01	0.35787E+05	0.16303E+03	0.71156E+03	0.72884E+00
4980.00	0.12200E-01	0.98825E+00	0.36680E+04	0.15868E+03	0.54985E+03	0.64625E+00
4985.00	0.12114E-01	0.11365E+01	0.38908E+04	0.15860E+03	0.57535E+03	0.61546E+00
4990.00	0.11950E-01	0.93265E+00	0.79380E+04	0.15943E+03	0.72599E+03	0.53852E+00
4995.00	0.12419E-01	0.42500E+00	0.50467E+04	0.15820E+03	0.70203E+03	0.33364E+00

continued opposite

Table 3—*continued*

5000.00	0.11640E-01	0.10043E+01	0.25875E+04	0.16163E+03	0.45831E+03	0.78783E+00
5005.00	0.11090E-01	0.17837E+01	0.17542E+04	0.16475E+03	0.41495E+03	0.87707E+00
5010.00	0.12334E-01	0.14305E+01	0.41652E+04	0.16230E+03	0.54376E+03	0.64314E+00
5015.00	0.12803E-01	0.32333E+00	0.25772E+04	0.15731E+03	0.67770E+03	0.24687E+00
5020.00	0.11775E-01	0.86331E+00	0.33632E+04	0.15876E+03	0.47902E+03	0.80245E+00
5025.00	0.10982E-01	0.19491E+01	0.20820E+04	0.15913E+03	0.37935E+03	0.99961E+00
5030.00	0.11780E-01	0.14252E+01	0.22398E+04	0.15722E+03	0.42259E+03	0.81289E+00
5035.00	0.11915E-01	0.41805E+00	0.91986E+03	0.15595E+03	0.51563E+03	0.36951E+00
5040.00	0.11139E-01	0.12694E+01	0.24098E+04	0.15705E+03	0.38496E+03	0.97859E+00
5045.00	0.10620E-01	0.17676E+01	0.12262E+04	0.16298E+03	0.31458E+03	0.10496E+01
5050.00	0.11037E-01	0.11111E+01	0.10725E+04	0.15547E+03	0.37863E+03	0.84046E+00
5055.00	0.10790E-01	0.10233E+01	0.93583E+03	0.16059E+03	0.39672E+03	0.93217E+00
5060.00	0.10760E-01	0.12030E+01	0.87473E+03	0.16044E+03	0.32957E+03	0.11171E+01
5065.00	0.10662E-01	0.11306E+01	0.10922E+04	0.15969E+03	0.30909E+03	0.11390E+01
5070.00	0.10601E-01	0.98022E+00	0.94201E+03	0.15825E+03	0.38154E+03	0.10330E+01
5075.00	0.10480E-01	0.14441E+01	0.11398E+04	0.15674E+03	0.34150E+03	0.96242E+00
5080.00	0.99496E-02	0.15456E+01	0.69989E+03	0.15769E+03	0.33906E+03	0.10789E+01
5085.00	0.10477E-01	0.17218E+01	0.70072E+03	0.16024E+03	0.33263E+03	0.12655E+01
5090.00	0.10635E-01	0.19835E+01	0.70641E+03	0.16549E+03	0.24018E+03	0.14092E+01
5095.00	0.10779E-01	0.14162E+01	0.49728E+03	0.16113E+03	0.29182E+03	0.16996E+01
5100.00	0.97057E-02	0.16491E+01	0.48011E+03	0.16436E+03	0.30280E+03	0.13919E+01
5105.00	0.95962E-02	0.15782E+01	0.51864E+03	0.15349E+03	0.29156E+03	0.11517E+01
5110.00	0.95326E-02	0.15388E+01	0.52297E+03	0.15455E+03	0.28611E+03	0.11833E+01
5115.00	0.96671E-02	0.18952E+01	0.62796E+03	0.15825E+03	0.23942E+03	0.13996E+01
5120.00	0.10129E-01	0.13813E+01	0.62152E+03	0.16092E+03	0.32934E+03	0.13253E+01
5125.00	0.11154E-01	0.22331E+01	0.48815E+03	0.15157E+03	0.41110E+03	0.10650E+01
5130.00	0.85728E-02	0.38505E+01	0.30613E+03	0.14995E+03	0.29491E+03	0.14215E+01
5135.00	0.88292E-02	0.37541E+01	0.34880E+03	0.16117E+03	0.19348E+03	0.14889E+01
5140.00	0.91292E-02	0.25339E+01	0.51781E+03	0.16318E+03	0.19839E+03	0.13355E+01
5145.00	0.95542E-02	0.21165E+01	0.68499E+03	0.16342E+03	0.20305E+03	0.13331E+01
5150.00	0.94687E-02	0.19721E+01	0.73880E+03	0.15522E+03	0.23398E+03	0.12513E+01
5155.00	0.84631E-02	0.18915E+01	0.50042E+03	0.15280E+03	0.29570E+03	0.13181E+01
5160.00	0.83091E-02	0.21551E+01	0.33886E+03	0.15874E+03	0.29169E+03	0.14494E+01
5165.00	0.86550E-02	0.18862E+01	0.32158E+03	0.15806E+03	0.27346E+03	0.15917E+01
5170.00	0.81305E-02	0.23356E+01	0.24721E+03	0.15869E+03	0.29009E+03	0.16850E+01
5175.00	0.77375E-02	0.33330E+01	0.16205E+03	0.13858E+03	0.29149E+03	0.15168E+01
5180.00	0.96680E-02	0.27811E+01	0.28736E+03	0.14598E+03	0.30576E+03	0.12340E+01
5185.00	0.93883E-02	0.25955E+01	0.44306E+03	0.15962E+03	0.29211E+03	0.16031E+01
5190.00	0.93097E-02	0.42117E+01	0.38935E+03	0.16164E+03	0.23259E+03	0.16300E+01
5195.00	0.85612E-02	0.48519E+01	0.28363E+03	0.13858E+03	0.23339E+03	0.15404E+01
5200.00	0.86558E-02	0.55618E+01	0.99978E+02	0.55041E+02	0.25979E+03	0.13493E+01
5205.00	0.93131E-02	0.75785E+01	0.86694E+02	0.61756E+02	0.27872E+03	0.13090E+01
5210.00	0.15368E-01	0.56761E+01	0.30781E+03	0.14399E+03	0.31542E+03	0.12243E+01
5215.00	0.82839E-02	0.32102E+01	0.33283E+03	0.14845E+03	0.32588E+03	0.14308E+01
5220.00	0.80904E-02	0.38982E+01	0.33227E+03	0.15223E+03	0.30427E+03	0.14357E+01
5225.00	0.77910E-02	0.46659E+01	0.23713E+03	0.13618E+03	0.29399E+03	0.14173E+01
5230.00	0.84165E-02	0.55290E+01	0.17104E+03	0.90220E+02	0.31242E+03	0.13007E+01
5235.00	0.92163E-02	0.45793E+01	0.29180E+03	0.14629E+03	0.36173E+03	0.12870E+01
5240.00	0.77875E-02	0.41153E+01	0.23107E+03	0.16176E+03	0.33773E+03	0.14833E+01
5245.00	0.80583E-02	0.32845E+01	0.22766E+03	0.15690E+03	0.36639E+03	0.15286E+01
5250.00	0.84187E-02	0.30005E+01	0.20372E+03	0.15714E+03	0.40514E+03	0.15437E+01
5255.00	0.82274E-02	0.37206E+01	0.18754E+03	0.15731E+03	0.38741E+03	0.15407E+01
5260.00	0.89432E-02	0.29365E+01	0.21896E+03	0.15812E+03	0.44773E+03	0.16009E+01
5265.00	0.99273E-02	0.23378E+01	0.17628E+03	0.15718E+03	0.49908E+03	0.18254E+01
5270.00	0.89499E-02	0.32148E+01	0.17605E+03	0.14342E+03	0.45962E+03	0.13963E+01
5275.00	0.94854E-02	0.30389E+01	0.20828E+03	0.14362E+03	0.48172E+03	0.12884E+01
5280.00	0.10058E-01	0.22038E+01	0.20042E+03	0.15632E+03	0.52957E+03	0.16399E+01
5285.00	0.91077E-02	0.29543E+01	0.15353E+03	0.15689E+03	0.49965E+03	0.15246E+01
5290.00	0.87238E-02	0.32920E+01	0.12402E+03	0.15764E+03	0.54984E+03	0.16600E+01
5295.00	0.94900E-02	0.26076E+01	0.13954E+03	0.15722E+03	0.57883E+03	0.18631E+01

continued overleaf

Table 3—*continued*

5300.00	0.88571E-02	0.26410E+01	0.12710E+03	0.15718E+03	0.52228E+03	0.18093E+01
5305.00	0.93016E-02	0.29819E+01	0.12199E+03	0.16066E+03	0.55649E+03	0.21153E+01
5310.00	0.87885E-02	0.36486E+01	0.11747E+03	0.15711E+03	0.56054E+03	0.18038E+01
5315.00	0.81381E-02	0.38999E+01	0.10281E+03	0.15738E+03	0.53466E+03	0.17518E+01
5320.00	0.86146E-02	0.33390E+01	0.11620E+03	0.15697E+03	0.52942E+03	0.18558E+01
5325.00	0.86143E-02	0.35157E+01	0.12773E+03	0.15664E+03	0.54479E+03	0.17863E+01
5330.00	0.83225E-02	0.45062E+01	0.12801E+03	0.15071E+03	0.52923E+03	0.15752E+01
5335.00	0.82169E-02	0.50990E+01	0.12500E+03	0.15576E+03	0.55832E+03	0.16049E+01
5340.00	0.80685E-02	0.56023E+01	0.13011E+03	0.15945E+03	0.57336E+03	0.15917E+01
5345.00	0.76535E-02	0.60422E+01	0.12198E+03	0.17066E+03	0.48449E+03	0.15891E+01
5350.00	0.78480E-02	0.59175E+01	0.12696E+03	0.17180E+03	0.48396E+03	0.16038E+01
5355.00	0.73420E-02	0.73606E+01	0.14667E+03	0.17689E+03	0.47433E+03	0.15774E+01
5360.00	0.69567E-02	0.11205E+02	0.13591E+03	0.16819E+03	0.43776E+03	0.15179E+01
5365.00	0.79742E-02	0.10285E+02	0.12723E+03	0.11589E+03	0.44436E+03	0.15093E+01
5370.00	0.92186E-02	0.86492E+01	0.16767E+03	0.14361E+03	0.40166E+03	0.15655E+01
5375.00	0.96223E-02	0.11455E+02	0.18507E+03	0.16666E+03	0.34368E+03	0.15457E+01
5380.00	0.10231E-01	0.15051E+02	0.17462E+03	0.16699E+03	0.37430E+03	0.15293E+01
5385.00	0.10458E-01	0.14058E+02	0.14433E+03	0.16875E+03	0.43148E+03	0.15763E+01
5390.00	0.98033E-02	0.11452E+02	0.12456E+03	0.16894E+03	0.43567E+03	0.16394E+01
5395.00	0.10663E-01	0.13887E+02	0.12903E+03	0.16795E+03	0.38742E+03	0.15704E+01
5400.00	0.10342E-01	0.18028E+02	0.13714E+03	0.17586E+03	0.34573E+03	0.15411E+01
5405.00	0.89618E-02	0.19724E+02	0.10720E+03	0.17499E+03	0.37502E+03	0.15512E+01
5410.00	0.94992E-02	0.18593E+02	0.98688E+02	0.19887E+03	0.39058E+03	0.15280E+01
5415.00	0.10664E-01	0.17046E+02	0.98548E+02	0.15341E+03	0.36854E+03	0.15879E+01
5420.00	0.10685E-01	0.16444E+02	0.97729E+02	0.10509E+03	0.39891E+03	0.16118E+01
5425.00	0.12467E-01	0.24860E+02	0.11648E+03	0.11299E+03	0.39935E+03	0.16726E+01
5430.00	0.11265E-01	0.25856E+02	0.15305E+03	0.18203E+03	0.35485E+03	0.15217E+01
5435.00	0.10186E-01	0.24382E+02	0.10591E+03	0.15062E+03	0.39813E+03	0.15072E+01
5440.00	0.97218E-02	0.29471E+02	0.84347E+02	0.15155E+03	0.41754E+03	0.15775E+01
5445.00	0.10735E-01	0.32410E+02	0.10788E+03	0.16736E+03	0.41551E+03	0.16433E+01
5450.00	0.10710E-01	0.35234E+02	0.10348E+03	0.14315E+03	0.45398E+03	0.16267E+01
5455.00	0.96170E-02	0.29595E+02	0.10809E+03	0.15954E+03	0.47318E+03	0.14975E+01
5460.00	0.10474E-01	0.26594E+02	0.13771E+03	0.20169E+03	0.48243E+03	0.14072E+01
5465.00	0.11776E-01	0.24736E+02	0.15353E+03	0.16491E+03	0.46919E+03	0.15932E+01
5470.00	0.14922E-01	0.40339E+02	0.10812E+03	0.81829E+02	0.45091E+03	0.18371E+01
5475.00	0.12283E-01	0.43764E+02	0.13394E+03	0.15179E+03	0.44820E+03	0.16860E+01
5480.00	0.12599E-01	0.24791E+02	0.15893E+03	0.23737E+03	0.45339E+03	0.13493E+01
5485.00	0.16762E-01	0.39303E+02	0.15815E+03	0.15710E+03	0.45372E+03	0.18628E+01
5490.00	0.16887E-01	0.59588E+02	0.17722E+03	0.13210E+03	0.40350E+03	0.21064E+01
5495.00	0.18472E-01	0.52627E+02	0.13257E+03	0.91688E+02	0.38357E+03	0.21166E+01
5500.00	0.18137E-01	0.45792E+02	0.16671E+03	0.13716E+03	0.42290E+03	0.20896E+01
5505.00	0.13774E-01	0.29799E+02	0.13378E+03	0.17322E+03	0.42382E+03	0.16238E+01
5510.00	0.20245E-01	0.64373E+02	0.16270E+03	0.13535E+03	0.35713E+03	0.22753E+01
5515.00	0.17933E-01	0.75744E+02	0.19356E+03	0.12925E+03	0.30778E+03	0.21391E+01
5520.00	0.20146E-01	0.64328E+02	0.20623E+03	0.13424E+03	0.32014E+03	0.23214E+01
5525.00	0.22388E-01	0.47894E+02	0.20270E+03	0.14881E+03	0.35664E+03	0.21496E+01
5530.00	0.18940E-01	0.44885E+02	0.19561E+03	0.15282E+03	0.32505E+03	0.19397E+01
5535.00	0.17728E-01	0.69598E+02	0.17808E+03	0.13206E+03	0.26307E+03	0.21090E+01
5540.00	0.17722E-01	0.48331E+02	0.15946E+03	0.16083E+03	0.31811E+03	0.19364E+01
5545.00	0.21397E-01	0.58540E+02	0.14828E+03	0.14409E+03	0.34873E+03	0.22278E+01
5550.00	0.20681E-01	0.47676E+02	0.11040E+03	0.15352E+03	0.37360E+03	0.21973E+01
5555.00	0.19056E-01	0.46938E+02	0.93100E+02	0.14684E+03	0.34632E+03	0.21560E+01
5560.00	0.17522E-01	0.67724E+02	0.92331E+02	0.13397E+03	0.31695E+03	0.22311E+01
5565.00	0.15400E-01	0.73569E+02	0.87188E+02	0.13258E+03	0.37645E+03	0.20745E+01
5570.00	0.15514E-01	0.10886E+03	0.90452E+02	0.12680E+03	0.38447E+03	0.21012E+01
5575.00	0.16285E-01	0.17759E+03	0.89990E+02	0.13105E+03	0.32569E+03	0.21695E+01
5580.00	0.16739E-01	0.28811E+03	0.93361E+02	0.11708E+03	0.23391E+03	0.21893E+01
5585.00	0.20184E-01	0.28707E+03	0.92119E+02	0.86332E+02	0.17997E+03	0.23694E+01
5590.00	0.21460E-01	0.14270E+03	0.10310E+03	0.10070E+03	0.26440E+03	0.27567E+01
5595.00	0.18359E-01	0.84820E+02	0.10137E+03	0.16929E+03	0.30734E+03	0.21753E+01

continued opposite

Table 3—*continued*

5600.00	0.17449E-01	0.10832E+03	0.89448E+02	0.14824E+03	0.21937E+03	0.21343E+01
5605.00	0.16866E-01	0.97454E+02	0.10346E+03	0.14011E+03	0.13721E+03	0.22244E+01
5610.00	0.17735E-01	0.52624E+02	0.13870E+03	0.16585E+03	0.15916E+03	0.21167E+01
5615.00	0.17448E-01	0.40837E+02	0.14615E+03	0.16016E+03	0.17393E+03	0.19289E+01
5620.00	0.20167E-01	0.75891E+02	0.18304E+03	0.11388E+03	0.10142E+03	0.23545E+01
5625.00	0.18620E-01	0.93042E+02	0.19984E+03	0.15485E+03	0.93535E+02	0.22314E+01
5630.00	0.17905E-01	0.16192E+03	0.10790E+03	0.10706E+03	0.12180E+03	0.22072E+01
5635.00	0.17783E-01	0.18602E+03	0.76427E+02	0.13285E+03	0.20927E+03	0.22515E+01
5640.00	0.18005E-01	0.12643E+03	0.80576E+02	0.15491E+03	0.26763E+03	0.22449E+01
5645.00	0.19745E-01	0.12121E+03	0.11903E+03	0.16305E+03	0.23972E+03	0.24357E+01
5650.00	0.17635E-01	0.92325E+02	0.13051E+03	0.14875E+03	0.21952E+03	0.21893E+01
5655.00	0.17365E-01	0.88586E+02	0.11726E+03	0.12150E+03	0.24500E+03	0.21843E+01
5660.00	0.18688E-01	0.11217E+03	0.10337E+03	0.10708E+03	0.28540E+03	0.23070E+01
5665.00	0.16795E-01	0.97709E+02	0.11760E+03	0.13525E+03	0.30346E+03	0.20928E+01
5670.00	0.15830E-01	0.85066E+02	0.98823E+02	0.13837E+03	0.36296E+03	0.19592E+01
5675.00	0.13923E-01	0.73424E+02	0.73840E+02	0.12288E+03	0.42796E+03	0.18891E+01
5680.00	0.14312E-01	0.61927E+02	0.78246E+02	0.15889E+03	0.40907E+03	0.18171E+01
5685.00	0.16200E-01	0.64240E+02	0.71822E+02	0.16376E+03	0.42802E+03	0.19212E+01
5690.00	0.14127E-01	0.56776E+02	0.59392E+02	0.14232E+03	0.46479E+03	0.18999E+01
5695.00	0.16191E-01	0.65552E+02	0.71062E+02	0.14512E+03	0.40959E+03	0.19169E+01
5700.00	0.17640E-01	0.79265E+02	0.85300E+02	0.14484E+03	0.38732E+03	0.20092E+01
5705.00	0.15933E-01	0.60014E+02	0.80961E+02	0.15558E+03	0.42473E+03	0.19139E+01
5710.00	0.15761E-01	0.62060E+02	0.87912E+02	0.15613E+03	0.43896E+03	0.19796E+01
5715.00	0.16097E-01	0.79921E+02	0.86500E+02	0.13322E+03	0.39808E+03	0.21070E+01
5720.00	0.15681E-01	0.79584E+02	0.81904E+02	0.14195E+03	0.37645E+03	0.20843E+01
5725.00	0.17493E-01	0.84303E+02	0.12127E+03	0.15144E+03	0.43230E+03	0.21675E+01
5730.00	0.16461E-01	0.10010E+03	0.11143E+03	0.12911E+03	0.40804E+03	0.20570E+01
5735.00	0.15507E-01	0.95437E+02	0.10625E+03	0.15067E+03	0.37385E+03	0.20176E+01
5740.00	0.16911E-01	0.87679E+02	0.11764E+03	0.14977E+03	0.40884E+03	0.21299E+01
5745.00	0.18472E-01	0.11850E+03	0.99573E+02	0.13375E+03	0.38975E+03	0.21515E+01
5750.00	0.21549E-01	0.14985E+03	0.12645E+03	0.20024E+03	0.37013E+03	0.22958E+01
5755.00	0.21164E-01	0.12356E+03	0.92273E+02	0.15310E+03	0.41956E+03	0.22478E+01
5760.00	0.22129E-01	0.14465E+03	0.80253E+02	0.13240E+03	0.40954E+03	0.21833E+01
5765.00	0.23382E-01	0.16946E+03	0.81191E+02	0.15576E+03	0.37336E+03	0.21768E+01
5770.00	0.20910E-01	0.17092E+03	0.69680E+02	0.12795E+03	0.36218E+03	0.20880E+01
5775.00	0.21302E-01	0.23761E+03	0.75776E+02	0.13014E+03	0.31840E+03	0.21422E+01
5780.00	0.20836E-01	0.22632E+03	0.74833E+02	0.14084E+03	0.29931E+03	0.22522E+01
5785.00	0.20008E-01	0.22101E+03	0.84517E+02	0.13070E+03	0.24199E+03	0.22768E+01
5790.00	0.18397E-01	0.28290E+03	0.99381E+02	0.13875E+03	0.18739E+03	0.21995E+01
5795.00	0.17433E-01	0.25758E+03	0.12016E+03	0.16920E+03	0.15633E+03	0.21125E+01
5800.00	0.17794E-01	0.24541E+03	0.14481E+03	0.18489E+03	0.11819E+03	0.20583E+01
5805.00	0.17515E-01	0.22751E+03	0.17246E+03	0.16872E+03	0.96472E+02	0.20611E+01
5810.00	0.18036E-01	0.15989E+03	0.21291E+03	0.19252E+03	0.86910E+02	0.20909E+01
5815.00	0.18321E-01	0.10577E+03	0.21350E+03	0.20830E+03	0.13077E+03	0.21088E+01
5820.00	0.20469E-01	0.82562E+02	0.19418E+03	0.19341E+03	0.19451E+03	0.21503E+01
5825.00	0.21785E-01	0.72525E+02	0.16604E+03	0.17891E+03	0.25432E+03	0.22542E+01
5830.00	0.20309E-01	0.82675E+02	0.89645E+02	0.12967E+03	0.28200E+03	0.22445E+01
5835.00	0.22052E-01	0.13309E+03	0.89397E+02	0.16348E+03	0.24578E+03	0.23419E+01
5840.00	0.23478E-01	0.16275E+03	0.85192E+02	0.15241E+03	0.26572E+03	0.22377E+01
5845.00	0.23765E-01	0.18974E+03	0.10780E+03	0.14772E+03	0.20837E+03	0.23462E+01
5850.00	0.22014E-01	0.26757E+03	0.12092E+03	0.13622E+03	0.11956E+03	0.23684E+01
5855.00	0.21196E-01	0.35322E+03	0.81957E+02	0.11911E+03	0.18780E+03	0.23281E+01
5860.00	0.18256E-01	0.38138E+03	0.76211E+02	0.13489E+03	0.19688E+03	0.22260E+01
5865.00	0.17251E-01	0.29838E+03	0.72232E+02	0.13805E+03	0.22858E+03	0.22667E+01
5870.00	0.17440E-01	0.27610E+03	0.65780E+02	0.13725E+03	0.28076E+03	0.22842E+01
5875.00	0.17514E-01	0.29401E+03	0.68678E+02	0.14233E+03	0.32745E+03	0.22830E+01
5880.00	0.18418E-01	0.23227E+03	0.66057E+02	0.13739E+03	0.37141E+03	0.22700E+01
5885.00	0.18359E-01	0.16530E+03	0.63282E+02	0.12647E+03	0.36874E+03	0.21879E+01
5890.00	0.20479E-01	0.17677E+03	0.66902E+02	0.11282E+03	0.41347E+03	0.25436E+01
5895.00	0.22564E-01	0.14256E+03	0.69760E+02	0.96502E+02	0.43272E+03	0.27484E+01

continued overleaf

Table 3—*continued*

5900.00	0.23122E-01	0.14759E+03	0.91730E+02	0.10161E+03	0.38036E+03	0.26418E+01
5905.00	0.22881E-01	0.17676E+03	0.10643E+03	0.11634E+03	0.35182E+03	0.25524E+01
5910.00	0.21913E-01	0.13504E+03	0.98442E+02	0.11267E+03	0.36871E+03	0.23477E+01
5915.00	0.20744E-01	0.12469E+03	0.13422E+03	0.10708E+03	0.35637E+03	0.22769E+01
5920.00	0.18571E-01	0.90746E+02	0.14025E+03	0.13962E+03	0.35950E+03	0.19922E+01
5925.00	0.19406E-01	0.12122E+03	0.13475E+03	0.13890E+03	0.34666E+03	0.21756E+01
5930.00	0.19345E-01	0.10958E+03	0.13271E+03	0.16344E+03	0.35015E+03	0.22225E+01
5935.00	0.19372E-01	0.11000E+03	0.13276E+03	0.13047E+03	0.35544E+03	0.22256E+01
5940.00	0.21362E-01	0.87471E+02	0.15496E+03	0.13851E+03	0.40355E+03	0.22781E+01
5945.00	0.19701E-01	0.90372E+02	0.12540E+03	0.13186E+03	0.39395E+03	0.22668E+01
5950.00	0.21216E-01	0.87239E+02	0.14982E+03	0.13243E+03	0.39035E+03	0.23713E+01
5955.00	0.21046E-01	0.36129E+02	0.13282E+03	0.21000E+03	0.41801E+03	0.16169E+01
5960.00	0.22884E-01	0.74642E+02	0.12967E+03	0.11228E+03	0.35990E+03	0.25432E+01
5965.00	0.23379E-01	0.75318E+02	0.97362E+02	0.98024E+02	0.39013E+03	0.26878E+01
5970.00	0.23900E-01	0.63114E+02	0.11817E+03	0.15350E+03	0.38028E+03	0.23377E+01
5975.00	0.24735E-01	0.80383E+02	0.11337E+03	0.15206E+03	0.40578E+03	0.23799E+01
5980.00	0.22553E-01	0.81671E+02	0.73714E+02	0.12712E+03	0.47116E+03	0.22551E+01
5985.00	0.22294E-01	0.11185E+03	0.57779E+02	0.10666E+03	0.50661E+03	0.22506E+01
5990.00	0.19878E-01	0.16232E+03	0.51437E+02	0.81929E+02	0.57996E+03	0.23391E+01
5995.00	0.22043E-01	0.34272E+03	0.76801E+02	0.68780E+02	0.54588E+03	0.24538E+01
6000.00	0.30299E-01	0.11797E+04	0.16243E+03	0.13833E+03	0.34155E+03	0.27660E+01
6005.00	0.52838E-01	0.70518E+03	0.28159E+03	0.75442E+02	0.17014E+03	0.21860E+01
6010.00	0.23546E-01	0.44077E+02	0.24664E+03	0.22428E+03	0.21695E+03	0.17733E+01
6015.00	0.21082E-01	0.52842E+02	0.22401E+03	0.16410E+03	0.22277E+03	0.19136E+01
6020.00	0.23573E-01	0.48704E+02	0.25210E+03	0.14793E+03	0.29430E+03	0.20837E+01
6025.00	0.24620E-01	0.58142E+02	0.25177E+03	0.15072E+03	0.29472E+03	0.21351E+01
6030.00	0.26166E-01	0.63649E+02	0.16693E+03	0.17938E+03	0.43455E+03	0.20313E+01
6035.00	0.25975E-01	0.12849E+03	0.81687E+02	0.63272E+02	0.46458E+03	0.23111E+01
6040.00	0.18859E-01	0.16402E+03	0.10807E+03	0.85799E+02	0.25660E+03	0.20421E+01
6045.00	0.18397E-01	0.13655E+03	0.37696E+03	0.18061E+03	0.11799E+03	0.21533E+01
6050.00	0.26251E-01	0.10511E+03	0.52694E+03	0.16949E+03	0.16919E+03	0.24005E+01
6055.00	0.23014E-01	0.14436E+03	0.17706E+03	0.65222E+02	0.14547E+03	0.21528E+01
6060.00	0.18195E-01	0.19698E+03	0.12197E+03	0.12246E+03	0.13984E+03	0.21612E+01
6065.00	0.19330E-01	0.20220E+03	0.77054E+02	0.89906E+02	0.19429E+03	0.23023E+01
6070.00	0.22182E-01	0.15139E+03	0.81793E+02	0.77209E+02	0.26155E+03	0.25830E+01
6075.00	0.26292E-01	0.11548E+03	0.19999E+03	0.17413E+03	0.31379E+03	0.25767E+01
6080.00	0.27760E-01	0.11184E+03	0.30309E+03	0.17017E+03	0.33136E+03	0.25875E+01
6085.00	0.27973E-01	0.10273E+03	0.30362E+03	0.16445E+03	0.35007E+03	0.27912E+01
6090.00	0.25275E-01	0.10073E+03	0.33750E+03	0.14657E+03	0.35168E+03	0.24254E+01
6095.00	0.25349E-01	0.10613E+03	0.36105E+03	0.13341E+03	0.33456E+03	0.24190E+01
6100.00	0.21826E-01	0.14062E+03	0.30445E+03	0.11957E+03	0.32511E+03	0.23022E+01
6105.00	0.20064E-01	0.14714E+03	0.27136E+03	0.10015E+03	0.33920E+03	0.22455E+01
6110.00	0.20511E-01	0.25021E+03	0.22015E+03	0.59634E+02	0.30025E+03	0.22482E+01
6115.00	0.17967E-01	0.11879E+03	0.24926E+03	0.11494E+03	0.33313E+03	0.20014E+01
6120.00	0.15236E-01	0.16755E+03	0.12161E+03	0.57583E+02	0.35912E+03	0.18604E+01
6125.00	0.16216E-01	0.16974E+03	0.11448E+03	0.51799E+02	0.36397E+03	0.20128E+01
6130.00	0.17545E-01	0.11716E+03	0.18631E+03	0.78024E+02	0.40356E+03	0.21308E+01
6135.00	0.18509E-01	0.10257E+03	0.14019E+03	0.54639E+02	0.45977E+03	0.21224E+01
6140.00	0.15965E-01	0.84246E+02	0.13852E+03	0.71300E+02	0.48187E+03	0.19611E+01
6145.00	0.16004E-01	0.10563E+03	0.14235E+03	0.63385E+02	0.50307E+03	0.19035E+01
6150.00	0.16711E-01	0.71418E+02	0.11520E+03	0.58334E+02	0.53628E+03	0.19360E+01
6155.00	0.15694E-01	0.66964E+02	0.92269E+02	0.53767E+02	0.59973E+03	0.18454E+01
6160.00	0.13392E-01	0.52931E+02	0.12925E+03	0.89571E+02	0.62669E+03	0.16571E+01
6165.00	0.10105E-01	0.41159E+02	0.14135E+03	0.11373E+03	0.63632E+03	0.15321E+01
6170.00	0.11266E-01	0.35390E+02	0.11404E+03	0.72193E+02	0.65639E+03	0.15578E+01
6175.00	0.11809E-01	0.27924E+02	0.11669E+03	0.10217E+03	0.69759E+03	0.15335E+01
6180.00	0.12857E-01	0.27699E+02	0.86163E+02	0.62474E+02	0.72843E+03	0.14833E+01
6185.00	0.12517E-01	0.17594E+02	0.94336E+02	0.50536E+02	0.74922E+03	0.15668E+01
6190.00	0.10166E-01	0.14311E+02	0.13252E+03	0.10854E+03	0.71367E+03	0.16168E+01
6195.00	0.11578E-01	0.12199E+02	0.93105E+02	0.74400E+02	0.74703E+03	0.14957E+01

continued opposite

Table 3—*continued*

6200.00	0.14161E-01	0.78702E+01	0.13883E+03	0.11933E+03	0.79658E+03	0.16141E+01
6205.00	0.13232E-01	0.76493E+01	0.17146E+03	0.12088E+03	0.79703E+03	0.15674E+01
6210.00	0.14335E-01	0.56238E+01	0.16548E+03	0.12068E+03	0.85050E+03	0.16478E+01
6215.00	0.16628E-01	0.50196E+01	0.18396E+03	0.12063E+03	0.86807E+03	0.18173E+01
6220.00	0.15982E-01	0.46332E+01	0.21723E+03	0.12172E+03	0.89107E+03	0.17045E+01
6225.00	0.19835E-01	0.28450E+01	0.22878E+03	0.12397E+03	0.92400E+03	0.21523E+01
6230.00	0.20477E-01	0.30053E+01	0.25067E+03	0.13221E+03	0.98721E+03	0.21010E+01
6235.00	0.19545E-01	0.26016E+01	0.31398E+03	0.12333E+03	0.98000E+03	0.18232E+01
6240.00	0.22314E-01	0.15121E+01	0.38459E+03	0.13218E+03	0.98881E+03	0.29337E+01
6245.00	0.21738E-01	0.16806E+01	0.39907E+03	0.12943E+03	0.11025E+04	0.22800E+01
6250.00	0.20861E-01	0.15563E+01	0.47698E+03	0.12954E+03	0.11018E+04	0.20005E+01
6255.00	0.21306E-01	0.12564E+01	0.50175E+03	0.12889E+03	0.10733E+04	0.25918E+01
6260.00	0.20769E-01	0.11321E+01	0.60693E+03	0.12850E+03	0.11142E+04	0.18276E+01
6265.00	0.21066E-01	0.88894E+00	0.71118E+03	0.12836E+03	0.11388E+04	0.12470E+01
6270.00	0.21511E-01	0.74110E+00	0.83572E+03	0.12749E+03	0.10826E+04	0.10397E+01
6275.00	0.22877E-01	0.55238E+00	0.10015E+04	0.12388E+03	0.98761E+03	0.36234E+00
6280.00	0.23441E-01	0.47344E+00	0.13001E+04	0.12664E+03	0.89403E+03	0.23974E+00
6285.00	0.23298E-01	0.42529E+00	0.98654E+03	0.11560E+03	0.87748E+03	0.41950E+00
6290.00	0.25837E-01	0.30610E+00	0.14989E+04	0.12105E+03	0.63343E+03	0.37405E+00
6295.00	0.25634E-01	0.28449E+00	0.21929E+04	0.12874E+03	0.58239E+03	0.20532E+00
6300.00	0.24300E-01	0.28853E+00	0.13911E+04	0.13310E+03	0.62952E+03	0.67594E+00
6305.00	0.24628E-01	0.26576E+00	0.29334E+04	0.11924E+03	0.56094E+03	0.39049E-01
6310.00	0.25663E-01	0.26274E+00	0.58710E+04	0.12527E+03	0.42109E+03	0.10841E+00
6315.00	0.24018E-01	0.26719E+00	0.36697E+04	0.12501E+03	0.50600E+03	0.38089E-01
6320.00	0.24274E-01	0.26924E+00	0.52141E+04	0.12513E+03	0.43977E+03	0.12417E+00
6325.00	0.24730E-01	0.18979E+00	0.44371E+04	0.12461E+03	0.36941E+03	0.10481E+01
6330.00	0.24354E-01	0.27113E+00	0.77890E+04	0.12487E+03	0.38256E+03	0.37012E+00
6335.00	0.24255E-01	0.24170E+00	0.57760E+04	0.12508E+03	0.40124E+03	0.16776E+00
6340.00	0.23521E-01	0.23904E+00	0.57036E+04	0.12277E+03	0.40475E+03	0.16092E+00
6345.00	0.23753E-01	0.22947E+00	0.61139E+04	0.13454E+03	0.40792E+03	0.48975E+01
6350.00	0.23936E-01	0.18041E+00	0.38191E+04	0.11136E+03	0.37085E+03	0.10661E+01
6355.00	0.22933E-01	0.21050E+00	0.56702E+04	0.12302E+03	0.37447E+03	0.44247E+01
6360.00	0.22176E-01	0.23484E+00	0.59575E+04	0.13019E+03	0.40782E+03	0.43044E+00
6365.00	0.21559E-01	0.21521E+00	0.34106E+04	0.12380E+03	0.41034E+03	0.61420E-01
6370.00	0.19569E-01	0.23591E+00	0.19531E+04	0.12236E+03	0.46922E+03	0.47747E+00
6375.00	0.18491E-01	0.27196E+00	0.21327E+04	0.12364E+03	0.55209E+03	0.87064E+00
6380.00	0.18152E-01	0.30583E+00	0.31498E+04	0.12317E+03	0.55412E+03	0.15238E+01
6385.00	0.17802E-01	0.31899E+00	0.34574E+04	0.12304E+03	0.56284E+03	0.17494E+01
6390.00	0.17024E-01	0.35170E+00	0.34466E+04	0.12292E+03	0.53975E+03	0.27216E+01
6395.00	0.16588E-01	0.33358E+00	0.15138E+04	0.12297E+03	0.43479E+03	0.46147E+01
6400.00	0.16216E-01	0.33422E+00	0.14379E+04	0.11681E+03	0.47569E+03	0.42627E+01
6405.00	0.15884E-01	0.28354E+00	0.16657E+04	0.12276E+03	0.54098E+03	0.46373E+00
6410.00	0.15690E-01	0.27193E+00	0.17040E+04	0.12278E+03	0.55130E+03	0.31907E+00
6415.00	0.15591E-01	0.27289E+00	0.40489E+04	0.12361E+03	0.54172E+03	0.96884E+00
6420.00	0.16021E-01	0.25487E+00	0.64245E+04	0.12283E+03	0.42079E+03	0.88895E+00
6425.00	0.15041E-01	0.25435E+00	0.29917E+04	0.12259E+03	0.48061E+03	0.90311E+00
6430.00	0.14638E-01	0.26013E+00	0.20966E+04	0.12256E+03	0.50125E+03	0.47251E+00
6435.00	0.14793E-01	0.25168E+00	0.19179E+04	0.12917E+03	0.57746E+03	0.94881E-01
6440.00	0.15300E-01	0.20411E+00	0.22031E+04	0.12223E+03	0.52117E+03	0.27927E-01
6445.00	0.15917E-01	0.19046E+00	0.49527E+04	0.12245E+03	0.40332E+03	0.83375E-01
6450.00	0.13898E-01	0.21308E+00	0.57165E+04	0.12268E+03	0.53081E+03	0.27641E+00
6455.00	0.14233E-01	0.21040E+00	0.75972E+04	0.12110E+03	0.46176E+03	0.40809E+00
6460.00	0.14842E-01	0.19565E+00	0.26850E+04	0.12208E+03	0.51947E+03	0.77180E-03
6465.00	0.14579E-01	0.21102E+00	0.17389E+04	0.12174E+03	0.54336E+03	0.12518E-02
6470.00	0.14201E-01	0.20535E+00	0.18679E+04	0.12171E+03	0.51061E+03	0.48831E-04
6475.00	0.13686E-01	0.20250E+00	0.97603E+03	0.12106E+03	0.45761E+03	0.12486E-04
6480.00	0.13716E-01	0.20936E+00	0.81579E+03	0.12070E+03	0.50263E+03	0.12894E-02
6485.00	0.13970E-01	0.18175E+00	0.88561E+03	0.12074E+03	0.54993E+03	0.16370E-02
6490.00	0.13513E-01	0.20871E+00	0.79977E+03	0.13013E+03	0.51859E+03	0.23555E-02
6495.00	0.13288E-01	0.23220E+00	0.55130E+03	0.11979E+03	0.48557E+03	0.35915E-03

continued overleaf

Table 3—*continued*

6500.00	0.13382E-01	0.20129E+00	0.59273E+03	0.11980E+03	0.52635E+03	0.84636E-03
6505.00	0.13190E-01	0.21748E+00	0.42640E+03	0.11911E+03	0.51053E+03	0.12173E-01
6510.00	0.13094E-01	0.23577E+00	0.38604E+03	0.11877E+03	0.49785E+03	0.91511E-02
6515.00	0.13149E-01	0.22046E+00	0.31003E+03	0.11793E+03	0.52225E+03	0.58466E+00
6520.00	0.13418E-01	0.20371E+00	0.21168E+03	0.11787E+03	0.54647E+03	0.38042E+00
6525.00	0.13588E-01	0.18762E+00	0.23199E+03	0.12045E+03	0.56628E+03	0.25698E-02
6530.00	0.13198E-01	0.23926E+00	0.23764E+03	0.11811E+03	0.52152E+03	0.10403E-01
6535.00	0.13367E-01	0.30695E+00	0.10106E+03	0.11318E+03	0.43166E+03	0.76457E+00
6540.00	0.13369E-01	0.28417E+00	0.22665E+03	0.11644E+03	0.40419E+03	0.55659E+00
6545.00	0.13675E-01	0.24525E+00	0.16645E+03	0.11493E+03	0.46646E+03	0.19334E+00
6550.00	0.13459E-01	0.26840E+00	0.62412E+02	0.12911E+03	0.47988E+03	0.22864E+01
6555.00	0.13160E-01	0.29987E+00	0.75897E+02	0.12080E+03	0.44683E+03	0.80834E-01
6560.00	0.13310E-01	0.33920E+00	0.38329E+02	0.11121E+03	0.45010E+03	0.90756E-01
6565.00	0.13322E-01	0.33487E+00	0.31648E+02	0.11068E+03	0.43945E+03	0.13808E+00
6570.00	0.13184E-01	0.36602E+00	0.46292E+02	0.11134E+03	0.47029E+03	0.43397E+00
6575.00	0.12956E-01	0.41148E+00	0.42854E+02	0.11059E+03	0.48163E+03	0.24811E+01
6580.00	0.12811E-01	0.41570E+00	0.48384E+02	0.11098E+03	0.43439E+03	0.15495E+00
6585.00	0.12488E-01	0.48653E+00	0.47258E+02	0.12932E+03	0.43040E+03	0.32911E+00
6590.00	0.12693E-01	0.49975E+00	0.63762E+02	0.11168E+03	0.42498E+03	0.37916E+00
6595.00	0.12811E-01	0.49971E+00	0.63053E+02	0.11113E+03	0.45501E+03	0.40460E+00
6600.00	0.12492E-01	0.56829E+00	0.67637E+02	0.11176E+03	0.45586E+03	0.17637E+01
6605.00	0.12580E-01	0.59898E+00	0.11495E+03	0.11588E+03	0.37703E+03	0.81321E+01
6610.00	0.12136E-01	0.72091E+00	0.11888E+03	0.11262E+03	0.35937E+03	0.27524E+01
6615.00	0.12256E-01	0.67325E+00	0.85727E+02	0.11146E+03	0.38658E+03	0.12718E+01
6620.00	0.12846E-01	0.56983E+00	0.73719E+02	0.11045E+03	0.40216E+03	0.23313E+01
6625.00	0.12594E-01	0.67319E+00	0.10987E+03	0.11222E+03	0.38313E+03	0.22117E+01
6630.00	0.12185E-01	0.83076E+00	0.95457E+02	0.11170E+03	0.41707E+03	0.20704E+01
6635.00	0.12273E-01	0.89251E+00	0.80461E+02	0.11109E+03	0.39931E+03	0.16570E+01
6640.00	0.11895E-01	0.96084E+00	0.84488E+02	0.11119E+03	0.35563E+03	0.22209E+01
6645.00	0.12274E-01	0.88389E+00	0.89576E+02	0.11085E+03	0.36793E+03	0.21919E+01
6650.00	0.12862E-01	0.80231E+00	0.10121E+03	0.11152E+03	0.37391E+03	0.14322E+01
6655.00	0.12516E-01	0.86525E+00	0.98078E+02	0.11124E+03	0.40009E+03	0.20108E+01
6660.00	0.12642E-01	0.81308E+00	0.86716E+02	0.11085E+03	0.43781E+03	0.20208E+01
6665.00	0.12796E-01	0.84122E+00	0.82160E+02	0.12711E+03	0.48243E+03	0.10274E+01
6670.00	0.12582E-01	0.89636E+00	0.62635E+02	0.10923E+03	0.47196E+03	0.23896E+01
6675.00	0.12373E-01	0.94309E+00	0.74254E+02	0.11004E+03	0.38703E+03	0.25307E+01
6680.00	0.11625E-01	0.12726E+01	0.87120E+02	0.11034E+03	0.39003E+03	0.24075E+01
6685.00	0.10774E-01	0.15579E+01	0.89776E+02	0.10879E+03	0.42926E+03	0.17430E+01
6690.00	0.11007E-01	0.16061E+01	0.12844E+03	0.11147E+03	0.46260E+03	0.11118E+01
6695.00	0.12413E-01	0.12806E+01	0.21478E+03	0.11305E+03	0.50857E+03	0.74308E+00
6700.00	0.11835E-01	0.11338E+01	0.14242E+03	0.10631E+03	0.48631E+03	0.13477E+01
6705.00	0.10147E-01	0.16323E+01	0.10549E+03	0.11032E+03	0.43432E+03	0.16881E+01
6710.00	0.90032E-02	0.22439E+01	0.12304E+03	0.12507E+03	0.41015E+03	0.16068E+01
6715.00	0.90859E-02	0.22330E+01	0.10548E+03	0.12562E+03	0.43529E+03	0.16503E+01
6720.00	0.95727E-02	0.20784E+01	0.12480E+03	0.13208E+03	0.43318E+03	0.17504E+01
6725.00	0.87542E-02	0.28446E+01	0.17590E+03	0.12878E+03	0.36159E+03	0.16218E+01
6730.00	0.88482E-02	0.28508E+01	0.16165E+03	0.12341E+03	0.35306E+03	0.16335E+01
6735.00	0.88803E-02	0.29244E+01	0.14737E+03	0.12928E+03	0.35757E+03	0.16460E+01
6740.00	0.89184E-02	0.37856E+01	0.13710E+03	0.13001E+03	0.32105E+03	0.16453E+01
6745.00	0.95727E-02	0.34876E+01	0.14407E+03	0.12331E+03	0.33881E+03	0.16334E+01
6750.00	0.91948E-02	0.35776E+01	0.12979E+03	0.12368E+03	0.34061E+03	0.16390E+01
6755.00	0.80774E-02	0.52626E+01	0.10887E+03	0.13931E+03	0.31508E+03	0.15539E+01
6760.00	0.87052E-02	0.88545E+01	0.12288E+03	0.14001E+03	0.25706E+03	0.15190E+01
6765.00	0.94057E-02	0.78199E+01	0.12876E+03	0.11360E+03	0.22477E+03	0.14749E+01
6770.00	0.10867E-01	0.37242E+01	0.13126E+03	0.14775E+03	0.28063E+03	0.18070E+01
6775.00	0.10314E-01	0.35701E+01	0.12700E+03	0.12664E+03	0.26796E+03	0.16731E+01
6780.00	0.10499E-01	0.46803E+01	0.13740E+03	0.12279E+03	0.25108E+03	0.15788E+01
6785.00	0.10982E-01	0.61525E+01	0.13798E+03	0.13783E+03	0.23371E+03	0.15488E+01
6790.00	0.10526E-01	0.67046E+01	0.12633E+03	0.15459E+03	0.23750E+03	0.15447E+01
6795.00	0.91698E-02	0.78564E+01	0.96591E+02	0.11832E+03	0.24212E+03	0.14920E+01

continued opposite

Table 3—*continued*

6800.00	0.88489E-02	0.83519E+01	0.76852E+02	0.11258E+03	0.31603E+03	0.14728E+01
6805.00	0.84862E-02	0.63660E+01	0.72784E+02	0.14045E+03	0.42067E+03	0.14919E+01
6810.00	0.95765E-02	0.49352E+01	0.57270E+02	0.13377E+03	0.39126E+03	0.13957E+01
6815.00	0.11875E-01	0.39038E+01	0.56749E+02	0.12527E+03	0.32559E+03	0.16662E+01
6820.00	0.11607E-01	0.41802E+01	0.58718E+02	0.12516E+03	0.31397E+03	0.16272E+01
6825.00	0.10539E-01	0.42013E+01	0.48957E+02	0.12542E+03	0.33820E+03	0.14821E+01
6830.00	0.11263E-01	0.38112E+01	0.52260E+02	0.12517E+03	0.33360E+03	0.15031E+01
6835.00	0.10663E-01	0.39993E+01	0.50416E+02	0.12525E+03	0.30458E+03	0.15557E+01
6840.00	0.11060E-01	0.41629E+01	0.45569E+02	0.12539E+03	0.33526E+03	0.16196E+01
6845.00	0.10868E-01	0.52457E+01	0.71112E+02	0.13291E+03	0.32405E+03	0.15720E+01
6850.00	0.10158E-01	0.54600E+01	0.66705E+02	0.14286E+03	0.30987E+03	0.15432E+01
6855.00	0.10581E-01	0.50407E+01	0.53568E+02	0.13333E+03	0.30992E+03	0.16908E+01
6860.00	0.10521E-01	0.55005E+01	0.66468E+02	0.14194E+03	0.29362E+03	0.14607E+01
6865.00	0.10033E-01	0.58423E+01	0.62117E+02	0.14000E+03	0.31896E+03	0.15168E+01
6870.00	0.93403E-02	0.66517E+01	0.54273E+02	0.15202E+03	0.35280E+03	0.14812E+01
6875.00	0.94108E-02	0.69720E+01	0.49099E+02	0.14204E+03	0.32878E+03	0.15738E+01
6880.00	0.10035E-01	0.65902E+01	0.60839E+02	0.15237E+03	0.29445E+03	0.15475E+01
6885.00	0.98259E-02	0.72410E+01	0.58027E+02	0.15078E+03	0.27046E+03	0.15129E+01
6890.00	0.10009E-01	0.79185E+01	0.35928E+02	0.10467E+03	0.33260E+03	0.14734E+01
6895.00	0.10061E-01	0.75547E+01	0.45226E+02	0.11470E+03	0.37790E+03	0.15547E+01
6900.00	0.10969E-01	0.74045E+01	0.67905E+02	0.14985E+03	0.32265E+03	0.13804E+01
6905.00	0.10510E-01	0.85388E+01	0.71919E+02	0.16925E+03	0.32933E+03	0.15903E+01
6910.00	0.85380E-02	0.10930E+02	0.43623E+02	0.13734E+03	0.36029E+03	0.15579E+01
6915.00	0.89794E-02	0.11518E+02	0.45791E+02	0.16114E+03	0.39323E+03	0.15819E+01
6920.00	0.10361E-01	0.99809E+01	0.49131E+02	0.17098E+03	0.39891E+03	0.14556E+01
6925.00	0.10931E-01	0.94384E+01	0.50131E+02	0.16423E+03	0.41264E+03	0.16048E+01
6930.00	0.98459E-02	0.10469E+02	0.55886E+02	0.14348E+03	0.41127E+03	0.16950E+01
6935.00	0.92348E-02	0.13250E+02	0.51225E+02	0.12606E+03	0.37393E+03	0.16167E+01
6940.00	0.93522E-02	0.11489E+02	0.38422E+02	0.12046E+03	0.39812E+03	0.16241E+01
6945.00	0.94589E-02	0.11267E+02	0.35349E+02	0.11422E+03	0.41933E+03	0.16199E+01
6950.00	0.97239E-02	0.14763E+02	0.44843E+02	0.13480E+03	0.37303E+03	0.15389E+01
6955.00	0.10037E-01	0.16103E+02	0.45728E+02	0.12071E+03	0.37862E+03	0.15527E+01
6960.00	0.10169E-01	0.16638E+02	0.42590E+02	0.12040E+03	0.42583E+03	0.15850E+01
6965.00	0.95609E-02	0.15426E+02	0.46441E+02	0.14508E+03	0.43354E+03	0.15215E+01
6970.00	0.94608E-02	0.17105E+02	0.49730E+02	0.14436E+03	0.40637E+03	0.14766E+01
6975.00	0.10176E-01	0.21122E+02	0.51869E+02	0.14674E+03	0.38328E+03	0.14875E+01
6980.00	0.10562E-01	0.22812E+02	0.48922E+02	0.12739E+03	0.36747E+03	0.15647E+01
6985.00	0.10102E-01	0.22931E+02	0.48333E+02	0.13848E+03	0.34548E+03	0.15614E+01
6990.00	0.10097E-01	0.21871E+02	0.57483E+02	0.15793E+03	0.35703E+03	0.14994E+01
6995.00	0.13049E-01	0.28931E+02	0.58144E+02	0.11217E+03	0.34396E+03	0.18429E+01
7000.00	0.12476E-01	0.31294E+02	0.55906E+02	0.12665E+03	0.30563E+03	0.18984E+01
7005.00	0.10610E-01	0.29239E+02	0.63738E+02	0.18855E+03	0.33671E+03	0.15193E+01
7010.00	0.11903E-01	0.30562E+02	0.71516E+02	0.17931E+03	0.33675E+03	0.14724E+01
7015.00	0.12351E-01	0.32959E+02	0.66472E+02	0.15045E+03	0.27998E+03	0.15473E+01
7020.00	0.12367E-01	0.34267E+02	0.62057E+02	0.12891E+03	0.27238E+03	0.16700E+01
7025.00	0.11710E-01	0.30011E+02	0.57031E+02	0.13056E+03	0.29537E+03	0.15773E+01
7030.00	0.12504E-01	0.33111E+02	0.61960E+02	0.15547E+03	0.28989E+03	0.15212E+01
7035.00	0.13806E-01	0.31613E+02	0.59483E+02	0.12310E+03	0.29523E+03	0.16516E+01
7040.00	0.15659E-01	0.34764E+02	0.64444E+02	0.11829E+03	0.29734E+03	0.17216E+01
7045.00	0.16698E-01	0.42354E+02	0.78465E+02	0.14824E+03	0.27855E+03	0.17335E+01
7050.00	0.17191E-01	0.41960E+02	0.71256E+02	0.14974E+03	0.27077E+03	0.18162E+01
7055.00	0.16950E-01	0.44991E+02	0.63006E+02	0.11897E+03	0.27090E+03	0.20376E+01
7060.00	0.16856E-01	0.49144E+02	0.69356E+02	0.11774E+03	0.25590E+03	0.19790E+01
7065.00	0.16733E-01	0.53421E+02	0.61925E+02	0.13091E+03	0.25149E+03	0.20296E+01
7070.00	0.15627E-01	0.44624E+02	0.47134E+02	0.10338E+03	0.27292E+03	0.21156E+01
7075.00	0.15944E-01	0.47309E+02	0.51301E+02	0.10666E+03	0.24482E+03	0.20339E+01
7080.00	0.15497E-01	0.60357E+02	0.50143E+02	0.13050E+03	0.20713E+03	0.20465E+01
7085.00	0.15292E-01	0.61790E+02	0.45311E+02	0.14149E+03	0.24511E+03	0.20143E+01
7090.00	0.16074E-01	0.72518E+02	0.43031E+02	0.14585E+03	0.27231E+03	0.21372E+01
7095.00	0.17313E-01	0.11242E+03	0.42746E+02	0.11906E+03	0.21934E+03	0.24625E+01

continued overleaf

Table 3—*continued*

7100.00	0.18066E-01	0.11304E+03	0.44887E+02	0.10262E+03	0.19423E+03	0.26076E+01
7105.00	0.17283E-01	0.75092E+02	0.50118E+02	0.12579E+03	0.21363E+03	0.22215E+01
7110.00	0.17874E-01	0.76676E+02	0.51990E+02	0.13378E+03	0.19850E+03	0.20471E+01
7115.00	0.17782E-01	0.70486E+02	0.48263E+02	0.11811E+03	0.19594E+03	0.22121E+01
7120.00	0.18560E-01	0.59507E+02	0.59990E+02	0.13299E+03	0.20341E+03	0.21411E+01
7125.00	0.18983E-01	0.76891E+02	0.72186E+02	0.12877E+03	0.16181E+03	0.21949E+01
7130.00	0.17143E-01	0.94827E+02	0.56190E+02	0.13132E+03	0.15438E+03	0.21147E+01
7135.00	0.16828E-01	0.87517E+02	0.48767E+02	0.13620E+03	0.21520E+03	0.21116E+01
7140.00	0.17163E-01	0.90790E+02	0.44198E+02	0.12368E+03	0.26968E+03	0.22418E+01
7145.00	0.16751E-01	0.10212E+03	0.39432E+02	0.11673E+03	0.28021E+03	0.22362E+01
7150.00	0.17380E-01	0.10085E+03	0.44568E+02	0.12442E+03	0.25010E+03	0.21743E+01
7155.00	0.18552E-01	0.93031E+02	0.50083E+02	0.12664E+03	0.22071E+03	0.23380E+01
7160.00	0.18218E-01	0.66318E+02	0.51043E+02	0.13422E+03	0.24509E+03	0.23401E+01
7165.00	0.15956E-01	0.48278E+02	0.52178E+02	0.15900E+03	0.28342E+03	0.19745E+01
7170.00	0.16820E-01	0.55349E+02	0.58138E+02	0.14129E+03	0.26187E+03	0.19965E+01
7175.00	0.17896E-01	0.76470E+02	0.62277E+02	0.13967E+03	0.20786E+03	0.21330E+01
7180.00	0.17081E-01	0.77850E+02	0.57886E+02	0.13137E+03	0.19439E+03	0.20786E+01
7185.00	0.17157E-01	0.85589E+02	0.49036E+02	0.12103E+03	0.19355E+03	0.21315E+01
7190.00	0.19503E-01	0.98330E+02	0.48544E+02	0.14345E+03	0.21049E+03	0.21507E+01
7195.00	0.19847E-01	0.98188E+02	0.50653E+02	0.13821E+03	0.23908E+03	0.22093E+01
7200.00	0.18554E-01	0.89018E+02	0.41887E+02	0.12634E+03	0.26697E+03	0.22584E+01
7205.00	0.18914E-01	0.99008E+02	0.42485E+02	0.13090E+03	0.24765E+03	0.22238E+01
7210.00	0.19088E-01	0.10438E+03	0.45133E+02	0.13740E+03	0.25295E+03	0.21959E+01
7215.00	0.17457E-01	0.88602E+02	0.45393E+02	0.13052E+03	0.28145E+03	0.21445E+01
7220.00	0.17724E-01	0.96110E+02	0.47584E+02	0.12213E+03	0.26169E+03	0.22591E+01
7225.00	0.17332E-01	0.97646E+02	0.44995E+02	0.12394E+03	0.26590E+03	0.23241E+01
7230.00	0.16955E-01	0.10800E+03	0.42418E+02	0.11556E+03	0.28287E+03	0.23816E+01
7235.00	0.17167E-01	0.10764E+03	0.43380E+02	0.12134E+03	0.27927E+03	0.23173E+01
7240.00	0.16933E-01	0.10232E+03	0.46069E+02	0.11987E+03	0.25266E+03	0.21816E+01
7245.00	0.16318E-01	0.96759E+02	0.44742E+02	0.11872E+03	0.25057E+03	0.21733E+01
7250.00	0.16463E-01	0.88167E+02	0.45800E+02	0.12199E+03	0.27127E+03	0.21465E+01
7255.00	0.17487E-01	0.92786E+02	0.49538E+02	0.11540E+03	0.26273E+03	0.20785E+01
7260.00	0.16862E-01	0.88617E+02	0.46685E+02	0.12456E+03	0.25413E+03	0.20364E+01
7265.00	0.17347E-01	0.81600E+02	0.47669E+02	0.11792E+03	0.28776E+03	0.21417E+01
7270.00	0.18557E-01	0.76393E+02	0.50955E+02	0.12992E+03	0.30801E+03	0.20712E+01
7275.00	0.17933E-01	0.74245E+02	0.47409E+02	0.13626E+03	0.30083E+03	0.19907E+01
7280.00	0.17169E-01	0.79323E+02	0.43700E+02	0.12148E+03	0.31990E+03	0.20440E+01
7285.00	0.16890E-01	0.85820E+02	0.36968E+02	0.12618E+03	0.31337E+03	0.20358E+01
7290.00	0.17720E-01	0.95893E+02	0.35982E+02	0.12269E+03	0.28043E+03	0.22960E+01
7295.00	0.17237E-01	0.89036E+02	0.41491E+02	0.95399E+02	0.28585E+03	0.25777E+01
7300.00	0.14373E-01	0.58158E+02	0.45901E+02	0.11070E+03	0.30736E+03	0.21638E+01
7305.00	0.15115E-01	0.58659E+02	0.52124E+02	0.12215E+03	0.26914E+03	0.20050E+01
7310.00	0.15480E-01	0.63193E+02	0.57025E+02	0.12191E+03	0.21022E+03	0.20564E+01
7315.00	0.15109E-01	0.56961E+02	0.54439E+02	0.11275E+03	0.19218E+03	0.20570E+01
7320.00	0.15669E-01	0.70439E+02	0.50399E+02	0.10078E+03	0.18274E+03	0.22585E+01
7325.00	0.16105E-01	0.81174E+02	0.45589E+02	0.11602E+03	0.18252E+03	0.23172E+01
7330.00	0.15748E-01	0.72727E+02	0.46539E+02	0.12287E+03	0.20618E+03	0.21333E+01
7335.00	0.16698E-01	0.75011E+02	0.50910E+02	0.10088E+03	0.22521E+03	0.22137E+01
7340.00	0.18836E-01	0.77383E+02	0.52907E+02	0.91954E+02	0.23228E+03	0.24007E+01
7345.00	0.18168E-01	0.55459E+02	0.55845E+02	0.11225E+03	0.25991E+03	0.22694E+01
7350.00	0.17940E-01	0.56844E+02	0.51805E+02	0.11300E+03	0.23420E+03	0.20923E+01
7355.00	0.18831E-01	0.69544E+02	0.53819E+02	0.14147E+03	0.20843E+03	0.20115E+01
7360.00	0.18183E-01	0.66702E+02	0.48808E+02	0.14511E+03	0.24449E+03	0.20057E+01
7365.00	0.19943E-01	0.12269E+03	0.41649E+02	0.10419E+03	0.23127E+03	0.26389E+01
7370.00	0.18332E-01	0.12425E+03	0.40035E+02	0.12252E+03	0.22893E+03	0.25267E+01
7375.00	0.15912E-01	0.68417E+02	0.41153E+02	0.13110E+03	0.26567E+03	0.21178E+01
7380.00	0.16177E-01	0.58068E+02	0.46700E+02	0.11777E+03	0.28830E+03	0.21372E+01
7385.00	0.17967E-01	0.61259E+02	0.55258E+02	0.11946E+03	0.26283E+03	0.21458E+01
7390.00	0.18162E-01	0.71846E+02	0.60574E+02	0.13504E+03	0.26702E+03	0.21555E+01
7395.00	0.16137E-01	0.61213E+02	0.50855E+02	0.12046E+03	0.32617E+03	0.21116E+01

continued opposite

Table 3—*continued*

7400.00	0.14625E-01	0.55637E+02	0.50859E+02	0.13180E+03	0.33819E+03	0.19722E+01
7405.00	0.14293E-01	0.61956E+02	0.55482E+02	0.14038E+03	0.34091E+03	0.19368E+01
7410.00	0.13635E-01	0.52145E+02	0.62344E+02	0.11799E+03	0.34345E+03	0.18456E+01
7415.00	0.14487E-01	0.63379E+02	0.74075E+02	0.12244E+03	0.31581E+03	0.18804E+01
7420.00	0.14487E-01	0.73737E+02	0.72300E+02	0.13744E+03	0.29765E+03	0.19148E+01
7425.00	0.14717E-01	0.67599E+02	0.70865E+02	0.11764E+03	0.26712E+03	0.19690E+01
7430.00	0.14940E-01	0.64821E+02	0.66630E+02	0.11231E+03	0.25466E+03	0.20064E+01
7435.00	0.17298E-01	0.65049E+02	0.88522E+02	0.12838E+03	0.27143E+03	0.20440E+01
7440.00	0.18602E-01	0.66431E+02	0.10697E+03	0.14258E+03	0.25914E+03	0.20728E+01
7445.00	0.18951E-01	0.69801E+02	0.11203E+03	0.13286E+03	0.24260E+03	0.21543E+01
7450.00	0.19295E-01	0.73112E+02	0.13731E+03	0.13906E+03	0.23258E+03	0.21754E+01
7455.00	0.19103E-01	0.66042E+02	0.12315E+03	0.14748E+03	0.22734E+03	0.21582E+01
7460.00	0.20216E-01	0.52739E+02	0.99627E+02	0.97256E+02	0.26185E+03	0.22136E+01
7465.00	0.20758E-01	0.46021E+02	0.12100E+03	0.95883E+02	0.29919E+03	0.20736E+01
7470.00	0.20652E-01	0.43049E+02	0.12663E+03	0.10338E+03	0.29889E+03	0.19882E+01
7475.00	0.20511E-01	0.39136E+02	0.11140E+03	0.93898E+02	0.28316E+03	0.20055E+01
7480.00	0.19439E-01	0.31574E+02	0.95923E+02	0.94645E+02	0.33397E+03	0.18884E+01
7485.00	0.16459E-01	0.26992E+02	0.79034E+02	0.10508E+03	0.39286E+03	0.17632E+01
7490.00	0.14743E-01	0.25697E+02	0.58511E+02	0.10511E+03	0.40594E+03	0.16825E+01
7495.00	0.11604E-01	0.26431E+02	0.40730E+02	0.99288E+02	0.45273E+03	0.16668E+01
7500.00	0.11689E-01	0.29370E+02	0.39621E+02	0.11753E+03	0.53979E+03	0.17129E+01
7505.00	0.30844E-01	0.77124E+02	0.48649E+02	0.33543E+02	0.51633E+03	0.39387E+01
7510.00	0.26303E-01	0.20176E+03	0.44017E+02	0.28933E+02	0.29904E+03	0.38126E+01
7515.00	0.21232E-01	0.12205E+03	0.41499E+02	0.35775E+02	0.29255E+03	0.27843E+01
7520.00	0.18358E-01	0.42792E+02	0.56465E+02	0.60089E+02	0.40116E+03	0.18585E+01
7525.00	0.15666E-01	0.19056E+02	0.47555E+02	0.58822E+02	0.52952E+03	0.16587E+01
7530.00	0.15608E-01	0.10911E+02	0.99103E+02	0.12882E+03	0.46838E+03	0.17156E+01
7535.00	0.19300E-01	0.78532E+01	0.12413E+03	0.13647E+03	0.42031E+03	0.18580E+01
7540.00	0.19159E-01	0.92267E+01	0.15090E+03	0.12532E+03	0.34537E+03	0.17700E+01
7545.00	0.18073E-01	0.15693E+02	0.10407E+03	0.80887E+02	0.35633E+03	0.19158E+01
7550.00	0.22439E-01	0.22915E+02	0.76234E+02	0.56776E+02	0.38153E+03	0.19760E+01
7555.00	0.21971E-01	0.15722E+02	0.24466E+03	0.10101E+03	0.26387E+03	0.18735E+01
7560.00	0.24959E-01	0.23683E+02	0.65740E+03	0.11343E+03	0.21653E+03	0.21054E+01
7565.00	0.26318E-01	0.25059E+02	0.62634E+03	0.11220E+03	0.25148E+03	0.20024E+01
7570.00	0.21915E-01	0.16773E+02	0.38675E+03	0.95023E+02	0.30346E+03	0.19904E+01
7575.00	0.19981E-01	0.14287E+02	0.32610E+03	0.10944E+03	0.24368E+03	0.18578E+01
7580.00	0.14445E-01	0.99304E+01	0.20140E+03	0.15373E+03	0.21958E+03	0.16000E+01
7585.00	0.21210E-01	0.17701E+02	0.15240E+03	0.95927E+02	0.21814E+03	0.20454E+01
7590.00	0.22420E-01	0.17435E+02	0.71236E+02	0.29832E+02	0.28274E+03	0.18213E+01
7595.00	0.21810E-01	0.22350E+02	0.22030E+03	0.10044E+03	0.33695E+03	0.19214E+01
7600.00	0.25497E-01	0.20699E+02	0.36461E+03	0.10486E+03	0.40367E+03	0.18596E+01
7605.00	0.16635E-01	0.18385E+02	0.86778E+02	0.22929E+02	0.38124E+03	0.14965E+01
7610.00	0.25622E-01	0.19907E+02	0.37416E+03	0.92638E+02	0.41704E+03	0.17566E+01
7615.00	0.13681E-01	0.12538E+02	0.98340E+02	0.34166E+02	0.44437E+03	0.14672E+01
7620.00	0.10745E-01	0.15288E+02	0.11020E+03	0.65436E+02	0.43011E+03	0.15581E+01
7625.00	0.90602E-02	0.10901E+02	0.12943E+03	0.86123E+02	0.47463E+03	0.15461E+01
7630.00	0.89680E-02	0.11455E+02	0.13333E+03	0.10498E+03	0.48884E+03	0.15756E+01
7635.00	0.94686E-02	0.87755E+01	0.13353E+03	0.11218E+03	0.53604E+03	0.15368E+01
7640.00	0.10208E-01	0.68362E+01	0.12885E+03	0.12166E+03	0.60187E+03	0.15550E+01
7645.00	0.10506E-01	0.59646E+01	0.10816E+03	0.12482E+03	0.56467E+03	0.16219E+01
7650.00	0.13888E-01	0.44210E+01	0.11162E+03	0.95314E+02	0.58120E+03	0.14551E+01
7655.00	0.15492E-01	0.39505E+01	0.99310E+02	0.10971E+03	0.65593E+03	0.15358E+01
7660.00	0.13937E-01	0.37193E+01	0.80584E+02	0.11103E+03	0.59174E+03	0.18733E+01
7665.00	0.15902E-01	0.30024E+01	0.10268E+03	0.11069E+03	0.62383E+03	0.18332E+01
7670.00	0.17929E-01	0.24978E+01	0.11832E+03	0.95944E+02	0.72744E+03	0.15099E+01
7675.00	0.18376E-01	0.20572E+01	0.10391E+03	0.11064E+03	0.65480E+03	0.26712E+01
7680.00	0.18575E-01	0.18492E+01	0.10413E+03	0.94855E+02	0.69735E+03	0.18200E+01
7685.00	0.20475E-01	0.13131E+01	0.18241E+03	0.97904E+02	0.74690E+03	0.18336E+01
7690.00	0.19904E-01	0.13214E+01	0.20487E+03	0.98180E+02	0.69851E+03	0.19302E+01
7695.00	0.19372E-01	0.12077E+01	0.20441E+03	0.98312E+02	0.72490E+03	0.17055E+01

continued overleaf

Table 3—*continued*

7700.00	0.19982E-01	0.87639E+00	0.30978E+03	0.99703E+02	0.80022E+03	0.10364E+01
7705.00	0.19870E-01	0.82825E+00	0.36411E+03	0.99907E+02	0.80888E+03	0.10281E+01
7710.00	0.19167E-01	0.80392E+00	0.39376E+03	0.10008E+03	0.77648E+03	0.97901E+00
7715.00	0.19795E-01	0.62138E+00	0.52306E+03	0.10049E+03	0.84095E+03	0.32749E+00
7720.00	0.20096E-01	0.54473E+00	0.55710E+03	0.10184E+03	0.86159E+03	0.11694E+00
7725.00	0.19740E-01	0.57369E+00	0.56083E+03	0.10055E+03	0.87062E+03	0.20028E+00
7730.00	0.20583E-01	0.41253E+00	0.64557E+03	0.10030E+03	0.85065E+03	0.18052E-01
7735.00	0.21138E-01	0.30806E+00	0.59956E+03	0.10577E+03	0.73281E+03	0.62908E+00
7740.00	0.20997E-01	0.29017E+00	0.54589E+03	0.10013E+03	0.70259E+03	0.46897E-03
7745.00	0.22880E-01	0.23470E+00	0.15197E+04	0.10139E+03	0.54364E+03	0.18242E-02
7750.00	0.22955E-01	0.23215E+00	0.15509E+04	0.10139E+03	0.53396E+03	0.12283E-02
7755.00	0.18418E-01	0.30301E+00	0.14330E+04	0.10057E+03	0.77628E+03	0.34868E+00
7760.00	0.18721E-01	0.25841E+00	0.22838E+04	0.91824E+02	0.51866E+03	0.17284E-01
7765.00	0.19099E-01	0.25008E+00	0.30359E+04	0.10159E+03	0.49674E+03	0.17206E-02
7770.00	0.18893E-01	0.25330E+00	0.37602E+04	0.10191E+03	0.46116E+03	0.35760E-01
7775.00	0.18378E-01	0.24199E+00	0.34472E+04	0.10046E+03	0.48041E+03	0.62322E-02
7780.00	0.18090E-01	0.21275E+00	0.34803E+04	0.10116E+03	0.43306E+03	0.44362E-01
7785.00	0.17233E-01	0.23350E+00	0.33508E+04	0.93514E+02	0.41807E+03	0.89754E-01
7790.00	0.17121E-01	0.19886E+00	0.33947E+04	0.90175E+02	0.40799E+03	0.21087E+00
7795.00	0.16671E-01	0.29204E+00	0.80205E+04	0.10175E+03	0.40217E+03	0.42302E+00
7800.00	0.16293E-01	0.15250E+00	0.26321E+04	0.10788E+03	0.37896E+03	0.29921E-01
7805.00	0.16244E-01	0.15204E+00	0.20871E+04	0.10147E+03	0.38442E+03	0.76963E+01
7810.00	0.15470E-01	0.16906E+00	0.34762E+04	0.85374E+02	0.37637E+03	0.67863E-02
7815.00	0.15773E-01	0.17809E+00	0.33270E+04	0.93308E+02	0.48445E+03	0.68104E-01
7820.00	0.15147E-01	0.23204E+00	0.58181E+04	0.98597E+02	0.48361E+03	0.22665E-01
7825.00	0.14777E-01	0.26071E+00	0.72211E+04	0.94194E+02	0.47857E+03	0.18509E+00
7830.00	0.14172E-01	0.23032E+00	0.53903E+04	0.10149E+03	0.49126E+03	0.55575E-02
7835.00	0.14001E-01	0.22427E+00	0.51901E+04	0.10083E+03	0.50116E+03	0.15188E-01
7840.00	0.13526E-01	0.27947E+00	0.66238E+04	0.10119E+03	0.54226E+03	0.24273E+00
7845.00	0.11730E-01	0.40832E+00	0.45408E+04	0.10066E+03	0.78162E+03	0.13001E+01
7850.00	0.11537E-01	0.38312E+00	0.42727E+04	0.10058E+03	0.78125E+03	0.94293E+00
7855.00	0.11770E-01	0.30459E+00	0.42311E+04	0.10052E+03	0.72082E+03	0.35855E+00
7860.00	0.11187E-01	0.36750E+00	0.45832E+04	0.10047E+03	0.75098E+03	0.11382E+01
7865.00	0.11002E-01	0.39893E+00	0.47586E+04	0.10051E+03	0.75707E+03	0.14149E+01
7870.00	0.10718E-01	0.38763E+00	0.39110E+04	0.10028E+03	0.74992E+03	0.14967E+01
7875.00	0.10726E-01	0.35043E+00	0.44699E+04	0.10027E+03	0.76174E+03	0.12334E+01
7880.00	0.11215E-01	0.24315E+00	0.39233E+04	0.10075E+03	0.66065E+03	0.19699E+00
7885.00	0.10358E-01	0.35861E+00	0.41589E+04	0.99934E+02	0.70036E+03	0.14624E+01
7890.00	0.10179E-01	0.38051E+00	0.29963E+04	0.97393E+02	0.68119E+03	0.20567E+01
7895.00	0.10115E-01	0.34367E+00	0.29136E+04	0.99641E+02	0.74137E+03	0.12680E+01
7900.00	0.10174E-01	0.30366E+00	0.32546E+04	0.99728E+02	0.75076E+03	0.66856E+00
7905.00	0.10128E-01	0.26627E+00	0.34166E+04	0.99971E+02	0.71053E+03	0.21293E+00
7910.00	0.98440E-02	0.33540E+00	0.31716E+04	0.99369E+02	0.64995E+03	0.11593E+01
7915.00	0.13228E-01	0.19396E+00	0.51667E+03	0.98095E+02	0.37983E+03	0.96015E-03
7920.00	0.99917E-02	0.25508E+00	0.10432E+04	0.99000E+02	0.50510E+03	0.30359E-02
7925.00	0.94184E-02	0.31514E+00	0.22599E+04	0.99402E+02	0.64108E+03	0.69926E+00
7930.00	0.98808E-02	0.25562E+00	0.11344E+04	0.90910E+02	0.59641E+03	0.18065E-01
7935.00	0.97450E-02	0.25368E+00	0.11722E+04	0.98911E+02	0.62066E+03	0.37365E-02
7940.00	0.96339E-02	0.25869E+00	0.14135E+04	0.98996E+02	0.68061E+03	0.27084E-03
7945.00	0.97650E-02	0.26476E+00	0.97643E+03	0.89350E+02	0.64051E+03	0.24158E-01
7950.00	0.94643E-02	0.26878E+00	0.11571E+04	0.98715E+02	0.66506E+03	0.11502E-01
7955.00	0.91295E-02	0.30743E+00	0.20758E+04	0.98848E+02	0.78070E+03	0.53649E+00
7960.00	0.91496E-02	0.29043E+00	0.20479E+04	0.98950E+02	0.79069E+03	0.30509E+00
7965.00	0.94999E-02	0.25765E+00	0.10359E+04	0.89132E+02	0.66076E+03	0.12057E-01
7970.00	0.12482E-01	0.18524E+00	0.24409E+03	0.95823E+02	0.51926E+03	0.10997E-02
7975.00	0.12612E-01	0.21261E+00	0.34570E+03	0.96451E+02	0.48697E+03	0.19267E-02
7980.00	0.12760E-01	0.23925E+00	0.13440E+03	0.93592E+02	0.42710E+03	0.45127E-02
7985.00	0.12782E-01	0.26133E+00	0.12310E+03	0.92778E+02	0.43204E+03	0.63658E+00
7990.00	0.12751E-01	0.26050E+00	0.46158E+02	0.89871E+02	0.42496E+03	0.18531E+01
7995.00	0.12826E-01	0.26276E+00	0.66956E+02	0.91111E+02	0.44842E+03	0.95322E+00

continued opposite

Table 3—*continued*

8000.00	0.12703E-01	0.28103E+00	0.67575E+02	0.98946E+02	0.44749E+03	0.64629E-03
8005.00	0.12624E-01	0.30558E+00	0.16715E+03	0.86471E+02	0.39779E+03	0.13497E-01
8010.00	0.12528E-01	0.32104E+00	0.11615E+03	0.92293E+02	0.39984E+03	0.28454E+00
8015.00	0.12186E-01	0.36972E+00	0.80498E+02	0.90232E+02	0.43121E+03	0.92435E-02
8020.00	0.12320E-01	0.43148E+00	0.46790E+02	0.89187E+02	0.38612E+03	0.15832E+01
8025.00	0.12051E-01	0.47127E+00	0.40995E+02	0.89900E+02	0.34279E+03	0.73524E+00
8030.00	0.11997E-01	0.49667E+00	0.38257E+02	0.89259E+02	0.35685E+03	0.16355E+00
8035.00	0.11987E-01	0.50927E+00	0.50780E+02	0.98314E+02	0.35747E+03	0.39565E+00
8040.00	0.12324E-01	0.43710E+00	0.66898E+02	0.89963E+02	0.39542E+03	0.15215E+00
8045.00	0.12431E-01	0.45078E+00	0.71030E+02	0.90129E+02	0.39555E+03	0.92093E-01
8050.00	0.12029E-01	0.54036E+00	0.65297E+02	0.89914E+02	0.39086E+03	0.22014E+00
8055.00	0.12097E-01	0.54360E+00	0.79005E+02	0.90362E+02	0.39794E+03	0.29950E+00
8060.00	0.11884E-01	0.59236E+00	0.87679E+02	0.88425E+02	0.35179E+03	0.80130E+00
8065.00	0.11697E-01	0.64347E+00	0.65090E+02	0.89508E+02	0.34853E+03	0.22103E+01
8070.00	0.11703E-01	0.64546E+00	0.63669E+02	0.89678E+02	0.36737E+03	0.10604E+01
8075.00	0.11660E-01	0.67971E+00	0.94154E+02	0.91036E+02	0.38416E+03	0.58982E+00
8080.00	0.11266E-01	0.80987E+00	0.10028E+03	0.90324E+02	0.32757E+03	0.18934E+01
8085.00	0.10920E-01	0.87313E+00	0.71251E+02	0.89700E+02	0.30216E+03	0.16868E+01
8090.00	0.10813E-01	0.96811E+00	0.75970E+02	0.89271E+02	0.31970E+03	0.25276E+01
8095.00	0.10283E-01	0.13065E+01	0.59626E+02	0.89149E+02	0.29431E+03	0.14699E+01
8100.00	0.10726E-01	0.13466E+01	0.62375E+02	0.88339E+02	0.31742E+03	0.16479E+01
8105.00	0.11155E-01	0.10949E+01	0.68954E+02	0.89452E+02	0.38093E+03	0.14048E+01
8110.00	0.11015E-01	0.10815E+01	0.56457E+02	0.88815E+02	0.35691E+03	0.15169E+01
8115.00	0.10676E-01	0.11782E+01	0.52948E+02	0.90651E+02	0.31575E+03	0.31721E+01
8120.00	0.10300E-01	0.13606E+01	0.54354E+02	0.88618E+02	0.27794E+03	0.25242E+01
8125.00	0.99990E-02	0.15321E+01	0.57461E+02	0.10549E+03	0.25499E+03	0.19839E+01
8130.00	0.10444E-01	0.14471E+01	0.47672E+02	0.87909E+02	0.27742E+03	0.22010E+01
8135.00	0.10986E-01	0.13279E+01	0.52468E+02	0.88331E+02	0.29502E+03	0.15452E+01
8140.00	0.11394E-01	0.12606E+01	0.53748E+02	0.87440E+02	0.31916E+03	0.84426E+00
8145.00	0.11601E-01	0.11646E+01	0.41683E+02	0.87878E+02	0.34493E+03	0.10999E+01
8150.00	0.11957E-01	0.11021E+01	0.50786E+02	0.88327E+02	0.34742E+03	0.13745E+01
8155.00	0.12415E-01	0.10747E+01	0.59546E+02	0.88499E+02	0.38244E+03	0.95457E+00
8160.00	0.12351E-01	0.11752E+01	0.63037E+02	0.10558E+03	0.39498E+03	0.81702E+00
8165.00	0.12465E-01	0.11516E+01	0.59705E+02	0.88352E+02	0.39083E+03	0.73133E+00
8170.00	0.12763E-01	0.11494E+01	0.71770E+02	0.10498E+03	0.42020E+03	0.77174E+00
8175.00	0.13010E-01	0.11875E+01	0.73661E+02	0.88553E+02	0.44146E+03	0.78495E+00
8180.00	0.13566E-01	0.10785E+01	0.83383E+02	0.89303E+02	0.43724E+03	0.68149E+00
8185.00	0.13641E-01	0.11304E+01	0.66129E+02	0.88446E+02	0.44469E+03	0.95773E+00
8190.00	0.13128E-01	0.13629E+01	0.86456E+02	0.10426E+03	0.43338E+03	0.10695E+01
8195.00	0.13818E-01	0.12682E+01	0.10547E+03	0.10361E+03	0.45160E+03	0.93808E+00
8200.00	0.14472E-01	0.11515E+01	0.80567E+02	0.95904E+02	0.50939E+03	0.61330E+00
8205.00	0.14230E-01	0.13228E+01	0.80414E+02	0.10461E+03	0.47802E+03	0.10563E+01
8210.00	0.13402E-01	0.15778E+01	0.80336E+02	0.10477E+03	0.43637E+03	0.12174E+01
8215.00	0.12858E-01	0.17543E+01	0.62877E+02	0.10506E+03	0.44360E+03	0.13210E+01
8220.00	0.13002E-01	0.17623E+01	0.45172E+02	0.10559E+03	0.44333E+03	0.12344E+01
8225.00	0.12846E-01	0.18761E+01	0.46261E+02	0.10551E+03	0.45863E+03	0.13142E+01
8230.00	0.13673E-01	0.17732E+01	0.59958E+02	0.10509E+03	0.48490E+03	0.11141E+01
8235.00	0.13339E-01	0.20590E+01	0.64011E+02	0.10466E+03	0.44534E+03	0.11571E+01
8240.00	0.11206E-01	0.28025E+01	0.49147E+02	0.10528E+03	0.40782E+03	0.15003E+01
8245.00	0.11088E-01	0.29114E+01	0.54636E+02	0.10476E+03	0.40117E+03	0.14285E+01
8250.00	0.11848E-01	0.26767E+01	0.53749E+02	0.10471E+03	0.40443E+03	0.14904E+01
8255.00	0.11732E-01	0.29375E+01	0.47958E+02	0.10507E+03	0.40461E+03	0.16470E+01
8260.00	0.11275E-01	0.32817E+01	0.54080E+02	0.10472E+03	0.39157E+03	0.16863E+01
8265.00	0.11439E-01	0.33002E+01	0.52027E+02	0.10490E+03	0.39975E+03	0.17296E+01
8270.00	0.11805E-01	0.32329E+01	0.39755E+02	0.10524E+03	0.44113E+03	0.18700E+01
8275.00	0.10953E-01	0.37745E+01	0.36725E+02	0.10557E+03	0.43582E+03	0.16590E+01
8280.00	0.94688E-02	0.46974E+01	0.36290E+02	0.11394E+03	0.39443E+03	0.20143E+01
8285.00	0.92200E-02	0.49855E+01	0.37791E+02	0.12457E+03	0.38934E+03	0.16988E+01
8290.00	0.94281E-02	0.52602E+01	0.38889E+02	0.12455E+03	0.40074E+03	0.16151E+01
8295.00	0.86150E-02	0.58829E+01	0.38975E+02	0.14376E+03	0.38915E+03	0.15743E+01

continued overleaf

Table 3—*continued*

8300.00	0.83334E-02	0.61378E+01	0.33632E+02	0.14428E+03	0.36448E+03	0.13908E+01
8305.00	0.83262E-02	0.68152E+01	0.44526E+02	0.15195E+03	0.35782E+03	0.14400E+01
8310.00	0.82281E-02	0.79162E+01	0.48625E+02	0.13757E+03	0.33865E+03	0.15518E+01
8315.00	0.79220E-02	0.78816E+01	0.40146E+02	0.12802E+03	0.31923E+03	0.15385E+01
8320.00	0.77105E-02	0.82576E+01	0.46469E+02	0.14871E+03	0.31040E+03	0.14878E+01
8325.00	0.82770E-02	0.86982E+01	0.58229E+02	0.15777E+03	0.29928E+03	0.15873E+01
8330.00	0.79448E-02	0.95681E+01	0.54228E+02	0.14885E+03	0.29716E+03	0.15944E+01
8335.00	0.77530E-02	0.85624E+01	0.50267E+02	0.13764E+03	0.30755E+03	0.16202E+01
8340.00	0.79949E-02	0.88580E+01	0.48826E+02	0.12217E+03	0.32006E+03	0.16185E+01
8345.00	0.77922E-02	0.91836E+01	0.56805E+02	0.16873E+03	0.33074E+03	0.16642E+01
8350.00	0.84823E-02	0.92446E+01	0.55885E+02	0.15883E+03	0.30388E+03	0.17269E+01
8355.00	0.87300E-02	0.11545E+02	0.54581E+02	0.13676E+03	0.28045E+03	0.17158E+01
8360.00	0.78694E-02	0.11531E+02	0.48855E+02	0.14639E+03	0.27379E+03	0.17132E+01
8365.00	0.78505E-02	0.11585E+02	0.47801E+02	0.16309E+03	0.26696E+03	0.15910E+01
8370.00	0.82033E-02	0.11789E+02	0.44712E+02	0.14766E+03	0.26440E+03	0.15694E+01
8375.00	0.86465E-02	0.12925E+02	0.46651E+02	0.14532E+03	0.25475E+03	0.15281E+01
8380.00	0.86347E-02	0.13914E+02	0.41874E+02	0.14724E+03	0.25036E+03	0.14555E+01
8385.00	0.91089E-02	0.16295E+02	0.34460E+02	0.13581E+03	0.24488E+03	0.14751E+01
8390.00	0.95243E-02	0.17385E+02	0.32686E+02	0.14547E+03	0.26598E+03	0.14828E+01
8395.00	0.89661E-02	0.16712E+02	0.29143E+02	0.15279E+03	0.31257E+03	0.14520E+01
8400.00	0.89900E-02	0.16904E+02	0.31612E+02	0.15187E+03	0.34158E+03	0.15653E+01
8405.00	0.90529E-02	0.18695E+02	0.28952E+02	0.11375E+03	0.33519E+03	0.17943E+01
8410.00	0.95679E-02	0.23453E+02	0.30547E+02	0.12101E+03	0.28967E+03	0.19043E+01
8415.00	0.12125E-01	0.28780E+02	0.37746E+02	0.13024E+03	0.25084E+03	0.20007E+01
8420.00	0.13376E-01	0.33183E+02	0.38427E+02	0.11378E+03	0.24990E+03	0.24276E+01
8425.00	0.12660E-01	0.23554E+02	0.29850E+02	0.82779E+02	0.29113E+03	0.25118E+01
8430.00	0.10165E-01	0.18577E+02	0.32787E+02	0.12865E+03	0.29051E+03	0.19036E+01
8435.00	0.98931E-02	0.20429E+02	0.33348E+02	0.12973E+03	0.26953E+03	0.18562E+01
8440.00	0.92191E-02	0.19483E+02	0.28772E+02	0.13635E+03	0.29810E+03	0.17757E+01
8445.00	0.96741E-02	0.20850E+02	0.25781E+02	0.13414E+03	0.29868E+03	0.18689E+01
8450.00	0.96358E-02	0.20292E+02	0.25223E+02	0.14916E+03	0.32813E+03	0.15740E+01
8455.00	0.11705E-01	0.22915E+02	0.30288E+02	0.14802E+03	0.34723E+03	0.16005E+01
8460.00	0.12252E-01	0.24217E+02	0.30275E+02	0.13750E+03	0.33441E+03	0.16902E+01
8465.00	0.11104E-01	0.23649E+02	0.25862E+02	0.14193E+03	0.35337E+03	0.15479E+01
8470.00	0.12390E-01	0.28112E+02	0.31014E+02	0.15202E+03	0.34521E+03	0.15511E+01
8475.00	0.11488E-01	0.29982E+02	0.31517E+02	0.14947E+03	0.34969E+03	0.16339E+01
8480.00	0.10212E-01	0.29609E+02	0.28214E+02	0.14354E+03	0.38056E+03	0.16626E+01
8485.00	0.10715E-01	0.33217E+02	0.30136E+02	0.14299E+03	0.37894E+03	0.17938E+01
8490.00	0.10176E-01	0.32960E+02	0.28614E+02	0.14865E+03	0.37467E+03	0.19958E+01
8495.00	0.90745E-02	0.33393E+02	0.26039E+02	0.14007E+03	0.39618E+03	0.23162E+01
8500.00	0.93494E-02	0.35521E+02	0.28045E+02	0.13216E+03	0.38646E+03	0.23751E+01
8505.00	0.10196E-01	0.38448E+02	0.28258E+02	0.12739E+03	0.37066E+03	0.25760E+01
8510.00	0.10213E-01	0.41105E+02	0.29126E+02	0.14022E+03	0.36292E+03	0.25223E+01
8515.00	0.10572E-01	0.42397E+02	0.31734E+02	0.13827E+03	0.33440E+03	0.24245E+01
8520.00	0.10677E-01	0.46301E+02	0.30220E+02	0.14038E+03	0.31970E+03	0.24158E+01
8525.00	0.11339E-01	0.46518E+02	0.31126E+02	0.14347E+03	0.30092E+03	0.22912E+01
8530.00	0.13627E-01	0.50281E+02	0.36977E+02	0.12996E+03	0.27292E+03	0.22830E+01
8535.00	0.13938E-01	0.52040E+02	0.38263E+02	0.12399E+03	0.26172E+03	0.23207E+01
8540.00	0.14807E-01	0.54876E+02	0.38786E+02	0.12663E+03	0.26383E+03	0.23140E+01
8545.00	0.17372E-01	0.66215E+02	0.41555E+02	0.12383E+03	0.23527E+03	0.25007E+01
8550.00	0.17240E-01	0.66342E+02	0.41112E+02	0.12610E+03	0.21060E+03	0.25421E+01
8555.00	0.16665E-01	0.60019E+02	0.47637E+02	0.13382E+03	0.21433E+03	0.23137E+01
8560.00	0.16610E-01	0.62340E+02	0.47530E+02	0.13327E+03	0.19761E+03	0.22012E+01
8565.00	0.17392E-01	0.74821E+02	0.44867E+02	0.13708E+03	0.17913E+03	0.23073E+01
8570.00	0.17855E-01	0.77432E+02	0.43409E+02	0.14174E+03	0.20042E+03	0.24994E+01
8575.00	0.17021E-01	0.74628E+02	0.38572E+02	0.13671E+03	0.22987E+03	0.25888E+01
8580.00	0.16281E-01	0.86054E+02	0.32254E+02	0.12845E+03	0.25826E+03	0.26778E+01
8585.00	0.15921E-01	0.10318E+03	0.28945E+02	0.13248E+03	0.25439E+03	0.29673E+01
8590.00	0.15686E-01	0.10307E+03	0.32422E+02	0.13966E+03	0.20592E+03	0.26933E+01
8595.00	0.16104E-01	0.10547E+03	0.31809E+02	0.13204E+03	0.18243E+03	0.27205E+01

continued opposite

Table 3—*continued*

8600.00	0.17298E-01	0.12670E+03	0.34793E+02	0.12517E+03	0.13870E+03	0.28541E+01
8605.00	0.17365E-01	0.13213E+03	0.42002E+02	0.13090E+03	0.94614E+02	0.25685E+01
8610.00	0.17217E-01	0.95166E+02	0.44958E+02	0.11457E+03	0.10727E+03	0.25929E+01
8615.00	0.17990E-01	0.74183E+02	0.44799E+02	0.12586E+03	0.13435E+03	0.24115E+01
8620.00	0.18280E-01	0.68911E+02	0.40555E+02	0.12395E+03	0.16138E+03	0.26506E+01
8625.00	0.17071E-01	0.52524E+02	0.38095E+02	0.13480E+03	0.19992E+03	0.25004E+01
8630.00	0.17323E-01	0.50602E+02	0.37905E+02	0.12759E+03	0.23585E+03	0.24518E+01
8635.00	0.17758E-01	0.63282E+02	0.37364E+02	0.12031E+03	0.22718E+03	0.25699E+01
8640.00	0.19238E-01	0.91866E+02	0.40453E+02	0.13695E+03	0.18416E+03	0.25133E+01
8645.00	0.18474E-01	0.10513E+03	0.40008E+02	0.13761E+03	0.15596E+03	0.24368E+01
8650.00	0.16761E-01	0.10111E+03	0.36900E+02	0.13530E+03	0.14726E+03	0.25552E+01
8655.00	0.16671E-01	0.10759E+03	0.36764E+02	0.12833E+03	0.16526E+03	0.27491E+01
8660.00	0.16614E-01	0.10212E+03	0.37733E+02	0.12675E+03	0.19719E+03	0.27339E+01
8665.00	0.15249E-01	0.89070E+02	0.32077E+02	0.13120E+03	0.23325E+03	0.26881E+01
8670.00	0.15404E-01	0.90101E+02	0.32977E+02	0.12696E+03	0.26115E+03	0.27987E+01
8675.00	0.15213E-01	0.84960E+02	0.33261E+02	0.12542E+03	0.29237E+03	0.27374E+01
8680.00	0.13394E-01	0.74365E+02	0.28529E+02	0.13100E+03	0.33116E+03	0.25027E+01
8685.00	0.12781E-01	0.66108E+02	0.24573E+02	0.13654E+03	0.34982E+03	0.25295E+01
8690.00	0.12662E-01	0.57914E+02	0.22520E+02	0.13055E+03	0.38243E+03	0.24389E+01
8695.00	0.12300E-01	0.55462E+02	0.22003E+02	0.14487E+03	0.40358E+03	0.22187E+01
8700.00	0.12665E-01	0.52308E+02	0.20995E+02	0.14341E+03	0.40917E+03	0.22576E+01
8705.00	0.11816E-01	0.43489E+02	0.20591E+02	0.13814E+03	0.42443E+03	0.22625E+01
8710.00	0.11468E-01	0.39870E+02	0.21071E+02	0.14529E+03	0.43306E+03	0.20592E+01
8715.00	0.11335E-01	0.36767E+02	0.21412E+02	0.14980E+03	0.42635E+03	0.18768E+01
8720.00	0.10640E-01	0.32533E+02	0.20992E+02	0.14272E+03	0.41579E+03	0.20752E+01
8725.00	0.10630E-01	0.30548E+02	0.24024E+02	0.13388E+03	0.41533E+03	0.21446E+01
8730.00	0.11091E-01	0.30392E+02	0.28309E+02	0.12914E+03	0.38452E+03	0.23446E+01
8735.00	0.12039E-01	0.29834E+02	0.32891E+02	0.13254E+03	0.37681E+03	0.23234E+01
8740.00	0.12115E-01	0.28302E+02	0.38085E+02	0.14641E+03	0.35106E+03	0.21035E+01
8745.00	0.11901E-01	0.28937E+02	0.38975E+02	0.12674E+03	0.29839E+03	0.22302E+01
8750.00	0.12679E-01	0.25145E+02	0.37960E+02	0.99012E+02	0.30656E+03	0.22487E+01
8755.00	0.12705E-01	0.20973E+02	0.44918E+02	0.12126E+03	0.30570E+03	0.19192E+01
8760.00	0.14652E-01	0.21682E+02	0.58057E+02	0.12075E+03	0.26998E+03	0.18741E+01
8765.00	0.13684E-01	0.19175E+02	0.53902E+02	0.12531E+03	0.25774E+03	0.17711E+01
8770.00	0.14483E-01	0.19490E+02	0.41567E+02	0.97644E+02	0.26435E+03	0.18382E+01
8775.00	0.15237E-01	0.21445E+02	0.44464E+02	0.10268E+03	0.29005E+03	0.17938E+01
8780.00	0.13396E-01	0.21527E+02	0.41900E+02	0.12865E+03	0.32415E+03	0.15711E+01
8785.00	0.13463E-01	0.26927E+02	0.36213E+02	0.11987E+03	0.32880E+03	0.17122E+01
8790.00	0.14034E-01	0.33134E+02	0.38502E+02	0.11721E+03	0.29797E+03	0.18971E+01
8795.00	0.15816E-01	0.39853E+02	0.41524E+02	0.10670E+03	0.29220E+03	0.20979E+01
8800.00	0.15225E-01	0.51477E+02	0.37088E+02	0.12345E+03	0.28494E+03	0.22789E+01
8805.00	0.16523E-01	0.84810E+02	0.37014E+02	0.11331E+03	0.22464E+03	0.28473E+01
8810.00	0.15272E-01	0.71783E+02	0.29842E+02	0.35034E+02	0.17742E+03	0.26139E+01
8815.00	0.12396E-01	0.31777E+02	0.48197E+02	0.11338E+03	0.19882E+03	0.23219E+01
8820.00	0.11923E-01	0.29439E+02	0.48083E+02	0.12580E+03	0.18777E+03	0.21870E+01
8825.00	0.11801E-01	0.26576E+02	0.45455E+02	0.11519E+03	0.18954E+03	0.23197E+01
8830.00	0.12843E-01	0.27196E+02	0.48752E+02	0.11600E+03	0.19259E+03	0.22995E+01
8835.00	0.13934E-01	0.27034E+02	0.55099E+02	0.12607E+03	0.21209E+03	0.21232E+01
8840.00	0.16065E-01	0.27931E+02	0.77385E+02	0.12976E+03	0.20688E+03	0.19709E+01
8845.00	0.15398E-01	0.31842E+02	0.89247E+02	0.14638E+03	0.16207E+03	0.18302E+01
8850.00	0.15044E-01	0.35302E+02	0.69894E+02	0.12764E+03	0.17007E+03	0.18728E+01
8855.00	0.15141E-01	0.39923E+02	0.65330E+02	0.10799E+03	0.16819E+03	0.18997E+01
8860.00	0.14337E-01	0.36247E+02	0.59992E+02	0.11815E+03	0.17100E+03	0.18097E+01
8865.00	0.14562E-01	0.44361E+02	0.56525E+02	0.11066E+03	0.17567E+03	0.18935E+01
8870.00	0.14337E-01	0.45143E+02	0.55151E+02	0.11889E+03	0.21513E+03	0.18514E+01
8875.00	0.14390E-01	0.38721E+02	0.48987E+02	0.13863E+03	0.25952E+03	0.18407E+01
8880.00	0.14405E-01	0.40123E+02	0.56244E+02	0.13448E+03	0.28132E+03	0.18784E+01
8885.00	0.12224E-01	0.35196E+02	0.50995E+02	0.13049E+03	0.31866E+03	0.17890E+01
8890.00	0.11099E-01	0.33929E+02	0.37365E+02	0.11497E+03	0.36014E+03	0.21044E+01
8895.00	0.11548E-01	0.39362E+02	0.30151E+02	0.11225E+03	0.38158E+03	0.25039E+01

continued overleaf

Table 3—*continued*

8900.00	0.12975E-01	0.50610E+02	0.31940E+02	0.12773E+03	0.35212E+03	0.24994E+01
8905.00	0.14736E-01	0.51872E+02	0.38124E+02	0.92305E+02	0.31604E+03	0.29863E+01
8910.00	0.14347E-01	0.30591E+02	0.23957E+02	0.35973E+02	0.40595E+03	0.21232E+01
8915.00	0.97970E-02	0.19800E+02	0.35924E+02	0.10843E+03	0.48774E+03	0.20440E+01
8920.00	0.10777E-01	0.17150E+02	0.28855E+02	0.75984E+02	0.53114E+03	0.19646E+01
8925.00	0.10287E-01	0.14441E+02	0.28458E+02	0.88230E+02	0.55517E+03	0.20041E+01
8930.00	0.11671E-01	0.12087E+02	0.25759E+02	0.60424E+02	0.52157E+03	0.18693E+01
8935.00	0.12101E-01	0.11259E+02	0.49528E+02	0.13282E+03	0.47885E+03	0.17919E+01
8940.00	0.13577E-01	0.10835E+02	0.58896E+02	0.13241E+03	0.45936E+03	0.17408E+01
8945.00	0.15592E-01	0.10774E+02	0.75768E+02	0.11855E+03	0.41720E+03	0.17954E+01
8950.00	0.15907E-01	0.12952E+02	0.86087E+02	0.90790E+02	0.35282E+03	0.16963E+01
8955.00	0.14621E-01	0.10510E+02	0.78157E+02	0.89958E+02	0.34690E+03	0.17184E+01
8960.00	0.14324E-01	0.97443E+01	0.67894E+02	0.84274E+02	0.33239E+03	0.18379E+01
8965.00	0.14614E-01	0.79293E+01	0.50928E+02	0.51352E+02	0.35880E+03	0.18018E+01
8970.00	0.14619E-01	0.75437E+01	0.98404E+02	0.96979E+02	0.37229E+03	0.20222E+01
8975.00	0.12623E-01	0.99271E+01	0.90523E+02	0.10574E+03	0.33833E+03	0.19497E+01
8980.00	0.13097E-01	0.88616E+01	0.57615E+02	0.52011E+02	0.36838E+03	0.16902E+01
8985.00	0.13691E-01	0.69041E+01	0.88376E+02	0.78962E+02	0.40722E+03	0.18639E+01
8990.00	0.11770E-01	0.74365E+01	0.52077E+02	0.64488E+02	0.41314E+03	0.18759E+01
8995.00	0.14837E-01	0.61855E+01	0.47574E+02	0.32874E+02	0.47670E+03	0.17692E+01
9000.00	0.15078E-01	0.51252E+01	0.68592E+02	0.78863E+02	0.52338E+03	0.19093E+01
9005.00	0.13899E-01	0.53130E+01	0.63450E+02	0.10227E+03	0.52867E+03	0.19768E+01
9010.00	0.16501E-01	0.41123E+01	0.51252E+02	0.96952E+02	0.56850E+03	0.28645E+01
9015.00	0.17664E-01	0.36851E+01	0.50651E+02	0.96901E+02	0.57748E+03	0.33297E+01
9020.00	0.18289E-01	0.35308E+01	0.42850E+02	0.97012E+02	0.51499E+03	0.43676E+01
9025.00	0.16610E-01	0.37569E+01	0.33777E+02	0.97296E+02	0.51459E+03	0.44189E+01
9030.00	0.18239E-01	0.30623E+01	0.50404E+02	0.96612E+02	0.62188E+03	0.35983E+01
9035.00	0.22728E-01	0.23575E+01	0.96227E+02	0.94998E+02	0.68183E+03	0.47683E+01
9040.00	0.20888E-01	0.36670E+01	0.11810E+03	0.79581E+02	0.44111E+03	0.16418E+01
9045.00	0.19602E-01	0.35506E+01	0.14870E+03	0.81564E+02	0.35774E+03	0.13014E+01
9050.00	0.23022E-01	0.16781E+01	0.25449E+03	0.91152E+02	0.54142E+03	0.25160E+01
9055.00	0.25873E-01	0.13146E+01	0.31847E+03	0.90324E+02	0.63000E+03	0.51125E+01
9060.00	0.25018E-01	0.12931E+01	0.35862E+03	0.90169E+02	0.56525E+03	0.65679E+01
9065.00	0.25184E-01	0.12229E+01	0.40156E+03	0.88512E+02	0.58377E+03	0.48955E+01
9070.00	0.24556E-01	0.11246E+01	0.54069E+03	0.89091E+02	0.62086E+03	0.46364E+01
9075.00	0.23476E-01	0.11892E+01	0.61712E+03	0.87392E+02	0.54569E+03	0.34126E+01
9080.00	0.23128E-01	0.11321E+01	0.65042E+03	0.85377E+02	0.53251E+03	0.36894E+01
9085.00	0.23251E-01	0.15671E+01	0.76908E+03	0.86407E+02	0.46653E+03	0.18879E+01
9090.00	0.21448E-01	0.16451E+01	0.73750E+03	0.86111E+02	0.40094E+03	0.19037E+01
9095.00	0.20160E-01	0.11588E+01	0.49127E+03	0.89744E+02	0.40921E+03	0.42684E+01
9100.00	0.19937E-01	0.17366E+01	0.50886E+03	0.84755E+02	0.35944E+03	0.18393E+01
9105.00	0.19914E-01	0.16862E+01	0.54403E+03	0.84767E+02	0.38998E+03	0.17560E+01
9110.00	0.20169E-01	0.14981E+01	0.64399E+03	0.88767E+02	0.44811E+03	0.19448E+01
9115.00	0.19602E-01	0.15104E+01	0.54035E+03	0.88730E+02	0.42061E+03	0.20469E+01
9120.00	0.19704E-01	0.21027E+01	0.74017E+03	0.85771E+02	0.42358E+03	0.14914E+01
9125.00	0.19104E-01	0.21125E+01	0.53709E+03	0.84829E+02	0.42651E+03	0.14846E+01
9130.00	0.18266E-01	0.18310E+01	0.36586E+03	0.88968E+02	0.44148E+03	0.20692E+01
9135.00	0.19320E-01	0.16997E+01	0.46067E+03	0.85036E+02	0.48924E+03	0.18904E+01
9140.00	0.18582E-01	0.15804E+01	0.28481E+03	0.89765E+02	0.49797E+03	0.26831E+01
9145.00	0.18636E-01	0.14681E+01	0.30713E+03	0.88644E+02	0.53669E+03	0.28715E+01
9150.00	0.18897E-01	0.13226E+01	0.28406E+03	0.89844E+02	0.59722E+03	0.39014E+01
9155.00	0.18690E-01	0.13612E+01	0.29260E+03	0.89334E+02	0.60866E+03	0.36037E+01
9160.00	0.19407E-01	0.10674E+01	0.27975E+03	0.89612E+02	0.67401E+03	0.49317E+01
9165.00	0.19131E-01	0.11064E+01	0.23656E+03	0.89963E+02	0.70694E+03	0.52829E+01
9170.00	0.19286E-01	0.96330E+00	0.36088E+03	0.88943E+02	0.76268E+03	0.33966E+01
9175.00	0.18207E-01	0.79589E+00	0.42884E+03	0.84279E+02	0.81340E+03	0.38772E+01
9180.00	0.18132E-01	0.72585E+00	0.56722E+03	0.84167E+02	0.86035E+03	0.25128E+01
9185.00	0.17981E-01	0.66289E+00	0.62662E+03	0.84465E+02	0.86284E+03	0.15719E+01
9190.00	0.18019E-01	0.53874E+00	0.70173E+03	0.83020E+02	0.86808E+03	0.13253E+01
9195.00	0.17814E-01	0.47238E+00	0.61654E+03	0.84653E+02	0.89298E+03	0.11561E+01

continued opposite

Table 3—*continued*

9200.00	0.17915E-01	0.35423E+00	0.64213E+03	0.84437E+02	0.78483E+03	0.98130E-02
9205.00	0.19694E-01	0.42693E+00	0.59467E+04	0.84341E+02	0.46090E+03	0.75981E+00
9210.00	0.19708E-01	0.26571E+00	0.29804E+04	0.86578E+02	0.48141E+03	0.32664E+00
9215.00	0.17183E-01	0.60422E+00	0.10235E+05	0.86211E+02	0.26142E+03	0.17206E+01
9220.00	0.16867E-01	0.13480E+01	0.29817E+05	0.79989E+02	0.16830E+03	0.14509E+01
9225.00	0.15938E-01	0.27112E+00	0.50980E+04	0.81457E+02	0.21392E+03	0.10815E+01
9230.00	0.15116E-01	0.74755E+00	0.18507E+05	0.85194E+02	0.21503E+03	0.16775E+01
9235.00	0.15356E-01	0.20051E+00	0.51591E+04	0.77921E+02	0.12768E+03	0.52349E+01
9240.00	0.14949E-01	0.19063E+00	0.53723E+04	0.85654E+02	0.14869E+03	0.14617E+01
9245.00	0.15535E-01	0.11603E+00	0.41371E+04	0.72969E+02	0.14982E+03	0.33396E+00
9250.00	0.14846E-01	0.14129E+00	0.56784E+04	0.79427E+02	0.15071E+03	0.31841E+00
9255.00	0.14555E-01	0.13529E+00	0.70375E+04	0.87410E+02	0.15268E+03	0.21813E+00
9260.00	0.14377E-01	0.13557E+00	0.78155E+04	0.84086E+02	0.14877E+03	0.18582E+00
9265.00	0.14326E-01	0.14647E+00	0.78442E+04	0.86734E+02	0.13794E+03	0.45872E+01
9270.00	0.14084E-01	0.10772E+00	0.57531E+04	0.84496E+02	0.16598E+03	0.33526E-01
9275.00	0.13344E-01	0.11647E+00	0.52648E+04	0.78621E+02	0.15091E+03	0.10745E+00
9280.00	0.13018E-01	0.15593E+00	0.80024E+04	0.66912E+02	0.14010E+03	0.39416E+00
9285.00	0.12998E-01	0.13204E+00	0.85520E+04	0.74716E+02	0.12728E+03	0.40236E+00
9290.00	0.14069E-01	0.91279E-01	0.60160E+04	0.82283E+02	0.14327E+03	0.45259E+00
9295.00	0.13927E-01	0.94485E-01	0.76161E+04	0.85992E+02	0.13290E+03	0.67628E+00
9300.00	0.13729E-01	0.94279E-01	0.73374E+04	0.78207E+02	0.14668E+03	0.36070E+01
9305.00	0.13046E-01	0.92764E-01	0.77917E+04	0.85225E+02	0.13128E+03	0.11738E+01
9310.00	0.12331E-01	0.79949E-01	0.75068E+04	0.94244E+02	0.14094E+03	0.36335E+00
9315.00	0.11784E-01	0.11315E+00	0.11390E+05	0.90295E+02	0.15290E+03	0.26928E+01
9320.00	0.11799E-01	0.93223E-01	0.93453E+04	0.85559E+02	0.14130E+03	0.13990E+00
9325.00	0.12014E-01	0.89787E-01	0.74890E+04	0.79498E+02	0.13033E+03	0.99938E+01
9330.00	0.11822E-01	0.11306E+00	0.93104E+04	0.77791E+02	0.13620E+03	0.88293E+00
9335.00	0.13395E-01	0.13145E+00	0.25758E+05	0.84796E+02	0.14976E+03	0.10503E+02
9340.00	0.13243E-01	0.89711E-01	0.10882E+05	0.86766E+02	0.13921E+03	0.25161E-01
9345.00	0.12589E-01	0.94828E-01	0.88713E+04	0.84126E+02	0.13882E+03	0.12835E+01
9350.00	0.11882E-01	0.11667E+00	0.11111E+05	0.81871E+02	0.14213E+03	0.40310E+00
9355.00	0.11910E-01	0.97764E-01	0.98426E+04	0.91554E+02	0.13897E+03	0.17110E+00
9360.00	0.11837E-01	0.79147E-01	0.55404E+04	0.73180E+02	0.13696E+03	0.50303E+00
9365.00	0.11653E-01	0.88650E-01	0.61050E+04	0.71417E+02	0.14762E+03	0.56654E+00
9370.00	0.11579E-01	0.12054E+00	0.12853E+05	0.83611E+02	0.14456E+03	0.75128E+01
9375.00	0.11900E-01	0.50705E-01	0.62826E+04	0.81123E+02	0.15046E+03	0.24072E+01
9380.00	0.11570E-01	0.71899E-01	0.70383E+04	0.83785E+02	0.14087E+03	0.35951E-01
9385.00	0.11552E-01	0.79053E-01	0.84682E+04	0.81437E+02	0.14151E+03	0.24418E+01
9390.00	0.12669E-01	0.31436E-01	0.80166E+04	0.84299E+02	0.13915E+03	0.38023E-01
9395.00	0.12050E-01	0.68874E-01	0.94490E+04	0.82878E+02	0.15027E+03	0.36939E+00
9400.00	0.12427E-01	0.85362E-01	0.81153E+04	0.75798E+02	0.14654E+03	0.21010E-01
9405.00	0.12876E-01	0.73158E-01	0.58159E+04	0.84302E+02	0.15161E+03	0.89195E+00
9410.00	0.13026E-01	0.81354E-01	0.59122E+04	0.80520E+02	0.15702E+03	0.10041E+00
9415.00	0.13011E-01	0.10929E+00	0.10654E+05	0.91437E+02	0.16198E+03	0.15732E-01
9420.00	0.13406E-01	0.77867E-01	0.44205E+04	0.86181E+02	0.16404E+03	0.14840E+00
9425.00	0.13311E-01	0.95772E-01	0.54093E+04	0.76356E+02	0.16103E+03	0.54460E-02
9430.00	0.13343E-01	0.10503E+00	0.64913E+04	0.64588E+02	0.15218E+03	0.11039E+01
9435.00	0.12923E-01	0.81419E+00	0.68154E+05	0.84092E+02	0.13114E+03	0.60958E+00
9440.00	0.13007E-01	0.55010E+00	0.42573E+05	0.82582E+02	0.16081E+03	0.71496E+00
9445.00	0.13160E-01	0.98673E-01	0.56033E+04	0.85790E+02	0.21440E+03	0.67413E+00
9450.00	0.13441E-01	0.91211E-01	0.59064E+04	0.83156E+02	0.18509E+03	0.55083E-01
9455.00	0.12750E-01	0.12483E+00	0.79960E+04	0.83468E+02	0.16232E+03	0.26690E+01
9460.00	0.12541E-01	0.96051E-01	0.38234E+04	0.84295E+02	0.21110E+03	0.32841E-01
9465.00	0.12597E-01	0.72564E-01	0.44348E+02	0.89292E+02	0.28324E+03	0.27988E+01
9470.00	0.12201E-01	0.10190E+00	0.48313E+02	0.74360E+02	0.39725E+03	0.76198E+01
9475.00	0.12312E-01	0.11404E+00	0.26534E+03	0.82190E+02	0.40061E+03	0.11248E-01
9480.00	0.12342E-01	0.11436E+00	0.23332E+03	0.83502E+02	0.37631E+03	0.10659E+01
9485.00	0.12864E-01	0.12960E+00	0.14399E+02	0.93325E+02	0.33687E+03	0.25002E+01
9490.00	0.13088E-01	0.12596E+00	0.41741E+01	0.93397E+02	0.32060E+03	0.57270E+00
9495.00	0.12703E-01	0.12443E+00	0.21117E+03	0.78358E+02	0.34147E+03	0.63920E+00
9500.00	0.13043E-01	0.12698E+00	0.17526E+03	0.84152E+02	0.31930E+03	0.29750E-01

transmittance under the conditions of interest. Finally, the Goody–Voigt model was extrapolated to the laboratory conditions of some very low temperature CH_4 spectra available in the literature, allowing a comparison with laboratory data.

Ten Jovian paths were used in the extrapolations, selected from the Curtis–Godson paths to the top of the atmosphere from levels betwen 0.01 and 10.0 bar, which had been calculated previously from the Jovian models of Orton.[17] Of the 10 paths, one was chosen for having the lowest Curtis–Godson temperature of all five Jovian models (107 K, 0.010 bar, and 14.8 m-amagat of CH_4), one for having the highest Curtis–Godson pressure and CH_4 abundance of all five models (262 K, 5.0 bar, and 773 m-amagat), and one for having the lowest Curtis–Godson pressure and CH_4 abundance of all five models (142 K, 0.0050 bar, and 0.710 m-amagat). The remaining seven paths were chosen in logarithmic steps from 0.01 to 10.0 bar, from the nominal model.

In the first test of the reliability of the extrapolation of the Goody–Voigt model, both this and the fitted Malkmus–Voigt model were used to generate spectra over the entire 2000–9500 cm^{-1} range for these 10 Jovian paths. For each path, both the difference between the transmittances predicted by the two models and the sum of the r.m.s. residual errors for the two fits were plotted as functions of frequency. For the spectra generated from the fits to the self-broadened CH_4 spectra, the agreement was generally excellent, being well within the sum of the fitting errors. The only exceptions to this were some points in the 3000 and 4300 cm^{-1} bands for the two lowest temperature paths, but for these points the differences between the predicted transmittances were still less than 0.08. For the spectra generated from the fits to the combined set of self- and H_2-broadened CH_4 spectra, the agreement between the Goody–Voigt and Malkmus–Voigt transmittances was again generally within the sum of the fitting errors. The exceptions were a few points in the 3000 cm^{-1} region and in the region of H_2 absorption from 4900–5000 cm^{-1}, for which the difference between the predicted transmittances exceeded the sum of the fitting errors for several spectra, and the path with the highest pressure and CH_4 abundance, for which the difference in transmittance was as large as 0.15 in the window regions, although generally much smaller.

Thus, except for a few frequencies under the extremes of Jovian temperature and pressure, the transmittances obtained by extrapolating the Goody–Voigt and Malkmus–Voigt models agreed to within the sum of the fitting errors. However, although this calculation demonstrated consistency between the extrapolations of the two band models, it did not provide any external measure of their reliability. In order to address this question, the GENLN2 line-by-line program was used to calculate synthetic spectra for all 10 Jovian paths using CH_4 line parameters listed in the HITRAN 1991 database.[6] It should be noted that the Goody–Voigt model used in this test was that fitted to all of the self- and H_2-broadened CH_4 spectra, while the GENLN2 calculation used the self- and air-broadened half-widths listed in the HITRAN 1991 database. In general, air-broadened CH_4 lines have slightly smaller half-widths than H_2-broadened CH_4 lines[80–82] and so the GENLN2 spectra might be expected to slightly over-estimate the absorption at line centre.

Figure 13 shows both the Goody–Voigt and GENLN2 spectra calculated for the three extreme Jovian paths described above, over the 2000–6200 cm^{-1} region for which CH_4 line data were available. In Fig. 13(a), the weakly absorbing spectra generating for the smallest Curtis–Godson pressure and CH_4 abundance are plotted. In this case, the Goody–Voigt and GENLN2 spectra agree to within 0.05 in transmittance in the 3000 and 5800 cm^{-1} bands and within 0.10 in the 4300 cm^{-1} band. The agreement is poorer for the spectra generated for the lowest temperature path [Fig. 13(b)], with the GENLN2 absorption being generally larger in the 3000 and 4300 cm^{-1} bands, and the Goody–Voigt absorption being larger in the 5800 cm^{-1} band. It is difficult to determine the extent to which these differences are due to errors in the HITRAN 1991 line data and/or to errors in the extrapolation of the band model. The spectra generated for the largest Curtis–Godson pressure and CH_4 abundance [Fig. 13(c)] can be compared only in the 2000 cm^{-1} window, where the transmittances again agree to within 0.10 or better, as all of the bands are saturated. Comparisons between the Goody–Voigt and GENLN2 spectra were also made for the seven other Jovian paths, yielding similar results: reasonably good agreement for the weakly absorbing spectra, poorest agreement for the lowest temperature (117.5 K) spectrum, and saturation for the strongly absorbing spectra.

Unfortunately, there are few low-temperature or high-abundance CH_4 spectra available in the literature, particularly those with sufficient information on their laboratory conditions to allow

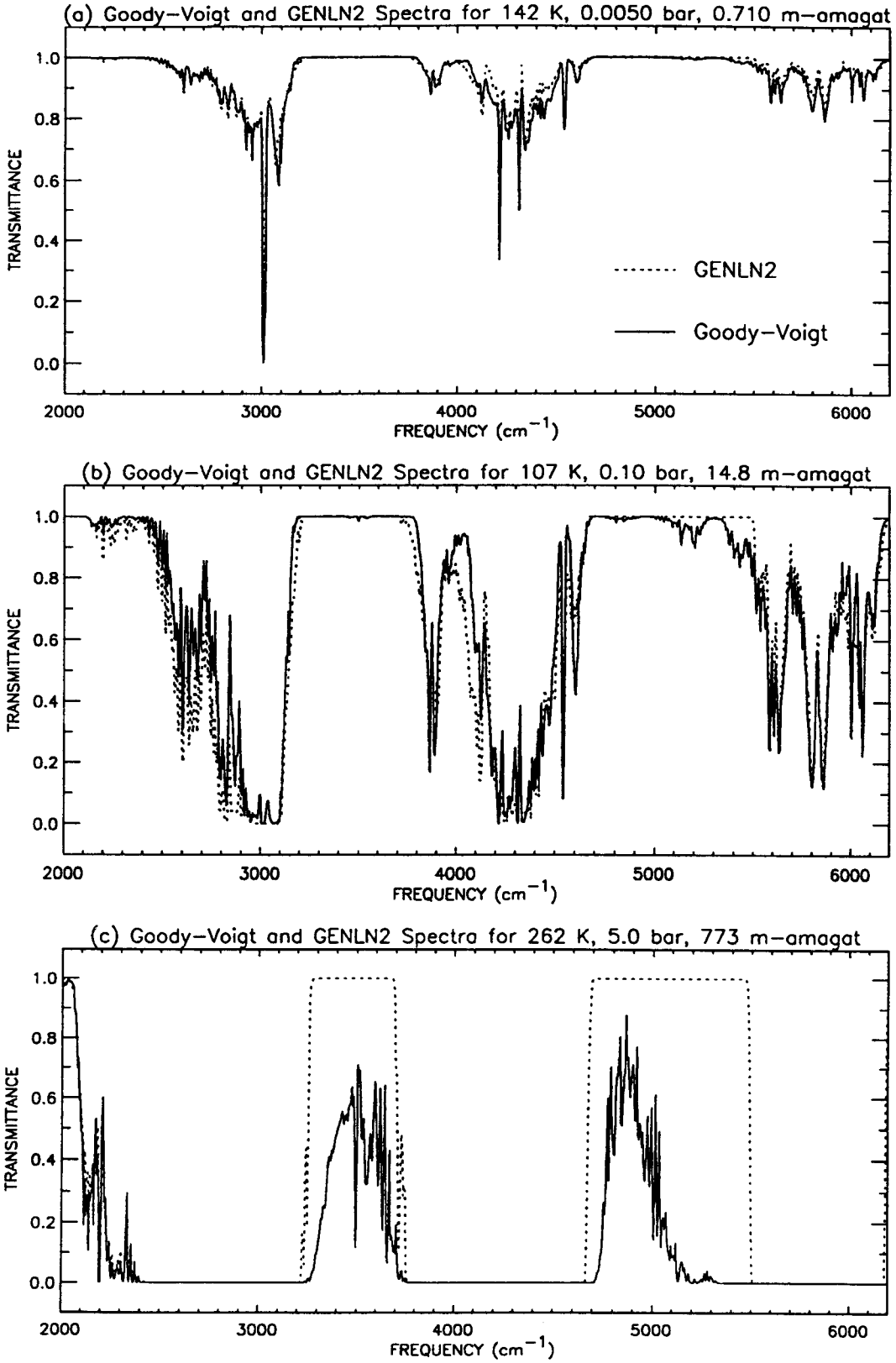

Fig. 13. Synthetic spectra generated by extrapolating the Goody–Voigt model (that fitted to all of the measured CH_4 spectra) to three extreme Jovian paths, and by applying the GENLN2 line-by-line program to the CH_4 data in the HITRAN 1991 database.

comparison with the extrapolations of the band models. One exception is the work of McKellar.[38] The Goody–Voigt fit to the combined set of self- and H_2-broadened CH_4 spectra was used to calculate spectra for each of his three sets of laboratory conditions (66 m, 0.0013 bar CH_4, 0.604 bar N_2; 88 m, 0.0083 bar CH_4, 0.355 bar N_2; and 88 m, 0.0115 bar CH_4, 0.368 bar N_2; all at 77 K), again assuming that H_2 and N_2-broadening are similar. For all three paths, the extrapolated spectra were found to under estimate the absorptions measured by McKellar.[38] This is shown in Fig. 14(a), in which the Goody–Voigt extrapolation has been superimposed on McKellar's 3800–4800 cm^{-1} spectrum at 10 cm^{-1} resolution (that for his first set of conditions). This figure also includes a line-by-line spectrum, generated using GENLN2 and the HITRAN 1991 database for the same set of conditions, which is seen to be in closer agreement with McKellar's spectrum. In addition to the extrapolation to 77 K, the Goody–Voigt model and GENLN2 were also used to generate synthetic spectra for the same CH_4 abundance and total pressure, but maintaining the temperature

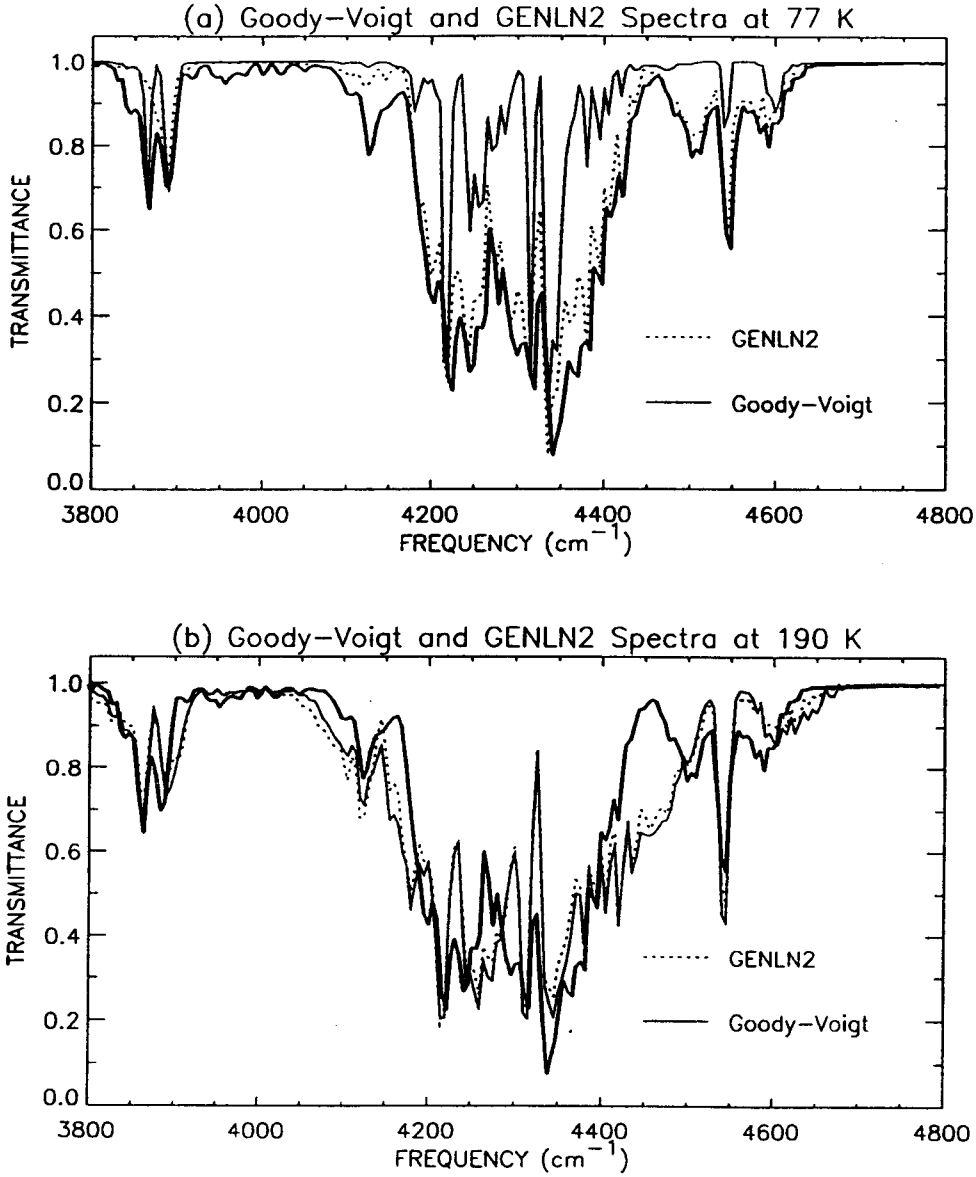

Fig. 14. The laboratory spectrum (line in boldface) measured by McKellar[38] at 77 K, 88 m, 0.0115 bar CH_4, and 0.368 bar N_2, along with spectra extrapolated to these conditions using the Goody–Voigt band model and the GENLN2 line-by-line program. In (a) the synthetic spectra have been generated using the correct temperature of 77 K. In (b), the synthetic spectra have been generated using a temperature of 190 K while leaving the total pressure and the CH_4 abundance unchanged.

at 190 K, i.e., avoiding extrapolation beyond the lowest laboratory temperature. These two spectra have been superimposed on McKellar's original spectrum in Fig. 14(b). This 190 K Goody–Voigt spectrum is in good agreement with the 190 K GENLN2 spectrum, and provides a closer match to McKellar's original spectrum. These results suggest that the Goody–Voigt band model greatly over-estimates the temperature dependence of the transmittance at low temperatures, which in turn suggests that extrapolation of the band model should be undertaken with caution. While the extrapolation attempted here was very large—113 K below the lowest laboratory temperature used to derive the model, and 30–40 K below the lowest temperature expected on Jupiter—it is clear that further measurements are desirable over the range from 100 to 190 K.

With CH_4 absorptions dominating near-infrared spectra of Jupiter, knowledge of the transmittance properties of CH_4 is a crucial first step in the interpretation of spectra recorded by NIMS. The Goody–Voigt band model which was fitted to the combined set of self- and H_2-broadened CH_4 spectra, thus covering a wide range of Jovian conditions, now provides a convenient means of calculating CH_4 transmittance over most of the NIMS spectral range. Analysis of NIMS spectra is likely to begin with simple models, approximating the Jovian atmosphere as clear (non-scattering) down to the level of the NH_3 cloud tops and in the regions between each of the NH_3, NH_4SH and H_2O cloud layers. In these reflecting-layer models, the band-model transmittances can readily be included in the equation of radiative transfer, and new information about cloud heights, temperature profiles, and the abundances of minor constituents should be retrievable.

Some insight into the usefulness of the fitted Goody–Voigt model for remote sounding of the Jovian atmosphere can be gained from a calculation of the optical depth, χ, of atmospheric CH_4 as a function of wavelength. Most of the information collected by a remote sensing instrument originates from the level where χ is close to unity.[83] Calculation of the mean $\chi = 1$ level for CH_4, which is uniformly mixed in the Jovian atmosphere, will therefore indicate the importance of CH_4 in the determination of the depths to which NIMS will be able to probe. This calculation was performed by first using the nominal Jovian atmospheric model of Orton[17] to generate a fine grid of Curtis–Godson paths to the top of the atmosphere at 0.5 km intervals over the entire 100–10^{-11} bar profile. Then for each 10 cm^{-1} frequency interval, the Goody–Voigt fit to all of the measured spectra was used to compute transmittance for each Curtis–Godson path, thereby determining to the nearest 0.5 km, the level at which $\bar{\tau} = \exp(-1)$. The resulting profile of atmospheric height (and pressure) versus frequency was then degraded to NIMS resolution by convolving it with a triangle of full-width-half-maximum of 0.025 μm, and sampling every 0.0125 μm. The final NIMS-resolution profile is plotted on a wavelength scale in Fig. 15.

From this figure, several interesting points emerge. Firstly, the $\chi = 1$ level varies significantly with wavelength, being located at pressures between 100 and 0.01 bar over 1–5 μm. In the absence of clouds or other absorbing gases, this suggests that CH_4 should be useful in temperature sounding over a height range of more than 300 km. The presence of NH_3 clouds near 0.3 bar, NH_4SH clouds near 2 bar, and H_2O clouds near 5 bar is likely to obscure the deeper levels, but it may be possible to sound to deeper levels through gaps in the clouds. Furthermore, the ability or inability to detect CH_4 at particular wavelengths should provide a means of determining cloud heights and locations. Figure 15 also reveals the windows in the CH_4 absorption, the spectral regions in which the concentrations of other minor constituents may be determined. The 5 μm window is obvious, allowing the detection of absorptions by GeH_4, PH_3, H_2O, CH_3D, H_2S, HCN, C_2H_2, C_2H_4, and C_2H_6. Additional windows are located at approx. 2.8, 2.0, 1.6, 1.3, and 1.1 μm. In these regions, the absorption of NH_3 becomes important, as NH_3 bands overlap the 2.8, 2.0, and 1.6 μm CH_4 windows. An analysis of the near-infrared spectral parameters of NH_3, similar to that performed for CH_4 in this work, clearly would be valuable.

The error budget for data retrieved from NIMS measurements will be determined by instrumental errors, assumptions made in the modelling and retrievals, and uncertainties in the knowledge of the transmittance properties of Jovian atmospheric gases. Of particular concern in the present study is how errors in the CH_4 transmittances calculated from the fitted Goody–Voigt model, quantified by the r.m.s. residual error σ, [Fig. 10(a)] will affect the accuracy of the retrieved atmospheric parameters. The calculation of the mean $\chi = 1$ level, performed above, provides a means of estimating this accuracy. The plot of the $\chi = 1$ level in Fig. 15 includes two curves for which $\bar{\tau}(\nu) = \exp(-1) \pm \sigma(\nu)$. In the three subsequent plots, these curves of the uncertainty in the

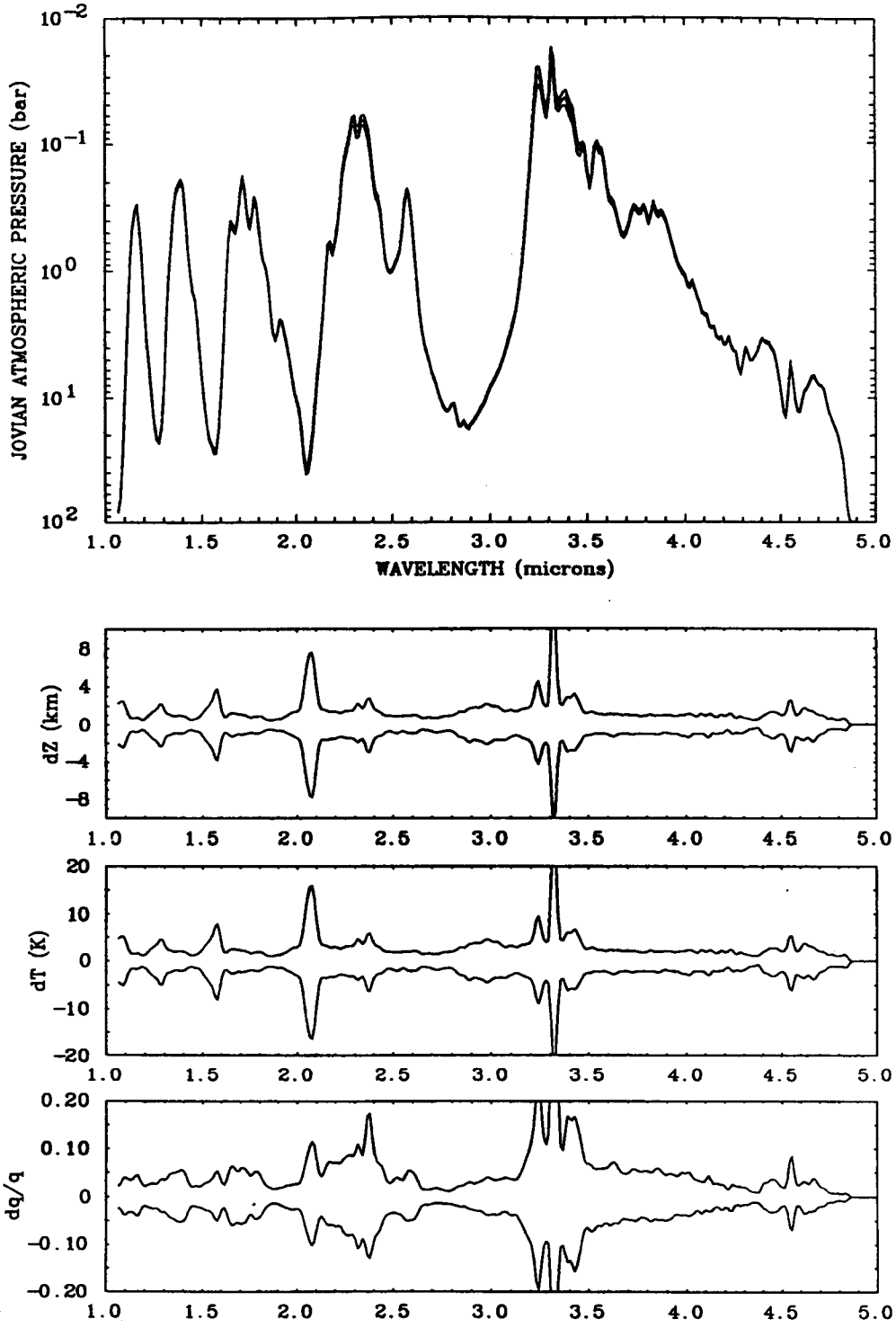

Fig. 15. The upper plot shows the pressure of the Jovian atmospheric level for which the optical depth to the top of the atmosphere is unity, as calculated using the nominal model of Orton[17] and the Goody–Voigt fit to all of the self- and H_2-broadened CH_4 spectra. Included in this plot are the levels for which $\bar{\tau} = \exp(-1) \pm \sigma$. The three lower plots show the uncertainties in height, temperature, and CH_4 mixing ratio which arise from the r.m.s. residual fitting errors, σ.

$\chi = 1$ level have been translated into uncertainties in height, temperature, and CH_4 mixing ratio. The uncertainty in height, Δz, is simply derived from the atmospheric heights at which $\tau(\nu) = \exp(-1) \pm \sigma(\nu)$. As expected, the largest values of Δz are for those wavelengths where σ is

large: at $\sim 2.1\ \mu$m, where the original spectra were contaminated by H_2 absorption, and at $\sim 3.3\ \mu$m, where the spectra were contaminated by pump oil and ice absorption and there was some difficulty in fitting the sharp Q branch of the band. Elsewhere, $|\Delta z|$ is consistently less than 3 km, and is generally closer to 1 km, implying that the uncertainty in the cloud heights retrieved by NIMS due to uncertainties in CH_4 transmittance, will be of this order of magnitude. Considering the current poor understanding of Jovian cloud structure and the large variations in modelled cloud heights, such uncertainties should allow a significant improvement in the determination of the vertical cloud structure.

Below the tropopause, at about 0.1 bar, temperatures in the Jovian atmosphere are believed to follow an adiabatic lapse rate of 2.1 K/km.[84] Assuming the CH_4 mixing ratio to be accurately known, and having calculated Δz, the uncertainty in tropospheric Jovian temperatures due to the r.m.s. residual error σ can be estimated as $\Delta T = (dT/dz)\,\Delta z$. This uncertainty in temperature has also been plotted in Fig. 15, and aside from the 2.1 and 3.3 μm regions, $|\Delta T|$ is generally less than 6 K, but mostly closer to 2 K. These values are comparable to current uncertainties in the Jovian temperature profile. For example, according to Orton,[17] errors in the tropospheric temperature profile derived from *Voyager* include a direct measurement error of ± 2 K, and an error of ± 1.1 K due to uncertainty in the composition. However, larger uncertainties exist in estimates of the temperature at the 1 bar level, which, with the adiabatic gradient, determines the vertical temperature profile. This temperature has been assigned values ranging from 153 to 170 K,[85] with Lindal *et al*[84] deriving a value of 165 ± 5 K. Thus, uncertainties in the temperatures retrieved by NIMS due to uncertainties in CH_4 transmittance should still allow refinement of the Jovian temperature profile, as well as measurements of horizontal temperature variations.

The third uncertainty plotted in Fig. 15 is the relative uncertainty in the CH_4 mixing ratio due to σ, in this case assuming the temperature profile to be accurately known. This has been calculated as $\Delta q/q$, where q is the CH_4 mixing ratio for a Curtis–Godson path from the $\bar{\tau}(\nu)$ level to the top of the atmosphere, and $\pm\Delta q$ is the difference in q for the $\bar{\tau}(\nu) \pm \sigma(\nu)$ levels, assuming the total atmospheric abundance to remain the same. The maxima in $\Delta q/q$ are determined by maxima in σ and minima in the CH_4 abundance. At most wavelengths, $|\Delta q/q|$ is well below 0.10. This compares favourably with the relative uncertainties of 0.22, 0.16, 0.11 and 0.33 in the values of the CH_4 mixing ratio derived by Sato and Hansen,[86] Knacke et al,[87] Gautier et al,[88] and Bjoraker et al.[89] Thus, the uncertainties in the band model CH_4 transmittance should also allow NIMS to improve measurements of the Jovian CH_4 mixing ratio. It should also be noted that the accuracy of the cloud heights, temperatures, and mixing ratios can be further increased by sounding the same levels at different wavelengths, thereby narrowing the range of allowable values for these parameters.

9. SUMMARY

Accurate knowledge of the line parameters or broad-band spectral parameters of CH_4 will be essential in order to make the most of the spectroscopic measurements of NIMS. However, the data available from both the HITRAN and GEISA databases and from previous band modelling studies have been shown to be inadequate for this purpose. Even the most recent compilation of CH_4 line parameters, HITRAN 1991, is completely lacking data in those weakly absorbing regions which will be an important source of information about the Jovian atmosphere. Although individual line parameters are the ideal form for spectral data, the complexity of the near-infrared spectrum of CH_4 makes this impossible on the time scale of the *Galileo* mission. However, because NIMS is a low-resolution instrument, the monochromatic transmittance can be replaced by a broad-band transmittance which is a well-defined function of temperature, pressure, and abundance.

Thus, an extensive set of CH_4 spectra was recorded under a wide range of frequencies, temperatures, CH_4 and H_2 pressures, and CH_4 abundances, for use in fitting a series of band models for future application in interpreting NIMS observations. The analysis began with the 108 self-broadened CH_4 spectra, which were fitted independently of the H_2-broadened spectra using four sequences of increasingly complex models, involving the Goody, Malkmus, Zachor–King/Gibson–Pierluissi, and Smith models, all with temperature dependence included. This choice of two random band models, two generalized band models, and an empirical transmittance model

allowed an assessment of which provided the best representation of the spectra. This showed the Goody–Voigt and Malkmus–Voigt models to give consistently better fits than any of the other models, generating an r.m.s. residual error which was less than 0.035 throughout 2000–9500 cm^{-1} and which generally lay between 0.005 and 0.02, comparable to the errors estimated in the original spectra and therefore considered acceptable. Having found that the two random band models provided the best fits to self-broadened CH_4 spectra, these two models were used to fit all 225 of the self- and H_2-broadened CH_4 spectra together. The Goody–Voigt model, fitted via a progression of increasingly complex models, and the Malkmus–Voigt model, fitted by initializing the parameters with the values obtained in the Malkmus–Voigt fit to the self-broadened CH_4 spectra, again provided the best fits to the spectra. For these two models, σ was comparable for all frequencies except the 3000 cm^{-1} band, where the Goody–Voigt model gave a better fit, with σ being less than 0.04 throughout the 2000–9500 cm^{-1} spectral range, and between 0.005 and 0.03 for all frequencies outside the 3000 and 4300 cm^{-1} bands, values again similar to the measurement errors in the spectra.

The present study has thus characterized the broad-band transmittance of self- and H_2-broadened CH_4 as a function of temperature, pressure, and abundance over the spectral range from 2000 to 9500 cm^{-1}. The resulting band-model fits are now ready for use in the interpretation of NIMS spectra once they become available. In addition, the original 0.25 cm^{-1} resolution CH_4 spectra are available for the identification of CH_4 lines and band centres. Meanwhile, the work undertaken in this study provides the basis for recommending several areas of investigation during the period prior to the December 1995 arrival of *Galileo* at Jupiter, investigations that will help to maximize the return of information from NIMS. These are as follows.

1. The lowest temperature achieved in the present work, as determined by the capabilities of the cryogenic system for the long White cell, was 190 K. Measurements of CH_4 spectra at the lowest Jovian temperatures (110 K at the tropopause) are clearly desirable, allowing band modelling which could reduce the need for extrapolating models beyond the original laboratory conditions, thus providing greater confidence in transmittances generated with these models.
2. Coverage of the visible region of NIMS spectral range was not possible during the measurements performed in this work. Although this region has been the subject of previous band modelling studies, these used only room temperature spectra. Measurement of visible, self- and H_2-broadened CH_4 spectra is recommended under conditions similar to those achieved in the infrared in this work, allowing the temperature-dependent band modelling to be extended across the entire NIMS range.
3. Although not as dominant as CH_4, NH_3 is also a significant absorber in the near-infrared spectrum of Jupiter. The line data available for NH_3 are also poor, while knowledge of the transmittance properties of NH_3 will be important in the analysis of NIMS spectra. Low-resolution spectroscopy of NH_3, again over the greatest possible range of conditions, and again followed by band-modelling analysis, would be useful in characterizing the near-infrared spectrum of this gas.
4. Scattering effects are likely to be significant in NIMS spectra of the Jovian atmosphere, and so more sophisticated analyses of these spectra are certain to require the use of atmospheric scattering models. The complex issue of reconciling band models with such models should therefore be addressed.
5. Considering the lack of line parameters for individual CH_4 lines over large regions of the near-infrared spectrum and the poor quality of the available weak line data, high-resolution measurements could be profitably undertaken in many bands. Even where line data are available, line widths listed are usually for air- or N_2-broadened CH_4, whereas it is H_2-broadened line widths that are relevant to Jupiter. The most useful measurements would be in the weak wings of bands which do not saturate under Jovian conditions and would not be contaminated by absorptions of NH_3 or H_2. These include both wings of the 8600 cm^{-1} band, the high frequency wing of the 7200 cm^{-1} band, and both wings of the 5600 cm^{-1} band.

Finally, the measurements and analysis performed in this work, although conducted primarily in support of the NIMS instrument, also have applications to other problems. They should be

directly applicable to the interpretation of ground-based observations of Jupiter, such as those recently made by Moreno et al[90] in the regions from 1.4 to 2.4 and 2.9 to 4.1 μm. Furthermore, with CH_4 also dominating the near-infrared spectra of Saturn, Titan, Neptune, and Uranus, the long-pathlength CH_4 spectra recorded in this work should prove to be useful in interpreting observations of all these planetary bodies. Griffith and Owen[91] have used CH_4 spectra from this work in demonstrating that CH_4 is the principle source of atmospheric opacity in the near-infrared spectrum of Titan. Lellouch et al[92] have also performed a preliminary analysis of the 1.1 μm window of Titan, using some of the original-resolution CH_4 spectra to identify approx. 95 new lines between 9050 and 9160 cm^{-1}. Further applications of the original-resolution CH_4 spectra and the fitted band models to studies of the outer planets are currently under consideration.

Acknowledgements—The authors would like to thank the many technical and engineering staff at R.A.L., particularly Mr Malcolm Page and Mr George Pullinger, whose efforts made it possible to perform the experiments described in this paper. They would also like to acknowledge Dr Brian Kerridge, Mr Rodney Knight, and Dr Graeme Mason for working shifts during the experimental phase of this study.

REFERENCES

1. H. P. Larson, in "Vibrational-Rotational Spectroscopy for Planetary Atmospheres", NASA CP-2223, M. J. Mumma, K. Fox, and J. Hornstein eds., p. 407 (1982).
2. S. T. Ridgway, H. P. Larson, and U. Fink, in *Jupiter*, T. Gehrels ed., Univ. of Arizona Press, Tucson, AZ (1976).
3. D. M. Hunten, L. Colin, and J. E. Hansen, *Space Sci. Rev.* **44,** 191 (1986).
4. F. W. Taylor and S. B. Calcutt, *JQSRT* **32,** 463 (1984).
5. L. S. Rothman, R. R. Gamache, A. Goldman, J. R. Gillis, L. R. Brown, R. A. Toth, H. M. Pickett, R. L. Poynter, J.-M. Flaud, C. Camy-Peyret, A. Barbe, N. Husson, C. P. Rinsland, and M. A. H. Smith, *Appl. Opt.* **26,** 4058 (1987).
6. L. S. Rothman, R. R. Gamache, R. H. Tipping, C. P. Rinsland, M. A. H. Smith, D. C. Benner, V. Malathy Devi, J.-M. Flaud, C. Camy-Peyret, A. Perrin, A. Goldman, S. T. Massie, L. R. Brown, and R. A. Toth, *JQSRT* **48,** 469 (1992).
7. A. Chedin, N. Husson, N. A. Scott, J. Cohen-Hallaleh, and A. Berroir, Internal Note 127, Laboratoire de Météorologie Dynamique du CNRS, Ecole Polytechnique, France (1985).
8. N. Husson, A. Chedin, N. A. Scott, D. Bailly, G. Graner, N. Lacome, A. Lévy, C. Rossetti, G. Tarrago, C. Camy-Peyret, J. M. Flaud, A. Bauer, J. M. Colmont, N. Monnanteuil, J. C. Hilico, G. Pierre, M. Loete, J. P. Champion, L. S. Rothman, L. R. Brown, G. Orton, P. Varanasi, C. P. Rinsland, M. A. H. Smith, and A. Goldman, *Ann. Geophys.* **86A,** 185 (1986).
9. G. Herzberg, *Molecular Spectra and Molecular Structure. II. Infrared and Raman Spectra of Polyatomic Molecules*, Van Nostrand-Reinhold, New York, NY (1945).
10. L. R. Brown, *Appl. Opt.* **27,** 3275 (1988).
11. D. P. Edwards, Internal Memorandum 87.2, Dept. of Atmospheric, Oceanic, and Planetary Physics, Univ. of Oxford (1987).
12. D. P. Edwards, in *SPIE Critical Review of Technology: Modelling of the Atmosphere*, Orlando, FL (1988).
13. K. Strong, D. Phil. Thesis. Univ. of Oxford (1992).
14. A. R. Curtis, *Q. J. R. Met. Soc.* **78,** 638 (1952).
15. W. L. Godson, *Proc. Toronto Met. Conf. 1953*, p. 35 (1954).
16. W. L. Godson, *J. Met.* **12,** 272 (1955).
17. G. S. Orton, NASA-JPL Report 1625-125, Jet Propulsion Laboratory, Pasadena, CA (1981).
18. H. L. Mayer, LA-647, Los Alamos (1947).
19. R. M. Goody, *Q. J. R. Met. Soc.* **78,** 165 (1952).
20. R. Mecke, *Z. Astrophys.* **6,** 144 (1933).
21. G. P. Kuiper, *Rep. Prog. Phys.* **13,** 247 (1950).
22. T. Dunham Jr., in *The Atmospheres of the Earth and Planets, Second Edition*, G. P. Kuiper ed., p. 288, Univ. of Chicago Press, Chicago, IL (1952).
23. T. Owen, *Icarus* **6,** 108 (1967).
24. B. Lutz and D. A. Ramsay, *Astrophys. J.* **176,** 521 (1972).
25. T. Owen, B. L. Lutz, C. C. Porco, and J. H. Woodman, *Astrophys. J.* **189,** 379 (1974).
26. B. L. Lutz, T. Owen, and R. D. Cess, *Astrophys. J.* **203,** 541 (1976).
27. K. A. Dick and U. Fink, *JQSRT* **18,** 447 (1977).
28. U. Fink, D. C. Benner, and K. A. Dick, *JQSRT* **18,** 447 (1977).
29. L. P. Giver, *JQSRT* **19,** 311 (1978).
30. M. Podolak and L. P. Giver, *Icarus* **37,** 361 (1979).
31. B. L. Lutz, T. Owen, and R. D. Cess, *Astrophys. J.* **258,** 886 (1982).
32. W. H. Smith, C. P. Conner, and K. H. Baines, *Icarus* **85,** 58 (1990).
33. M. E. Mickelson, L. E. Larson, and A. Schubert, *J.G.R.* **96(E2)** 17507.

34. U. Fink and H. P. Larson, *Astrophys. J.* **233,** 1021 (1979).
35. D. C. Benner and U. Fink, *Bull. Am. Astron. Soc.* **12,** 697.
36. U. Fink, in "Vibrational–Rotational Spectroscopy for Planetary Atmospheres", NASA CP-2223, M. J. Mumma, K. Fox, and J. Hornstein eds., p. 559 (1982).
37. J. Apt, J. V. Martonchik, and L. R. Brown, *JQSRT* **26,** 431 (1981).
38. A. R. W. McKellar, *Can. J. Phys.* **67,** 1027 (1989).
39. P. Silvaggio, in "Vibrational–Rotational Spectroscopy for Planetary Atmospheres", NASA CP-2223, M. J. Mumma, K. Fox, and J. Hornstein eds., p. 585 (1982).
40. S. B. Calcutt, D.Phil. Thesis, Univ. of Oxford (1984).
41. L. P. Giver, D. C. Benner, and R. W. Boese, *Bull. Am. Astron. Soc.* **16,** 711 (1984).
42. L. P. Giver, D. C. Benner, and C. B. Suárez, *Bull. Am. Astron. Soc.* **20,** 838 (1988).
43. J. J. Remedios, D.Phil. Thesis, Univ. of Oxford (1990).
44. J. White, *JOSA* **32,** 285 (1942).
45. J. Ballard, K. Strong, J. J. Remedios, W. B. Johnston, and M. Page, "A Coolable Long Path Absorption Cell for Laboratory Spectroscopic Studies of Gases", in preparation (1993).
46. W. L. Wolfe and G. J. Zissis eds., *The Infrared Handbook*, Office of Naval Research, Dept. of the Navy, Washington, DC (1978).
47. H. J. Bernstein and G. Herzberg, *J. Chem. Phys.* **16,** 30 (1948).
48. J. W. Brault, K. Fox, D. E. Jennings, and J. S. Margolis, *Astrophys. J.* **247,** L101 (1981).
49. J. A. Kaye, *Rev. Geophys.* **25,** 1609 (1987).
50. P. Drossart, R. Courtin, S. Atreya, and A. Tokunaga, in "Time-Variable Phenomena in the Jovian System", NASA SP-494, M. J. S. Belton, R. A. West, and J. Rahe eds., p. 211 (1989).
51. K. Strong, "Operation of the Rutherford Appleton Laboratory Long White Cell Using Methane and Hydrogen: Development and Implementation of Safety Measures and Operating Procedures", RAL-91-015, S.E.R.C. Rutherford Appleton Laboratory, Chilton, Didcot, Oxfordshire (1991).
52. R. H. Norton and R. Beer, *JOSA* **66,** 259 (1976).
53. "Multipoint Data Recorder PM8237A/02 Operating Manual", Philips Scientific & Industrial Equipment Division, York Street, Cambridge, U.K.
54. D. C. Benner, Ph.D. Dissertation, Univ. of Arizona (1979).
55. L. P. Giver, D. C. Benner, M. G. Tomasko, U. Fink and D. Kerola, in "First International Conference on Laboratory Research for Planetary Atmospheres", NASA CP-3077, K. Fox, J. E. Allen Jr., and D. T. Quillen eds., p. 147 (1990).
56. P. R. Griffiths and J. A. de Haseth, *Fourier Transform Infrared Spectroscopy*, pp. 39–42, Wiley, New York, NY (1986).
57. N. Ockman, *Adv. Cry. Eng.* **7,** 199 (1958).
58. J. Margolis, in "Vibrational–Rotational Spectroscopy for Planetary Atmospheres", NASA CP-2223, M. J. Mumma, K. Fox, and J. Hornstein eds., p. 431 (1982).
59. R. M. Goody, *Atmospheric Radiation. I. Theoretical Basis*, The Clarendon Press, Oxford (1964).
60. C. D. Rodgers, "Approximate Methods of Calculating Transmission by Bands of Spectral Lines", NCAR/TN-116 + 1A, National Center for Atmospheric Research, Boulder, CO (1976).
61. *NAG FORTRAN Library Manual, Mark 10, Volume 3. E04—Minimising or Maximising a Function*, pp. 3–27, Numerical Algorithms Group, Oxford (1983).
62. P. E. Gill and W. Murray, *SIAM J. Numer. Anal.* **15,** 977 (1978).
63. S. B. Calcutt, J. Ballard, W. B. Johnston and F. W. Taylor, "Spectroscopic Parameters for Methane from 1 to 2.5 Microns with Applications to Remote Sensing of the Atmosphere of Jupiter", unpublished manuscript (1988).
64. W. Malkmus, *JOSA* **57,** 323 (1967).
65. S. R. Drayson, *JQSRT* **16,** 611 (1976).
66. J. S. Vandergraft, *Introduction to Numerical Computations, Second Edition*, p. 156, Academic Press Inc., New York, NY (1983).
67. A. S. Zachor, *JQSRT* **8,** 771 (1968a).
68. A. S. Zachor, *JQSRT* **8,** 1341 (1968b).
69. J. I. F. King, *JQSRT* **4,** 705 (1964).
70. G. A. Gibson and J. H. Pierluissi, *Appl. Opt.* **10,** 1509 (1971).
71. W. H. Press, B. P. Flannery, S. A. Teulosky, and W. T. Vetterling, *Numerical Recipes: The Art of Scientific Computing*, Cambridge Univ. Press, Cambridge (1986).
72. W. L. Smith, "Polynomial Representation of Carbon Dioxide and Water Vapour Transmission", ESSA Technical Report NESC47 (1969).
73. D. P. Cruikshank and P. M. Silvaggio, *Astrophys. J.* **233,** 1016 (1979).
74. P. Silvaggio, Ph.D. Thesis, Cornell Univ. (1977).
75. P. Varanasi, S. Sarangi, and L. Pugh, *Astrophys. J.* **179,** 977 (1973).
76. J. Ballard and W. B. Johnston, *JQSRT* **36,** 365 (1986).
77. P. Varanasi and S. Chudmani, *JQSRT* **43,** 1 (1990).
78. D. H. Rank, U. Fink, and T. A. Wiggins, *Astrophys. J.* **143,** 980 (1966).
79. J. S. Margolis, *JQSRT* **11,** 69 (1971).
80. K. Fox and D. E. Jennings, *J. Molec. Struct.* **224,** 1 (1990).

81. K. Fox, D. E. Jennings, E. A. Stern, and R. Hubbard, *JQSRT* **39,** 473 (1988).
82. K. Fox, D. T. Quillen, D. E. Jennings, J. Wagner, and C. Plymate, *J.G.R.* **96(E2),** 17483 (1991).
83. F. W. Taylor, *J. Atmos. Sci.* **29,** 950 (1984).
84. G. F. Lindal, G. E. Wood, G. S. Levy, J. D. Anderson, D. N. Sweetnam, H. B. Hotz, B. J. Buckles, D. P. Holmes, P. E. Doms, V. R. Eshleman, G. L. Tyler, and T. A. Croft, *J.G.R.* **86,** 8721 (1981).
85. D. M. Hunten, M. Tomasko, and L. Wallace, *Icarus* **43,** 143 (1980).
86. M. Sato and J. E. Hansen, *J. Atmos. Sci.* **36,** 1133 (1979).
87. R. F. Knacke, S. J. Kim, S. T. Ridgway, and A. T. Tokunaga, *Astrophys. J.* **262,** 388 (1982).
88. D. Gautier, B. Bézard, A. Marten, J. P. Baluteau, N. Scott, A. Chedin, V. Kunde, and R. Hanel, *Astrophys. J.* **257,** 901 (1982).
89. G. L. Bjoraker, H. P. Larson, and V. G. Kunde, *Icarus* **66,** 579 (1986).
90. F. Moreno, A. Molina, and J. L. Ortiz, *Icarus* **96,** 129 (1992).
91. C. A. Griffith and T. Owen, in "Proceedings of the Toulouse Symposium on Titan", EAS SP-338 (1991).
92. E. Lellouch, A. Coustenis, J.-P. Maillard, K. Strong, N. Demé, C. Griffith, and B. Schmitt, in "Proceedings of the Toulouse Symposium on Titan", ESA SP-338 (1991).